Mathematics of the SARS-CoV-2 Pandemic

by

Salman Safdar

A Dissertation Presented in Partial Fulfillment
of the Requirements for the Degree
Doctor of Philosophy

Approved April 2023 by the
Graduate Supervisory Committee:

Abba B. Gumel, Chair
Eric Kostelich
Yun Kang
John Fricks
Malena Espanol

ARIZONA STATE UNIVERSITY

May 2023

ABSTRACT

A pneumonia-like illness emerged late in 2019 (coined COVID-19), caused by SARS-CoV-2, causing a devastating global pandemic on a scale never before seen since the 1918/1919 influenza pandemic. This dissertation contributes in providing deeper qualitative insights into the transmission dynamics and control of the disease in the United States. A basic mathematical model, which incorporates the key pertinent epidemiological features of SARS-CoV-2 and fitted using observed COVID-19 data, was designed and used to assess the population-level impacts of vaccination and face mask usage in mitigating the burden of the pandemic in the United States. Conditions for the existence and asymptotic stability of the various equilibria of the model were derived. The model was shown to undergo a vaccine-induced backward bifurcation when the associated reproduction number is less than one. Conditions for achieving vaccine-derived herd immunity were derived for three of the four FDA-approved vaccines (namely Pfizer, Moderna and Johnson & Johnson vaccine), and the vaccination coverage level needed to achieve it decreases with increasing coverage of moderately- and highly-effective face masks. It was also shown that using face masks as a singular intervention strategy could lead to the elimination of the pandemic if moderate or highly-effective masks are prioritized and pandemic elimination prospects are greatly enhanced if the vaccination program is combined with a face mask use strategy that emphasizes the use of moderate to highly-effective masks with at least moderate coverage. The model was extended in Chapter 3 to allow for the assessment of the impacts of waning and boosting of vaccine-derived and natural immunity against the BA.1 Omicron variant of SARS-CoV-2. It was shown that vaccine-derived herd immunity can be achieved in the United States *via* a vaccination-boosting strategy which entails fully vaccinating at least 72% of the susceptible populace. Boosting of vaccine-derived immunity was shown to be more beneficial than boosting of nat-

ural immunity. Overall, this study showed that the prospects of the elimination of the pandemic in the United States were highly promising using the two intervention measures.

DEDICATION

"Every good gift and every perfect gift is from above, and cometh down from the Father of lights, with whom is no variableness, neither shadow of turning"

James 1:17.

"As long as the earth remains, there will be planting and harvest, cold and heat, summer and winter, day and night"

Genesis 8:22.

To my parents Safdar Sardar and Nusrat Safdar, wife Rahela Salman, and kids Genesis Salman and Jonah Emmanuel Salman,

With tears in my eyes and joy in my heart, I would like to thank all of you for all your love and sacrifices to make me whom I am today. You saw the future and gave your life in order for me to achieve greatness in life. As long as I remain on earth, I will forever be indebted to you. I will proclaim to generations to come the sacrifices you made for them to have a good life.

ACKNOWLEDGEMENT

First and foremost, my appreciation goes to the almighty GOD for blessing me with this opportunity to pursue my PhD in the United States. I would like to express my sincere gratitude to my research advisor Professor Dr. Abba B. Gumel for his constant guidance and for his fatherly role during my studies. Sir, I am very thankful for your understanding and patience during the early stage of my graduate studies. Thank you for your constructive criticism that has very much improved me in all aspects of public life. Not only have you helped me grow academically, but you have taught me to be a great human being throughout my academic journey. Having you as a mentor has changed my life for the better. I will forever be grateful to you, Sir, for always motivating me during times of difficulty. I could not have done it without the help of my dissertation committee members: Dr. Eric Kostelich, Dr. Yun Kang, Dr. John Fricks and Dr. Malena Espanol, for sharing their expertise and for their insightful comments, support and guidance during the writing of this thesis. Most importantly, I would like to thank my amiable wife (Rahela Salman) and the wonderful kids God blessed us with (Genesis Salman and Jonah Emmanuel Salman) for constantly providing me love, encouragement, and inspiration during my research. A special thank you to my parents (Mr Safdar Sardar and Mrs Nusrat Safdar), for uplifting me and supporting me each and everyday. Especially, to my mother who never stopped praying and fasting for me, I am incredibly thankful for you. Indeed, I can attest to the fact that those prayers brought me this far. Also, I would like to thank my only brother (Mr Arslan Safdar) and all my sisters (Ms Sadaf Safdar, Mrs Najaf Nabil, Mrs Ishaf Howell, Mrs Bushra Naeem and Mrs Kiran John) for all your prayers, support, and encouragement during my graduate studies. I am also thankful to all of my brother-in-laws (Mr Nabil Salim, Mr Nelson Howell, Mr Naeem Sarfraz, Mr John Ghori and Mr Moses Rohel) and also to my sister-in-law (Mrs Rida

Arslan). This bond with all of you is extremely special to me, as it has only brought us all closer together. Also, I want to thank all my loving neices and nephews (Aroma, Abigail, Samuel, Joye, Joanna, Enoch, Hosanna, Rija and Eden). I also want to thank my father-in-law and my mother-in-law (Mr Parvez Iqbal and Mrs Mukhtari Sardar) whom were constantly praying for me while encouraging me during this time. I am also very thankful to Dr. Enahoro Iboi for encouraging me and for all his support and mentorship during my graduate studies. To my dependable friends (Waqas Iqbal and Ahmed Faraz), for bringing me joy and motivation. I am also thankful to Dr. Danish Khan, Dr. Munawar Hussain and Mr Maqsood Alam, who have remained close friends and mentors to me. Professor Adnan Khan (my mentor), thank you for exposing me to the immense field of mathematical biology. I am also thankful to Dr. Calistus Ngonghala for the valuable insight you provided me when I was writing my MATLAB Codes. I am also thankful to Dr. Tufail Malik and Dr. Chandranath Podder for their guidance during my research. I also want to express my gratitude to Dr. Sharon Crook and Ms Joelle Park for all their help during my four years at ASU. To all my friends at ASU, you are now family to me. My time at ASU was worth while due to our friendship, thank you. You all made my stay at Arizona State worth while. Last but not least, I must specially acknowledge my pastors (Pastor A. V. Chako, Pastor Shing Chow, Pastor Steve Joseph, Pastor Shamoun Ayub and Brother Michael) as this dissertation would not be possible without your love, prayers, and support from the first day they learn't of my desire for a graduate degree. I will forever be indebted to all my prayer group brothers and sisters (Nathan, Jake, Keely, Joshua, Ashton, Ethan, Jordan, Micah, Paige, David, Rebekah, Lauren, Annaliese, Lindsey, Tim, Joshua Pawlak, Jacqueline and Chris) for the wonderful fellowship during my stay in the United States of America for my graduate studies. I would also like to thank Fulbright Foreign Student Program for sponsoring my graduate studies.

TABLE OF CONTENTS

APPENDIX Page

LIST OF TABLES

Table Page

Table Page

LIST OF FIGURES

Figure Page

Figure Page

Figure Page

Figure Page

Chapter 1

INTRODUCTION

1.1 General Overview

A pneumonia-like illness of an unknown etiology emerged out of Wuhan city of China late in December 2019 (Srivastava *et al.*, 2020). Genomic sequencing analysis revealed that the disease is a member of the family of coronaviruses, caused by SARS-CoV-2 (Wang *et al.*, 2020). Within a few days and weeks, the disease (tagged COVID-19) rapidly spread across China and to almost every part of the world. The World Health Organization (WHO) declared COVID-19 to be a global pandemic on March 11, 2020 (Ohannessian *et al.*, 2020). The COVID-19 pandemic continues to inflict unprecedented burden globally. It has, as of March 16, 2023, caused over 682 million confirmed cases and over 6.8 million deaths globally (Figures 1.1 and 1.2 depict a map for the global cumulative confirmed cases and deaths, respectively (Dong *et al.*, 2020; Worldometer., 2023)). The COVID-19 pandemic has become the greatest public health and socio-economic challenge humans have faced since the 1918 influenza pandemic (Liang *et al.*, 2021; Ngonghala *et al.*, 2020b; Brozak *et al.*, 2021).

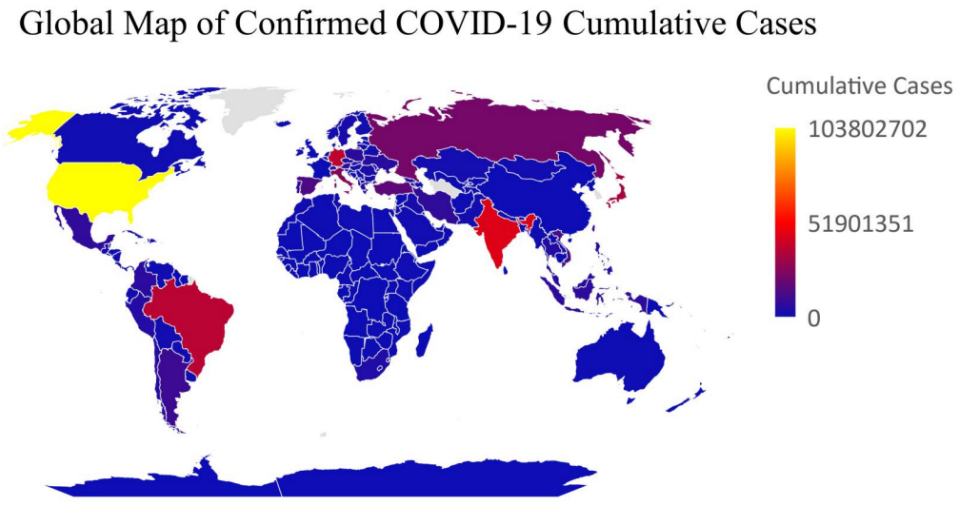

Figure 1.1: Global Map of Confirmed COVID-19 Cumulative Cases, as of March 9th, 2023. Map was Generated Using the Cumulative COVID-19 Case Data from the Johns Hopkins University Github (Dong *et al.*, 2020).

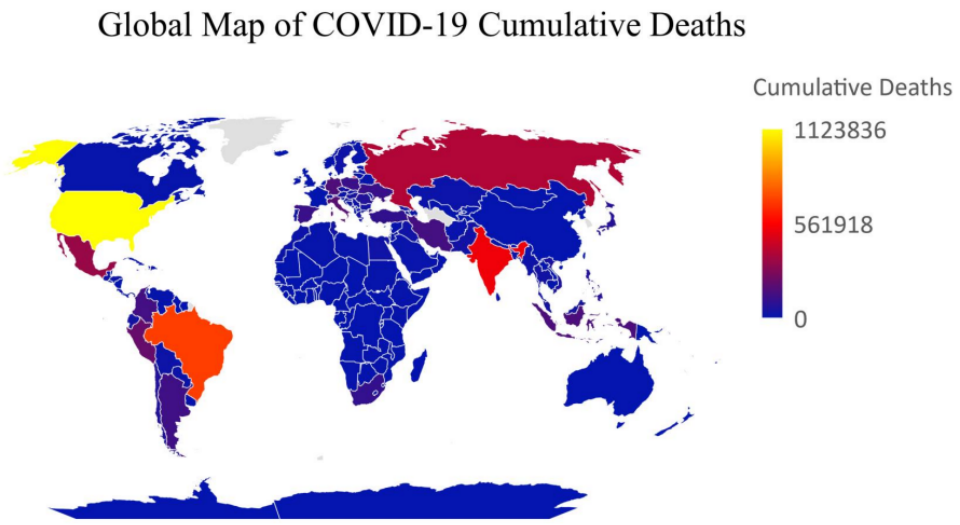

Figure 1.2: Global Map of COVID-19 Cumulative Deaths, as of March 9th, 2023. Map was Generated Using the Cumulative Mortality Data from the Johns Hopkins University Github (Dong *et al.*, 2020).

The United States suffers the brunt of the global burden of COVID-19, with nearly 105 million confirmed cases and over 1.1 million deaths (see Figures 1.3 and 1.4 for the map of the cumulative confirmed cases and deaths for the United States, respectively (Dong *et al.*, 2020; Worldometer., 2023)).

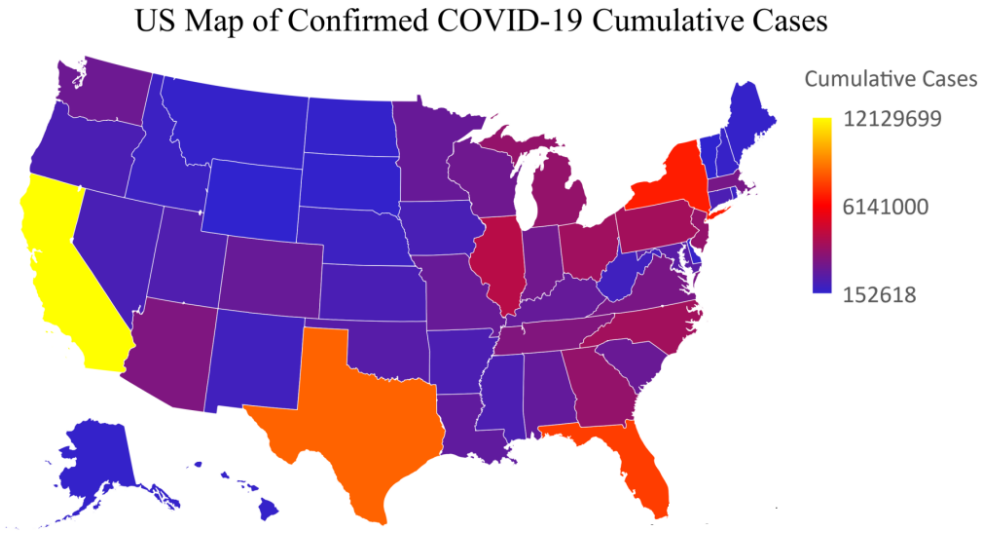

Figure 1.3: Map of Confirmed COVID-19 Cumulative Cases for the United States, as of March 9th, 2023, Generated Using the Cumulative Confirmed Case Data from the Johns Hopkins University Github (Dong *et al.*, 2020).

This dissertation is based on using mathematical modeling approaches, together with rigorous analysis, data analytics and computation, to gain insight into (and understanding on) the transmission dynamics and control of COVID-19 in the United States. Emphasis is on the assessment of the population-level impacts of various public health interventions, such as vaccination and the use of face mask in public.

1.2 Basic Background of COVID-19

Coronaviruses are a group of related RNA viruses that cause diseases in mammals and birds (Pal *et al.*, 2020). Specifically, these viruses cause respiratory tract infections

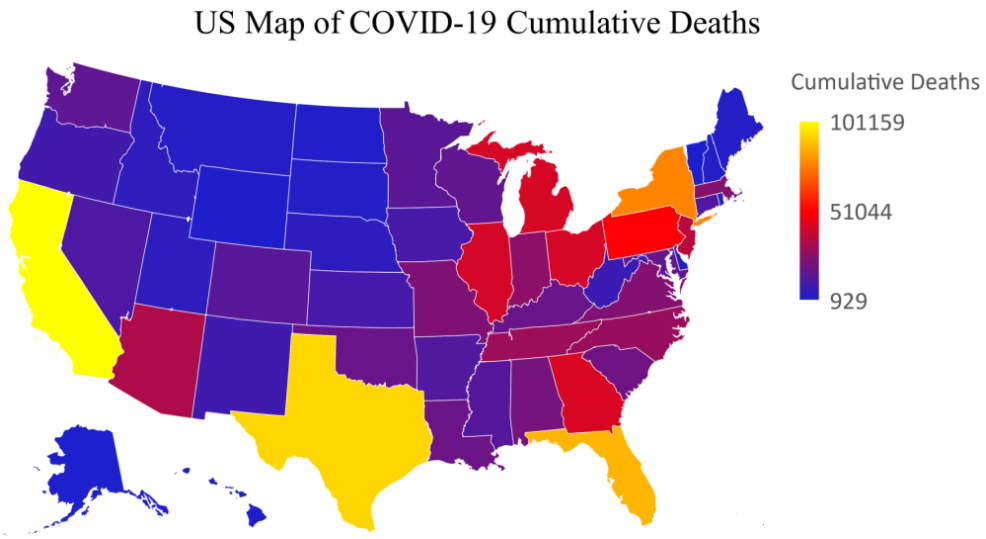

Figure 1.4: Map of COVID-19 Cumulative Deaths for the United States, as of March 9th, 2023, Generated Using the Cumulative Mortality Data from the Johns Hopkins University Github (Dong *et al.*, 2020).

in humans (Van der Hoek, 2007). The structure of coronavirus particles (depicted in Figure 1.5) consist of long stranded RNA viral genomes (the largest known viral RNA genome (Li *et al.*, 2020)) which are bounded by a protective *capsid* (a lattice of repeated protein molecules, called *nucleocapsid*). The viral genome and the *capsid* are enveloped into the center of the particle (Jonathan *et al.*, 2020). The core particle of the coronavirus (i.e., the RNA genome) is further surrounded by an outer membrane, which is made from a layer of lipids (fats) (Scripps Research, 2020). These outer membranes derive from the cells in which the virus was last assembled but are modified to contain specific viral proteins, including membrane, envelope and the spike proteins (regarded as the key set of the proteins in the outer membrane (Jonathan *et al.*, 2020)). It should be mentioned that the word "corona" is Latin for "crown", which refers to the appearance that Coronaviruses get from the spike proteins sticking out of them (Chorba, 2020). These spike proteins, which act as the grappling hooks that sticks tightly to, and cracks, the host cells, and eventually enters into the host cells by binding to a viral receptor known as *Angiotensin Converting Enzyme*

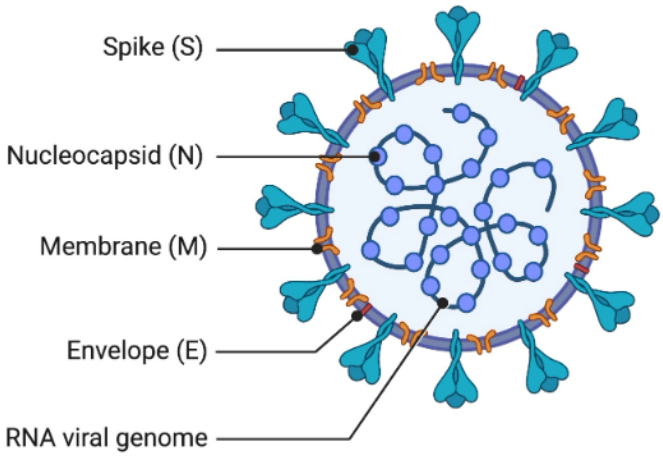

Figure 1.5: Structure of COVID-19 (spike protein). Source: Jonathan *et al.* (2020).

2 (ACE2) (Scripps Research, 2020; Zheng *et al.*, 2022; Jonathan *et al.*, 2020). This triggers the human immune response, namely the innate and the adaptive immune responses. The innate immune response (which includes both the humoral and T cell-mediated immune response) is the first line of host defense against the virus, and is triggered within minutes to hours of viral entry into the host's target cell. The adaptive immune response (which develops antibodies and white blood cells to attack and remember the virus, making it easier to fight with it again) removes any remaining virus and create a memory for fighting future infections (Billingsley, 2020). When SARS-CoV-2 virus enters a host cell, the pathogen recognition receptors (PRRs) of the innate immune response rapidly identifies and recognizes the external pathogen (i.e., the virus) (Zheng *et al.*, 2022; Qi *et al.*, 2022; Shah *et al.*, 2020). Upon this recognition, the adaptive immune response kicks in, and plays a key role in curtailing or neutralizing the spread of the SARS-CoV-2 virus within the host (Zheng *et al.*, 2022; Qi *et al.*, 2022; Shah *et al.*, 2020). Specific antibodies generated by the humoral immune response are significant in neutralizing the SARS-CoV-2 virus and have the potential to help activated immune T cells to destroy the virus-infected cells (Zheng

et al., 2022; Qi *et al.*, 2022; Shah *et al.*, 2020).

Figure 1.6: Diagrammatic Representation of the Theory Behind the Twin Mammals (i.e., Bats and Pangolins) and Emergence of COVID-19 in Humans. Source: Anjum (2020).

Two theories have been advanced as to the origin of SARS-CoV-2, the causative agent of COVID-19. The first is that the virus primarily emerged *via* a zoonotic transfer from wild animals or from consumption of meat of wild animals sold at the Huanan Seafood Wholesale Market in Wuhan city (Figure 1.6) (Wang *et al.*, 2020). Bats and many other non-human primates in the wild are implicated for the emergence of many of the deadly infectious diseases of humans, including SARS-CoV-2 (Figure 1.7). The second is that it came from a leak from the Wuhan Institute of Virology (Ruiz-Medina *et al.*, 2022; Maxmen *et al.*, 2022; Alanagreh *et al.*, 2020; Yuan *et al.*, 2020). SARS-CoV-2 is genetically similar to the severe acute respiratory syndrome (SARS-CoV-1), which emerged out of the Guandong province of China in 2002 and the middle eastern respiratory syndrome (MERS), which emerged from Saudi Arabia

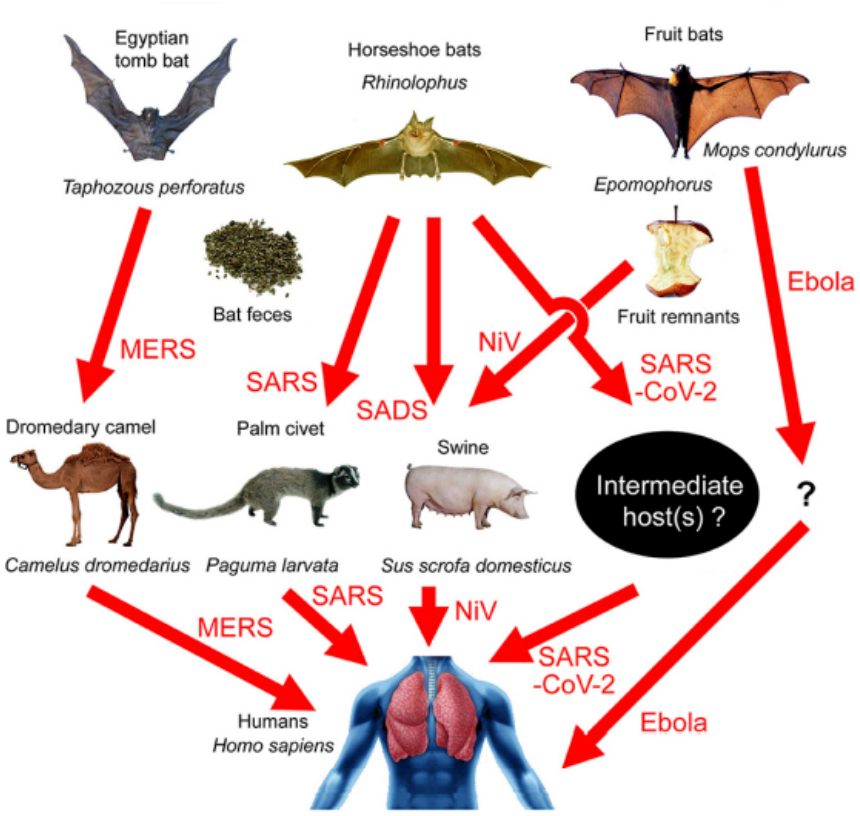

Figure 1.7: Transmission Pathways of Bat-borne Viral Diseases. MERS: Egyptian Tomb Bat → Dromedary Camel → Humans; SARS: Horseshoe Bats → Palm Civet → Humans; Sads: Horseshoe Bats → Swine; SARS-CoV-2: Horseshoe Bats → Unknown Intermediate Host → Humans; Nipah Virus (NiV): Fruit Bats → Swine → Humans; Ebola Virus: Angora Dog Bat (Mops Condylurus) → Unknown Intermediate Host → Humans. Source: Yuan *et al.* (2020).

and Jordan (Peiris and Poon, 2021) (the biology, burden and global distribution of these three members of the family of coronaviruses are compared in Table 1.1). SARS-CoV-2, the causative agent of the COVID-19 pandemic, is primarily transmitted from human-to-human through inhalation of respiratory droplets from both symptomatic and asymptomatically-infectious humans (van den Driessche and Watmough, 2000; Yin and Wunderink, 2018; Ngonghala *et al.*, 2020a). The incubation period of the disease is estimated to be between 2 and 14 days, and majority of the COVID-19

	SARS-CoV	**MERS-CoV**	**COVID-19**
Origin	China	Saudi Arabia	China
Duration	2002 − 2003	2012 − to date	Dec. 2019 − to date
Reservoir	Bats & civet	Bats/camels	Bats (Pangolins)
Countries	29	27	220
Incubation period	2 − 7 days	5 days	2 − 14 days
Confirmed cases	8,000	2,519	682,465,296
Global deaths	744	866	≈ 6.8 million
Case fatality ratio	9.5%	34.4%	≈ 99.9%

Table 1.1: Comparing Recent Coronaviruses: SARS-CoV, MERS-CoV and COVID-19. Sources: Open Literature (Wikipedia) and (Worldometer., 2023).

infected individuals show mild or no clinical symptoms (Ngonghala *et al.*, 2020a; Brozak *et al.*, 2021). Most common symptoms of the disease often resemble those of seasonal influenza, which typically include fever, difficulty breathing, fatigue, sore throat, and body aches (Brozak *et al.*, 2021; Mancuso *et al.*, 2021; Ngonghala *et al.*, 2020a). The elderly and those with underlying medical conditions (co-morbidities) such as people with diabetes, hypertension, obesity, kidney disease and other conditions that suppress or compromise the immune system, younger people who are in close contact with the infected individuals, and frontline healthcare workers are also at high risk of acquiring COVID-19 (World Health Organization, 2020; Brozak *et al.*, 2021; Ngonghala *et al.*, 2020a; Gumel *et al.*, 2021a).

1.3 Public Health Interventions

Two main types of interventions, namely non-pharmaceutical (NPI) and pharmaceutical, are used to control and mitigate the burden of the COVID-19 pandemic, as briefly described below.

1.3.1 Non-pharmaceutical interventions

Prior to the development, and subsequent FDA-EUA of a number of safe and effective vaccines for use in humans in December 2020, the control and mitigation strategies against COVID-19 have been limited to, and focused on, the use of NPIs (Eikenberry *et al.*, 2020; Ngonghala *et al.*, 2020a,b; Gumel *et al.*, 2021a). In particular, since the novel coronavirus is a respiratory disease, which is transmitted among people through respiratory droplets produced when an infected individual coughs, sneezes, or talks, the implementation of strict social-distancing and lockdown measures has proven to be effective in limiting the spread of the pandemic (Ngonghala *et al.*, 2020a; Bourouiba, 2020; Ngonghala *et al.*, 2020b). Another major public health strategy for controlling the spread of COVID-19 is by contact-tracing, which involves the identification of individuals who had close contact with a confirmed SARS-CoV-2 case within a certain time frame (e.g., two days prior to the onset of symptoms (Bi *et al.*, 2020)), interviewing, testing, and isolating or hospitalizing them if they have the disease (Michaud and Kates, 2020).

The use of face masks (i.e., respiratory protection) in public, hand-washing with sanitizers and quarantine of the detected cases of COVID-19 are some other important NPIs. The use of face masks in public, which was generally considered to be the most significant NPI for effectively curtailing COVID-19, has historically been a common practice to combat the transmission and the spread of respiratory diseases, dating back to at least the 1918 pandemic caused by the H1N1 influenza A virus (Luckingham, 1984; Bootsma and Ferguson, 2007; Morens *et al.*, 2009). Furthermore, the use of face masks may have been instrumental in limiting the community spread of the 2002/2003 SARS epidemic in many Asian counties (particularly in China, Singapore, Hong Kong and Taiwan) (Wu *et al.*, 2004; Lau *et al.*, 2004). Numerous research

studies have shown that the community wide compliance of face masks has been used as the most effective NPI in curbing the COVID-19 pandemic (Wang *et al.*, 2020; Eikenberry *et al.*, 2020; Ngonghala *et al.*, 2020b, 2021b, 2023; Gumel *et al.*, 2021b). Face masks have dual purposes. If worn by a susceptible individual, they provide efficacy against the acquisition of infection (i.e., primary protection). On the other hand, if the wearer is already infected, masks offer efficacy against their ability to transmit the disease to the susceptible individuals (i.e., secondary protection) (Aiello *et al.*, 2010, 2012; MacIntyre *et al.*, 2009; Eikenberry *et al.*, 2020).

Broadly, several categories of face masks exist based on their protective efficacy and

Figure 1.8: Different Types of Face Masks (with Their Pros and Cons) Used During the COVID-19 Pandemic. Source: Infection Control (2020).

their fitting. Face masks are mainly classified in following three categories (as shown in Figure 1.8); i.e., (*a*) cloth or fabric masks; which are loose fitting devices with protective efficacy ranging from 0 to 50% (Eikenberry *et al.*, 2020; Lindsley *et al.*, 2021; Ngonghala *et al.*, 2021b), (*b*) surgical or procedure masks; which are also loose fitting devices with protective efficacy about 70% (Ngonghala *et al.*, 2021b, 2023))

and (c) respirators (N95 masks); which are considered as tight-fitting respiratory protective devices that meet or exceed the National Institute for Occupational Safety and Health (NIOSH) N95 standard and have protective efficacy around 100% (Lindsley *et al.*, 2021; Qian *et al.*, 1998; Ngonghala *et al.*, 2021b). However, face masks and surgical masks are designed to be used as a source control and only have outward efficacy (i.e., protecting the transmission of the disease from the mask wearers to the those around them and not the protection of mask wearers from the infected individuals) whereas the respirators have both inward (i.e., primary protection against catching the infection) and outward efficacy (i.e., source control) (Ngonghala *et al.*, 2021b). Furthermore, it is worth mentioning that fitting of all the mask types discussed above (which are also shown in Figure 1.8), directly co-relates with the masking efficacy (Ngonghala *et al.*, 2021b). Poorly fitted device can eventually lead to decreased filtration efficiency, regardless of the masking type (O'Kelly *et al.*, 2021; Ngonghala *et al.*, 2021b). Furthermore, the design of face masks and surgical masks cannot ensure the tight seal and, thus, enable significant filter bypass. However, the construction and design of the respirators ensure tight seal (when properly fitted) that leads to the whooping reduction of 100-fold in the concentration of particles inside the device compared with particles outside of the device (Bergman *et al.*, 2012; Ngonghala *et al.*, 2021b).

1.3.2 Pharmaceutical interventions

To limit and curtail the burden of COVID-19 pandemic in the United States, the United States Food and Drug Authority (FDA) has authorized and deployed the following pharmaceutical interventions, which have been mainly classified into two

categories, namely treatments and vaccines, as briefly described below.

(A) Treatments

The United States Food and Drug Administration (FDA) has authorized three antiviral drugs and monoclonal antibodies (mABs) for the treatment of COVID-infected individuals, showing mild-to-moderate symptoms of the disease (Centers for Disease Control and Prevention, 2022). Following are the FDA approved pharmaceutical interventions available in the United States for the treatment of individuals, who are likely to develop severe symptoms of COVID-19 and eventually can get very sick with the SARS-CoV-2 virus.

(A1): Antiviral drugs Treatment

The United States Food and Drug Administration (FDA) approved the first antiviral drug (*remdesivir*; sold under the brand name *Veklury*, developed by the biopharmaceutical company *Gilead Sciences*) on October 22, 2020, for use to treat COVID-19 patients (Cohen and Kupferschmidt, 2020). This drug is administered *via* injection through the vein. Due to its limited supply, it was only reserved for use to treat the infected individuals in hospital who display severe symptoms of COVID-19 (Gumel *et al.*, 2021b). Furthermore, the overall treatment cost associated with this antiviral medication is quite high (costing around $390 *per* vial, this is equivalent to $2,340 for a 5-day course of treatment, or $4,680 for a 10-day course of treatment (Margaret Labban, 2020)).

In late December of 2021, the FDA issued Emergency Use Authorization (EUA) to two antiviral drugs, namely, *Paxlovid*, consists of two separate medications packaged together (i.e., *Nirmatrelvir* with *Ritonavi*, developed by *Pfizer* Inc.), be orally taken by individuals, 12 years of age and older weighing at least 40 kg and *Molnupiravir* (sold under the brand name *Lagevrio*, developed by *Merck* Inc.), be orally taken by

individuals, 18 years of age and older (Centers for Disease Control and Protection, 2022; Centers for Disease Control and Prevention, 2022). Each of these drugs is used to treat mild-to-moderate COVID-19 in individuals (must be taken within five days after symptoms begin) who are at high risk for progression to severe COVID-19, including hospitalization or death (Food and Drug Administration and others, 2022). Both of these antiviral drugs primarily work by altering the genetic code of SARS-CoV-2 and inhibiting it from replicating (Ngonghala *et al.*, 2023). Generally, all the FDA approved antivirals for the treatment of COVID-19 work by targeting specific parts of the SARS-CoV-2 virus to curtail its multiplying effect in the human body. *Paxlovid*, which is administered as three tablets (i.e., 2 *nirmatrelvir* tablets, 150 mg and 1 *ritonavir* tablet, 100 mg) taken together orally twice daily (i.e., morning and evening, same time each day) for five days, is estimated to reduce the risk of hospitalization or death by 88% (Centers for Disease Control and Protection, 2022). *Molnupiravir*, which is administered as four 200 milligram capsules taken orally every 12 hours for five days, is effective in reducing hospitalization or death by 31% (Ngonghala *et al.*, 2023). Furthermore, the FDA EUA states that *Molnupiravir* is not recommended for use in pregnant patients (National Institute of Health, 2022).

(A2): Monoclonal Antibody Treatment

On February 11th, 2022, the United States Food and Drug Administration (FDA) issued an EUA for a new monoclonal antibody (named *Bebtelovimab*, developed by *AbCellera and Eli Lilly*) for the treatment of the Omicron variant of COVID-19 (for individuals having mild-to-moderate symptoms) (U.S. Food and Drug Authority, 2022). Monoclonal antibody treatment works by helping the immune system to recognize and respond more effectively to the SAR-CoV-2 virus (Centers for Disease Control and Prevention, 2022). *Bebtelovimab* contains man made antibodies (not the

original SARS-CoV-2 virus) that bind to the spike protein of the SARS-CoV-2 virus and thus block the virus from entering the human body (Centers for Disease Control and Prevention, 2022). *Bebtelovimab*, which is administered for ages 12 years and older, as a single *Intravenous* (IV) injection, which must be taken within 7 days of onset of symptoms (U.S. Department of Health & Human Services, 2022). Furthermore, there is no cost associated with the antibodies themselves, but there may be treatment fees (U.S. Department of Health & Human Services, 2022).

(B) Vaccines

The most-awaited breakthrough and *game-changer* in the fight against COVID-19 was announced on December 11, 2020, when the FDA gave emergency use authorization (EUA) for the first vaccine against the pandemic (Pfizer, 2020; Self *et al.*, 2021). This vaccine, developed by Pfizer-BioNtech and based on the delivery of RNA (mRNA) encoding the SARS-CoV-2 spike protein (Mancuso *et al.*, 2021), was initially administered in a two-dose regimen 3 to 8 weeks apart. It showed 95% efficacy against symptomatic COVID-19 in clinical trials. The Pfizer vaccine was initially approved for use for people 16 years of age and older, but later also approved for use for infants and other children under the age of 16 (Katella, 2021). A week later (December 18, 2020), the FDA gave an EUA for another vaccine, developed by Moderna Inc. (Mahase, 2020; Self *et al.*, 2021). This vaccine, also based on mRNA technology, is administered in a two-dose regimen 4 to 8 weeks apart (and it showed efficacy of about 94.1% in initial clinical trials) (Mancuso *et al.*, 2021; Katella, 2021). The Moderna vaccine is also approved for use in people 6 months and older (Katella, 2021).

The Janssen vaccine, developed by Johnson & Johnson, received FDA EUA on February 27, 2021. It is administered as a single dose (it showed 67% efficacy in preventing moderate to severe COVID-19 14 days post-vaccination, in clinical trials (Mancuso

et al., 2021; Safdar *et al.*, 2023; Katella, 2021)). Unlike the mRNA-based Pfizer and Moderna vaccines, the Johnson & Johnson vaccine was developed based on using adenovirus vector encoding the SARS-CoV-2 spike protein.

The most recent vaccine to receive FDA EUA on July 13, 2022, is the Novavax COVID-19 Vaccine (available with brand names *Nuvaxovid* and *Covovax*). Unlike the mRNA and vector vaccines, this is a protein adjuvant (i.e., an ingredient used to strengthen the immune response). It is administered in individuals 18 years of age and older. Two doses of the vaccine administered 3 to 8 weeks apart showed 90% efficacy against lab-confirmed, symptomatic infection and 100% against moderate and severe disease in Phase 3 trial (Dunkle *et al.*, 2022). Table 1.2 compares the different features of the aforementioned four vaccines being deployed and administered in the United States. The table given below discusses the various classes of vaccines (or vaccine types) being administered in the United States.

Developer	**Pfizer-BioNTech**	**Moderna**	**J & J**	**Novavax**
Platform	mRNA-based	mRNA-based	adenovirus vector	protein adjuvant
Shell life	cold freezer (−94F)	standard freezer	standard freezer	refrigerator
FDA-EUA	12/11/2020	12/18/2020	02/27/2021	06/13/2022
Efficacy	95%	94.1%	67%	90%
Doses	3 (8 weeks apart)	4 (8 weeks apart)	single dose	3 (8 weeks apart)
Age group	6 months & older	6 months & older	18 years & older	12 years & older
Cost/dose	$\approx$ \$20	$\approx$ \$20 – \$25	$\approx$ \$10	$\approx$ \$16

Table 1.2: Comparative Summary of the COVID-19 Vaccines Currently Used in The United States (Katella, 2021). Notation: J&J Represents the Johnson & Johnson Vaccine.

(B1): mRNA vaccines

Numerous studies have shown that researchers have been studying and working on messenger RNA (abbreviated as mRNA) vaccines for decades (Schlake *et al.*, 2012;

Dolgin *et al.*, 2021; Centers for Disease Control and Prevention, 2020), and that mRNA vaccines have been studied in the past, for instance, in the context of influenza, Zika, rabies, and *cytomegalovirus* (CMV) (Centers for Disease Control and Prevention, 2020). The two mRNA vaccines developed against COVID-19 (i.e., the Pfizer and Moderna vaccines) work by sending instructions through a small piece of mRNA (i.e., a protein found on the outer surface of virus) to the host cells in the body for making copies of a spike protein (like the spikes, as shown in Figure 1.5). In response, it triggers the immune response in our bodies which immediately recognizes that this is a foreign pathogen, and the immune system reacts by activating immune cells and producing antibodies (i.e., a specialized protein) (Jain *et al.*, 2021). The antibodies produced through this process remain active in our bodies even after the original protein (that was inserted in the body) was attacked and destroyed by these antibodies. The developed antibodies recognize and attack the real SARS CoV-2 spike protein, if an individual becomes exposed to the actual SARS-CoV-2 virus. (Katella, 2021; Centers for Disease Control and Prevention, 2020).

(B2): Adenovirus vaccine

Adenovirus vector vaccine (on which the Johnson & Johnson vaccine is based on) is a carrier vaccine and works by sending a "harmless" adenovirus (i.e., a virus that cause common illnesses like fevers and coughs) as a shell to carry genetic code on the spike proteins to the cells (Katella, 2021). The genetic code being delivered to the cells is a message that will instruct the cells to temporarily make a few copies of the spike protein just to activate the immune system (American Society of Gene plus Cell Therapy, 2021; Centers for Disease Control and Prevention, 2020). The adenovirus vaccine cannot make the vaccinated individual to become sick because the genetic code sent to the cells are not given enough instructions to build the full

virus (Katella, 2021; American Society of Gene plus Cell Therapy, 2021). Once the genetic code is inside the cells, the cells produce a spike protein to train the body's immune system to produce antibodies and activates T-cells (i.e. memory cells) to protect against an actual COVID-19 infection (Katella, 2021; Centers for Disease Control and Prevention, 2020).

(B3): Protein adjuvant vaccine

The protein adjuvant (sub-unit) vaccine (on which the Novavax vaccine is based on) works by sending the spike protein of the coronavirus itself, but formulated as a nano-particle (i.e., the harmless spike protein), which cannot cause disease (Katella, 2021). This stimulates the immune system to produce antibodies and T-cell immune responses to protect against SARS-CoV-2 infection (Katella, 2021; Centers for Disease Control and Prevention, 2020).

Booster vaccine doses

Numerous research studies have shown that the protection efficacy of all the anti-COVID vaccines wanes over time (Gumel *et al.*, 2021b; Ngonghala *et al.*, 2023; Safdar *et al.*, 2023; Curley, 2021). Center for Disease Control and Prevention (CDC) recommended the booster doses to overcome this waning effect of mRNA vaccines (McConeghy, 2022; Ferdinands *et al.*, 2022). Booster dose is an additional administration of the vaccine given to those individuals who have completed the primary vaccination series. Booster doses are further classified into two categories (based on their effectiveness against the strains of SARS-CoV-2) (Washam, 2022), namely *monovalent* and *bivalent*, as briefly described below.

(a): Monovalent boosters

On November 19th, 2021, the first booster dose was recommended by CDC (i.e., an

extra dose of vaccine administered after the primary dose) specifically for those individuals who are at highest risk of serious disease and for the frontline healthcare workers (Pacific and Hasan, 2021). In late March 2022, the FDA authorized a second booster shot of COVID-19 vaccines for vulnerable populations in the United States (i.e., for people 50 years of age and older, and for individuals with certain immunocompromising conditions who are at higher risk of severe disease, hospitalization and death) (Safdar *et al.*, 2023). These boosters are called "*monovalent*", because they were designed to protect against the original virus that causes COVID-19. They also provide some protection against the Omicron variant (Centers for Disease Control and Prevention and others, 2022).

(b): Bivalent boosters

Bivalent boosters (which protect against both the original SARS-CoV-2 variant and the Omicron variants BA.4 and BA.5) was authorized by FDA in August 2022 and became available from September 2, 2022 (Centers for Disease Control and Prevention and others, 2022). Most adults (i.e., 18 years and older) should get an updated Pfizer-BioNTech or Moderna bivalent booster at least 2 months after their primary Pfizer, Moderna or Novavax, two dose vaccine series, or at least 2 months after 1st dose of Johnson & Johnson vaccine (Katella, 2021; Centers for Disease Control and Prevention and others, 2022).

Emergence of SARS-CoV-2 Variants

Despite the rapid development and deployment of the effective vaccines, the efficacy of all the vaccines are threatened by the emergence of deadly and highly-contagious SARS-CoV-2 variants of concern (notably the Alpha, Beta, Gamma, Delta and Omicron variants, as tabulated with their lineages and date of first detection, in Table 1.3) (Mahase, 2021; Gómez-Carballa *et al.*, 2021; Karim and Karim, 2021; Koyama

et al., 2020). Furthermore, numerous clinical studies have shown that the efficacy of the SARS-CoV-2 vaccines wane over time (Ngonghala *et al.*, 2023; Safdar *et al.*, 2023; Ngonghala *et al.*, 2021b; Gumel *et al.*, 2021b). To overcome the waning effect of vaccine-derived immunity, the FDA approved the administration of booster vaccine doses, for three of the four FDA-EUA vaccines (Pfizer vaccine, Moderna vaccine and Johnson & Johnson vaccine), during August-November of 2021. Booster vaccine was approved for Novavax in October of 2022. Primarily, the booster dose (for persons aged 18 years and above) were approved because of waning vaccine effectiveness over time (Fast *et al.*, 2021).

VoC	**Lineage (location)**	**Date of first detection**
Original	A (China)	December 31, 2019
Alpha	B.1.1.7 (UK)	September 20, 2020
Beta	B. 1.135 (South Africa)	May, 2020
Delta	B.1.617.2 (India)	October 5, 2020
Gamma	P.1 or B.1.1.28.1 (Brazil)	November, 2020
Omicron	B.1.1.529 (South Africa)	November 24, 2021
	BA.2 (UK/India/Denmark)	December, 2021
	BA.5 (South Africa)	January, 2022
	XBB.1.5 (United States)	October, 2022

Table 1.3: Lineage and Date of First Detection of Main Variants of Concern (VoC) for COVID-19 (He *et al.*, 2021; Parums, 2021; Yale Medicine, 2023).

1.4 Outline of the Dissertation

This dissertation contains two main technical chapters (i.e., Chapters 2 and 3), while Chapter 1 provides a comprehensive introduction of the dissertation. Below is a brief

description of the content of each of the two technical chapters.

Chapter 2 of this dissertation contains material on modeling the population-level impact of three of the four anti-COVID vaccines approved by the United States Food and Drug Administration (FDA), namely the Pfizer, Moderna and the Johnson & Johnson vaccines (U.S. Food and Drug Administration and others, 2009, 2021b; Pfizer, 2020), on the transmission dynamics and control of the SARS-CoV-2 pandemic in the United States. To achieve the objectives of this chapter, a new basic model is formulated for the spread of COVID-19 in the presence of vaccination. The basic model, which takes the form of a 9-dimensional deterministic system of nonlinear differential equations, is rigorously analysed to gain insight into its dynamical features. The basic model was fitted using observed daily case data for the period where the Omicron BA.1 variant of SARS-CoV-2 first emerged in the United States (i.e., starting from the fall of 2021) (Dong *et al.*, 2020). The model is shown to undergo a vaccine-induced *backward bifurcation*, where two stable equilibria co-exists when the control reproduction number of the model is less than one. Two main sufficient conditions for the existence of the backward bifurcation were identified. When the two sufficient conditions are violated (so that backward bifurcation does not occur), the analyses revealed that the disease-free equilibrium of the model is globally-asymptotically stable when the associated control reproduction number of the model is less than one.

A theoretical expression for the vaccine-induced herd immunity threshold is also derived. It is shown that the basic model has a unique endemic equilibrium, for a special case, whenever the associated reproduction number exceeds one. This equilibrium is shown, using a Krasnasolskii sub-linearity approach (Hethcote and Thieme, 1985; Safi and Gumel, 2010; Melesse and Gumel, 2010; Esteva *et al.*, 2009), to be locally-asymptotically stable when it exists. Numerical simulations are carried out

to determine the optimal vaccination coverage level needed to achieve herd immunity for the various vaccine types. Extensive numerical simulations are also carried out to assess the community-wide impact of masking as a singular intervention and the combined impact of vaccination with a public face mask use strategy, as measured in terms of reduction (of both) in the value of control reproduction number and on the daily number of new COVID-19 cases in the United States. Detailed global sensitivity analysis of the parameters of the model is also carried out to identify the parameters that have the most effect or influence on the dynamics of the disease (with respect to a chosen response function).

Chapter 3 of this dissertation is based on modeling the impact of waning and boosting of natural and vaccine-derived immunity against the BA.1 Omicron variant in the United States. This work is motivated by the fact that the efficacy of each of aforementioned FDA-approved SARS-CoV-2 vaccines wanes over time (Gumel *et al.*, 2021b; Ngonghala *et al.*, 2021b, 2023; Safdar *et al.*, 2023). Consequently, the FDA approved the administration of booster doses, for each of the three FDA-approved vaccines, during the period between August and November of 2021 (Fast *et al.*, 2021). As of March 9, 2023, at least 69.3% of the population of the United States is fully-vaccinated with any of the approved vaccines (Center for Disaster Philanthropy, 2023) (and approximately 16.3% have received a bivalent booster shot, i.e., the highest level of protection against the virus (Centers for Disease Control and Prevention, 2023a; Center for Disaster Philanthropy, 2023)).

The objective of this chapter is to use mathematical modeling approaches to asses the population-level impact of waning and boosting of both the natural and vaccine-derived immunity on the transmission dynamics and control of the pandemic in the United States. To achieve this objective, the basic model developed in Chapter 2

was extended to explicitly account for the waning and boosting of the two immunity types. In addition to conducting the rigorous analysis of the model, the extended model was fitted using available case data for COVID-19 (starting from the onset of the Omicron variant) in the United States.

Chapter 2

BASIC VACCINATION MODEL AGAINST COVID-19

2.1 Introduction

COVID-19, the pneumonia-like illness that emerged out of Wuhan city in China late in December of 2019, has caused a devastating pandemic on a scale never before seen since the 1918/1919 influenza pandemic (Liang *et al.*, 2021; Safdar and Gumel, 2023). It has, as of March 19, 2023, caused over 682 million confirmed cases and over 6.8 million deaths globally (Worldometer., 2023; Dong *et al.*, 2020). The United States suffers the highest burden of the pandemic globally (with over 105 million confirmed cases and over 1.1 million deaths, as of March 19, 2023) (Worldometer., 2023) (the index case for COVID-19 was reported in the United States on January 21, 2020 (Haynes *et al.*, 2020; Safdar and Gumel, 2023)). For most parts of the year 2020, the control and mitigation efforts against SARS-CoV-2 in the United States were restricted to the use of non-pharmaceutical interventions, such as social-distancing, quarantine of suspected cases, isolation of those with symptoms of SARS-CoV-2, the use of face coverings (i.e., face masks), community lockdowns, contact-tracing, etc. (Ngonghala *et al.*, 2020a,b, 2021a; Eikenberry *et al.*, 2020; Ngonghala *et al.*, 2021b; Safdar and Gumel, 2023), until the Food and Drug Administration (FDA) provided Emergency Use Authorization (EUA) to two safe and highly-efficacious vaccines (developed by Pfizer Inc. and Moderna Inc., respectively) in December of 2020 (Pfizer, 2020; Food *et al.*, 2020; Safdar and Gumel, 2023). Each of these two FDA-EUA vaccines was primarily administered in a two-dose regimen, within three to four weeks apart, and each offered an estimated protective efficacy against symptomatic COVID-19 infec-

tion of about 95% (Mahase, 2020; Self *et al.*, 2021; Safdar and Gumel, 2023). Another vaccine, developed by Johnson & Johnson (administered as a single dose), received FDA-EUA in late February 2021 (U.S. Food and Drug Administration and others, 2021b) (this vaccine has an estimated 75% efficacy in preventing severe/critical illness caused by COVID-19 (Sargent *et al.*, 2021)). The rapid development and deployment of effective anti-COVID vaccines has played a vital role in minimizing and mitigating the burden of the pandemic, in jurisdictions with high coverage of these vaccines, around the world (Polack *et al.*, 2020; Bar-On *et al.*, 2021; Safdar and Gumel, 2023).

This chapter focuses on using mathematical modeling approaches, coupled with data rigorous qualitative and data analytics together with computation, to assess the population-level impacts of the aforementioned three FDA-EUA vaccines on curtailing and mitigating the burden of the SARS-CoV-2 pandemic in the United States. Numerous clinical studies have shown that the efficacy of all the FDA-approved SARS-CoV-2 vaccines wane over time (with estimated waning time of about 9 months) (Gumel *et al.*, 2021b; Dan *et al.*, 2021; Safdar *et al.*, 2023; Ngonghala *et al.*, 2023; Curley, 2021; Safdar and Gumel, 2023). Consequently, this chapter will specifically assess the population-level impact of the vaccination program (based on the three FDA-EUA vaccines), keeping in mind the waning efficacies of the approved vaccines, on the dynamics of the current predominant SARS-CoV-2 variant (Omicron) in the United States. The population-level impact of the use of face masks, as a singular intervention and its combination with vaccination, will also be assessed (Safdar and Gumel, 2023).

Numerous mathematical models, of various types (such as compartmental (Ngonghala *et al.*, 2020a; Eikenberry *et al.*, 2020; Iboi *et al.*, 2020b; Ngonghala *et al.*, 2020b;

Gumel *et al.*, 2021a; Ngonghala *et al.*, 2021a; Schneider *et al.*, 2020), agents-based (Ferguson *et al.*, 2020; Wilder *et al.*, 2020; Cuevas, 2020), network (Xue *et al.*, 2020; Thurner *et al.*, 2020; Firth *et al.*, 2020) and statistical models (Srivastava and Chowell, 2020; Tariq *et al.*, 2020; IHME COVID-19 health service utilization forecasting team, 2020)) have been formulated and used to gain insight and understanding into the transmission dynamics and control of the COVID-19 pandemic (with majority of these models being of the form of compartmental deterministic systems of nonlinear differential equations (Ngonghala *et al.*, 2020a; Eikenberry *et al.*, 2020; Iboi *et al.*, 2020b; Ngonghala *et al.*, 2020b; Gumel *et al.*, 2021a; Ngonghala *et al.*, 2023)). In this chapter, a deterministic model will also be developed and used to study the dynamics of the COVID-19 pandemic. The model (which is relatively basic) will be rigorously analysed to, among others, derive the threshold vaccination coverage needed to achieve herd immunity in the United States (the determination of this threshold provides the sufficient condition, in parameter space, for effectively curtailing and eliminating the pandemic in a population) (Safdar and Gumel, 2023). Since the United States has been experiencing the brunt of the burden of the COVID-19 pandemic globally (i.e., the United States has so far recorded the highest number of confirmed cases and mortality) (Worldometer., 2023; Dong *et al.*, 2020), the emphasis of this chapter is on studying the dynamics of the COVID-19 pandemic (i.e., the current predominant Omicron variant) in the United States. Consequently, the model to be developed in this chapter will be parameterized using the daily new case data for the COVID-19 pandemic during the onset of the Omicron variant in the United States (Safdar and Gumel, 2023). The model will also be used to asses the population-level impact of the use of face masks (of various types and efficacy) on the disease dynamics. The chapter is organized as follows. The model for COVID-19 pandemic, in the presence of an imperfect vaccine, is formulated in Section 2.2. In addition to fitting

the model using the daily new case data, the basic qualitative properties of the model are also presented in this section. The model is rigorously analyzed, with respect to the existence and asymptotic stability properties of its equilibria (disease-free and endemic), in Section 2.3. Rigorous analysis for, and numerical illustration of, the existence of the dynamic phenomenon of backward bifurcation in the model are also provided. Conditions for achieving community-wide vaccine-derived *herd immunity* are derived and global parameter sensitivity analyses are also carried out in this section. Numerical simulations are reported in Section 2.4. The results of this chapter are discussed and summarized in Section 2.5 (Safdar and Gumel, 2023).

2.2 Formulation of Vaccination Model for COVID-19

To develop the vaccination model for the transmission dynamics of COVID-19 in a population, the total population at time t, denoted by $N(t)$, is sub-divided into the mutually-exclusive compartments of susceptible individuals ($S(t)$), fully-vaccinated individuals ($V((t))$, exposed or latent individuals (i.e., newly-infected individuals who are not yet infectious; $E(t)$), pre-symptomatic infectious individuals ($I_p(t)$), symptomatically-infectious individuals ($I_s(t)$), asymptomatically-infectious individuals ($I_a(t)$), hospitalized individuals ($I_h(t)$), recovered individuals with natural immunity ($R_n(t)$) and recovered individuals with natural plus vaccine-derived immunity ($R_{nv}(t)$), so that (Safdar and Gumel, 2023):

$$N(t) = S(t) + V(t) + E(t) + I_p(t) + I_s(t) + I_a(t) + I_h(t) + R_n(t) + R_{nv}(t).$$

The model for COVID-19 dynamics in a population, that incorporates the use of any of the aforementioned imperfect vaccines, is given by the following deterministic system of nonlinear differential equations (where, a dot represents differentiation with respect to time t) (Safdar *et al.*, 2023). The flow diagram of the vaccination model is

depicted in Figure 2.1, and the description of the state variables and parameters of the vaccination model are tabulated in Tables 2.1 and 2.2, respectively (Safdar and Gumel, 2023):

$$\begin{cases} \dot{S} &= \Pi + \omega_v V - (\lambda + \xi_v + \mu)S, \\ \dot{V} &= \xi_v S - [(1-\varepsilon_v)\lambda + \omega_v + \mu]V, \\ \dot{E} &= \lambda[S + (1-\varepsilon_v)V + (1-\varepsilon_n)R_n + (1-\varepsilon_{nv})R_{nv}] - (\sigma_E + \mu)E, \\ \dot{I}_p &= \sigma_E E - (\sigma_p + \delta_p + \mu)I_p, \\ \dot{I}_s &= r\sigma_p I_p - (\phi_s + \gamma_s + \delta_s + \mu)I_s, \\ \dot{I}_a &= (1-r)\sigma_p I_p - (\gamma_a + \delta_a + \mu)I_a, \\ \dot{I}_h &= \phi_s I_s - (\gamma_h + \delta_h + \mu)I_h, \\ \dot{R}_n &= \gamma_s I_s + \gamma_a I_a + \gamma_h I_h - [(1-\varepsilon_n)\lambda + \xi_v + \mu]R_n, \\ \dot{R}_{nv} &= \xi_v R_n - [(1-\varepsilon_{nv})\lambda + \mu]R_{nv}, \end{cases} \tag{2.1}$$

where, the infection rate (or *force of infection*), λ, is given by (Safdar and Gumel, 2023):

$$\lambda = \frac{(\beta_p I_p + \beta_s I_s + \beta_a I_a + \beta_h I_h)}{N}, \tag{2.2}$$

with β_p, β_s, β_a and β_h representing, respectively, the effective contact rates for pre-symptomatic (I_p), symptomatic (I_s), asymptomatic (I_a) and hospitalized (I_h) infectious individuals. In the vaccination model (2.1), Π is the rate of recruitment of individuals into the population, ω_v is the vaccine waning rate for fully-vaccinated individuals (i.e., the rate at which individuals in the V class revert to the wholly-susceptible class, S), λ is the infection rate (defined in Equation (2.2)), ξ_v is the *per capita* vaccination rate and μ is the natural death rate. The parameter $0 < \varepsilon_v < 1$

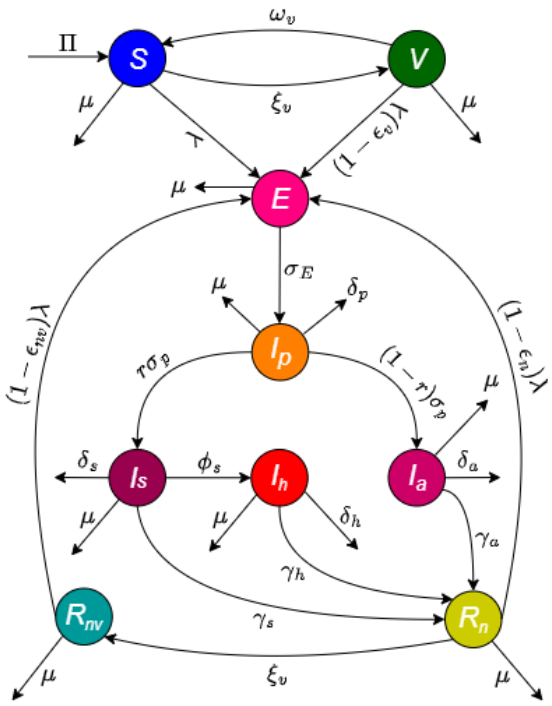

Figure 2.1: Flow diagram of the vaccination model (2.1) (Safdar and Gumel, 2023).

is the average protective efficacy of the vaccine for fully-vaccinated susceptible individuals (i.e., vaccine efficacy for individuals in the V class), while $0 \leq \varepsilon_n < 1$ is the efficacy of natural immunity to prevent recovered individuals (in the R_n class) from acquiring future SARS-CoV-2 infection and $0 < \varepsilon_{nv} \leq 1$ is the efficacy of natural and vaccine-derived immunity to prevent future SARS-CoV-2 infection of recovered individuals (in the R_{nv}, class) (Safdar and Gumel, 2023). Exposed individuals progress to the pre-symptomatic stage at the rate σ_E, and pre-symptomatic individuals progress to either become symptomatically-infectious, at a rate $r\sigma_p$ (where, $0 \leq r \leq 1$ is the proportion of these individuals that show clinical symptoms), or become asymptomatically-infectious, at the rate $(1-r)\sigma_p$. Symptomatic individuals are hospitalized at a rate ϕ_s, and infectious individuals in stage I_k recover at a rate γ_k (with $k = \{s, a, h\}$). Finally, disease-induced mortality occur in the I_j class at a

rate δ_j ($j = \{p, s, a, h\}$) (Safdar *et al.*, 2023; Safdar and Gumel, 2023).

Some of the main assumptions made in formulating the vaccination model (2.1) are (Safdar and Gumel, 2023):

(a) A homogeneously-mixed population: it is assumed that the population is well-mixed, so that every member of the community is equally likely to mix with (and acquire infection from or transmit infection to) every other member of the community.

(b) Vaccinated susceptible individuals (in the V class) are assumed to have received the full required doses (i.e., two doses for the Pfizer or the Moderna vaccine, one dose for the Johnson & Johnson vaccine), and that enough time has elapsed for the body to develop the full vaccine-derived immunity.

(c) The three SARS-CoV-2 vaccines that received FDA Emergency Use Authorization (i.e., the Pfizer, Moderna and Johnson & Johnson vaccines) are imperfect (Food and Drug Administration and others, 2020; U.S. Food and Drug Administration and others, 2009, 2021b) (i.e., the vaccines offer partial protective immunity with efficacy $0 < \varepsilon_v < 1$), which wanes over time (at a rate ω_v) (Curley, 2021; Gumel *et al.*, 2021b)). In other words, vaccinated individuals can experience breakthrough infection (Oliver *et al.*, 2020; U.S. Food and Drug Administration and others, 2021a).

(d) It is assumed that vaccine-derived immunity may wane over time in vaccinated individuals (V), resulting, ultimately, in reverting to the wholly-susceptible class (S) (Gumel *et al.*, 2021b).

(e) It is assumed, for mathematical tractability, that recovered individuals in the R_n and R_{nv} classes do not lose their natural (infection-acquired) immunity. This

assumption is relaxed in the model to be developed in Chapter 3.

(f) Vaccination is only offered to wholly-susceptible individuals or those who recovered naturally but their natural immunity has waned completely or recovered individuals who had acquired both natural and vaccine-derived immunity but their immunity has completely waned over time (i.e., the vaccines are not administered to individuals who are currently infected with SARS-CoV-2).

(g) It is assumed that presymptomatically-infectious individuals do not recover while at this class (owing to the short average duration in this compartment). They recover only after transitioning to the symptomatic infectious class (at the rate $r\sigma_p$) or to the asymptomatically-infectious class (at the rate $(1-r)\sigma_p$). It is also assumed that individuals in the presymptomatic and asymptomatic infectious classes do not die from SARS-CoV-2 infection (so that δ_p and δ_a are set to zero in the numerical simulations) (Mayo Clinic, 2022; Tan *et al.*, 2021; Vermund and Pitzer, 2021).

The vaccination model (2.1) extends numerous other (relatively basic) models for COVID-19 dynamics that incorporate the use of a vaccine, such as those in Gumel *et al.* (2021a); Iboi *et al.* (2020b), by *inter alia* (Safdar and Gumel, 2023):

(a) Adding an epidemiological class for pre-symptomatic infectious individuals (the vaccination model in Gumel *et al.* (2021a) does not explicitly account for disease transmission by pre-symptomatic infectious individuals).

(b) Incorporating two classes for recovered individuals based on immunity status (i.e., recovered individuals with either natural or vaccine-derived immunity). Only one recovered compartment is considered in Gumel *et al.* (2021a); Iboi

State variables	Description
S	Population of unvaccinated (wholly)-susceptible individuals
V	Population of fully-vaccinated susceptible individuals
E	Population of exposed (newly-infected) individuals
I_p	Population of pre-symptomatic infectious individuals
I_s	Population of infectious individuals with clinical symptoms of the disease
I_a	Population of asymptomatically-infectious individuals
I_h	Population of hospitalized individuals
R_n	Population of recovered individuals with natural immunity (i.e., unvaccinated)
R_{nv}	Population of recovered individuals with both natural and vaccine-derived immunity

Table 2.1: Description of the State Variables of the Vaccination Model (2.1) (Safdar *et al.*, 2023; Safdar and Gumel, 2023).

et al. (2020b).

(c) Allowing for the re-infection of recovered individuals. This is not considered in Gumel *et al.* (2021a); Iboi *et al.* (2020b). Furthermore, this study will contribute to the literature on the rigorous analyses of relatively basic vaccination models for COVID-19 by giving rigorous results for the existence and asymptotic stability of an endemic equilibrium of the (special case of) vaccination model (2.1).

Parameter	Description
Π	Recruitment rate
$\beta_p(\beta_s)(\beta_a)(\beta_h)$	Effective contact rate for individuals in the $I_p(I_s)(I_a)(I_h)$ compartment
ξ_v	*Per capita* vaccination rate
μ	Natural death rate
r	Proportion of pre-symptomatic individuals who show clinical symptoms of the disease
ω_v	Waning rate of fully-vaccinated individuals
ε_v	Vaccine efficacy for fully-vaccinated individuals
ε_n	Efficacy of natural immunity to prevent re-infection of recovered individuals in the R_n class
ε_{nv}	Efficacy of natural and vaccine derived immunity to prevent re-infection of recovered individuals in the R_{nv} class
σ_E	Progression rate from exposed class to pre-symptomatic class
σ_p	Progression rate from pre-symptomatic class to either symptomatic or asymptomatic class
$\gamma_k(k = \{s, a, h\})$	Recovery rate for individuals in the I_s, I_a and I_h class, respectively
ϕ_s	Hospitalization rate of individuals with clinical symptoms of the disease
$\delta_j(j = \{p, s, a, h\})$	Disease-induced mortality rate for individuals in the I_p, I_s, I_a and I_h class, respectively

Table 2.2: Description of the Parameters of the Vaccination Model (2.1) (Safdar *et al.*, 2023; Safdar and Gumel, 2023).

2.2.1 Data fitting and parameter estimation

The vaccination model (2.1) contains 22 parameters. Although the values of some of these parameters are known from the literature (as tabulated in Table 2.3), and the values of some other parameters are unknown. Specifically, the values of the effective contact rate parameters (β_p, β_a, β_a and β_h) are unknown. We fit the model with available data for COVID-19 for the United States, and use the fitted model to estimate the best values for the four unknown parameters. For fitting purposes, we use the daily new case data for the United States, obtained from the Johns Hopkins University COVID-19 repository (Dong *et al.*, 2020), for the period between November 28, 2021 (when the Omicron variant first emerged in the United States) to March 23, 2022 (Safdar and Gumel, 2023). The data fitting is done by splitting the data into two segments. The first segment of the data, from November 28, 2021 to February 23, 2022 (i.e., the region to the left of the dashed vertical cyan line in Figure 2.2), was used to fit the model (2.1) and to estimate the unknown parameters (Safdar *et al.*, 2023; Ngonghala *et al.*, 2023). The second segment (from February 24, 2022 to March 23, 2022) was used to cross validate the model (Safdar *et al.*, 2023; Ngonghala *et al.*, 2023). The model fitting was done using a standard nonlinear least squares approach, which involves using the inbuilt MATLAB's minimization function (i.e., *lsqcurvefit*) to minimize the sum of the squared differences between each observed daily new cases data points and the corresponding daily new cases points obtained from the vaccination model (2.1) (i.e., $r\sigma_p I_p$) (Safdar and Gumel, 2023).

Bootstrapping technique was used for the parameter estimation with 95% confidence intervals (Chowell, 2017; Ngonghala *et al.*, 2020a; Banks *et al.*, 2009; Safdar and Gumel, 2023). The process of bootstrapping involves producing a large collection of simulated data sets from a given data set by sampling from this given data set with

replacement and then using each generated data set for the parameter estimation (Ngonghala *et al.*, 2023, 2021b; Safdar and Gumel, 2023). The inbuilt bootstrapping function in MATLAB R2019b (i.e., *bootstrp*) was used to generate 10,000 bootstrap replicates to sample the residuals from the initial parameter estimation. Furthermore, the bootstrap data sets are generated by adding the re-sampled residuals to the best fit curve (Ngonghala *et al.*, 2023; Safdar and Gumel, 2023). Finally, the vaccination model (2.1) was then fitted to each bootstrap data set to create the bootstrap distribution of the estimated parameters. The inbuilt MATLAB R2019b function (i.e., *prctile*) is used for the bootstrap distribution to estimate the 95% credible intervals of the estimated parameters. Furthermore, it is significant to mention that fitting the model (2.1) to the daily new confirmed case data is much accurate data fitting approach which avoid mistakes that arise when cumulative case data is used for fitting the deterministic models (King *et al.*, 2015; Ngonghala *et al.*, 2023; Safdar and Gumel, 2023). The values of the unknown parameters, which are estimated from the model fitting, are presented in Table 2.4.

The results obtained from fitting the vaccination model (2.1) with the observed daily new case data, depicted in Figure 2.2, show a very good fit for the model output (blue curve) and the observed daily new case data (red dots) (Safdar *et al.*, 2023). This figure also shows a very good fit for the cross validation component of the fitting (green curve) of Figure 2.2. This segment of Figure 2.2 shows that the vaccination model (2.1) cross validates the observed daily new case data for the period from February 23, 2022 to March 23, 2022 perfectly (solid green curve) (Safdar *et al.*, 2023; Safdar and Gumel, 2023). The cross-validated model was used to make prediction for the trajectory of the pandemic for a five-week period after the cross validation period (March 24, 2022; as highlighted by the region to the right of the dashed vertical black line), as illustrated by the solid magenta curve in Figure 2.2 (Safdar *et al.*, 2023;

Safdar and Gumel, 2023).

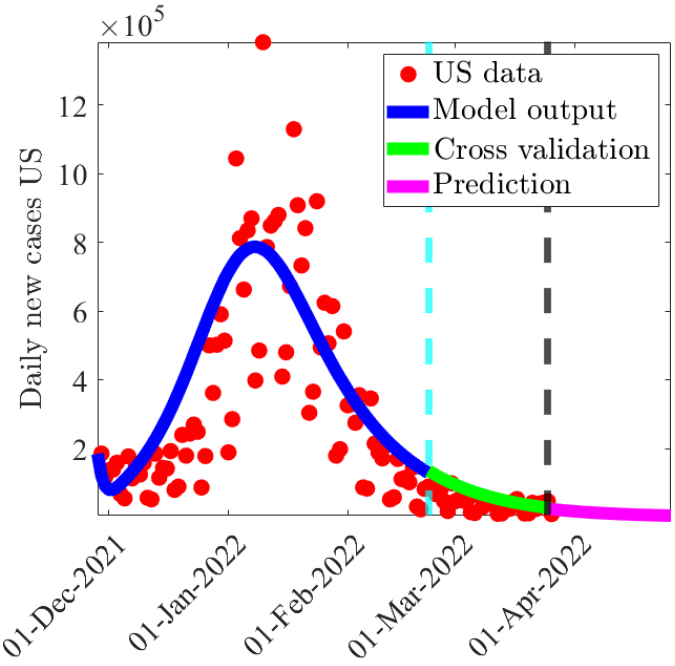

Figure 2.2: Time Series Illustration of the Least Squares Fit of the Vaccination Model (2.1), Showing the Model's Output for the Daily New Cases in the United States (Blue Curve) Compared to the Observed Confirmed Daily New Cases for the United States (Red Dots) from November 28, 2021 to February 23, 2022 (Segment to the Left of The Dashed Vertical Cyan Line), Using the Fixed and Estimated (Fitted) Baseline Parameter Values given in Tables 2.3 and 2.4, Respectively. The Segment from February 24, 2022 To April 30, 2022 (i.e., Solid Green and Magenta Curves or the Entire Segment to The Right of the Dashed Cyan Vertical Line) Illustrates the Performance of the Vaccination Model (2.1) in Predicting the Daily New COVID-19 Cases in the United States (Safdar *et al.*, 2023; Safdar and Gumel, 2023).

2.2.2 Basic qualitative properties

Before carrying out the asymptotic analysis and numerical simulations of the vaccination model (2.1), it is instructive to explore its basic qualitative features with respect to its well-posedness (i.e., with respect to the non-negativity, boundedness and invariance of its solutions). First of all, since the vaccination model (2.1) monitors the temporal dynamics of human populations, all its parameters are non-negative.

Parameter	Baseline Value	Source
σ_E	1/5 day^{-1}	Ngonghala *et al.* (2023)
σ_p	1/2 day^{-1}	Linton *et al.* (2020)
r	0.095 (dimensionless)	Weintraub (2022)
$(1-r)$	0.905 (dimensionless)	Weintraub (2022)
γ_s	1/10 day^{-1}	Gumel *et al.* (2021b); Mancuso *et al.* (2021)
γ_a	1/5 day^{-1}	Kissler *et al.* (2020)
γ_h	1/8 day^{-1}	Kissler *et al.* (2020)
ω_v	1/274 day^{-1}	Curley (2021)
ϕ_s	1/5 day^{-1}	Linton *et al.* (2020)
ξ_v	1.9×10^{-5} day^{-1}	Ngonghala *et al.* (2023)
Π	11,400 day^{-1}	Ngonghala *et al.* (2021b)
μ	3.4×10^{-5} day^{-1}	Ngonghala *et al.* (2021b)
δ_s	4.9804×10^{-5} day^{-1}	Safdar *et al.* (2023)
δ_h	5.0×10^{-5} day^{-1}	Ngonghala *et al.* (2021b)
δ_p	0 day^{-1}	Tan *et al.* (2021); Mayo Clinic (2022)
δ_a	0 day^{-1}	Vermund and Pitzer (2021); Mayo Clinic (2022)
ε_v	0.85 (dimensionless)	Safdar *et al.* (2023)
ε_n	0.85 (dimensionless)	Safdar *et al.* (2023)
ε_{nv}	0.95 (dimensionless)	Safdar *et al.* (2023)

Table 2.3: Baseline Values of the Fixed Parameters of the Vaccination Model (2.1) (Safdar *et al.*, 2023; Safdar and Gumel, 2023).

Parameter	Estimated Value	95% Confidence Interval
β_p	0.2309 day^{-1}	$[0.2177 - 0.2474]$ day^{-1}
β_s	9.9986×10^{-4} day^{-1}	$[1.0 \times 10^{-4} - 9.9 \times 10^{-4}]$ day^{-1}
β_a	0.5429 day^{-1}	$[0.5342 - 0.5523]$ day^{-1}
β_h	4.9989×10^{-5} day^{-1}	$[1.0 \times 10^{-6} - 4.9 \times 10^{-5}]$ day^{-1}

Table 2.4: Baseline Values of the Four Fitted (Estimated) Parameters (and Their Confidence Intervals (CIs)) of the Vaccination Model (2.1), Obtained by Fitting the Model with the Observed Daily New Case COVID-19 Data for the United States for the Period November 28, 2021 to February 23, 2022 (Safdar *et al.*, 2023; Safdar and Gumel, 2023).

It is convenient to define the following biologically-feasible region for the vaccination model (2.1) (Safdar and Gumel, 2023):

$$\Omega = \left\{ (S, V, E, I_p, I_s, I_a, I_h, R_n, R_{nv}) \in \mathbb{R}^9_+ : N(t) \leq \frac{\Pi}{\mu} \right\},$$

where, $N(t)$ is the total population. It should be stated that since the vaccination model (2.1) monitors human populations, all its initial conditions are non-negative (i.e., $S(0) > 0, V(0) \geq 0, E(0) \geq 0, I_p(0) \geq 0, I_s(0) \geq 0, I_a(0) \geq 0, I_h(0) \geq 0,$ $R_n(0) \geq 0, R_{nv}(0) \geq 0$). Furthermore, for the model to be mathematically- and biologically-meaningful, it is necessary that all solutions of the model remain non-negative for all non-negative initial conditions. That is, initial solutions of the model that start in the region Ω remain in Ω for all time $t > 0$ (i.e., Ω is positively-invariant with respect to the vaccination model (2.1)). This result is rigorously established below (Safdar and Gumel, 2023).

Theorem 2.2.1. *Let the initial data for the vaccination model* (2.1) *be* $S(0) > 0, V(0) \geq 0, E(0) \geq 0, I_p(0) \geq 0, I_s(0) \geq 0, I_a(0) \geq 0, I_h(0) \geq 0, R_n(0) \geq 0, R_{nv}(0) \geq 0$. *Then the solutions of the vaccination model* (2.1) *with positive initial data, will remain positive for all time* $t > 0$.

Proof. Let $t_1 = sup\{t > 0 : S(t) > 0, V(t) > 0, E(t) > 0, I_p(t) > 0, I_s(t) > 0, I_a(t) > 0, I_h(t) > 0, R_n(t) > 0, R_{nv}(t) > 0 \in [0, t]\}$. Thus, $t_1 > 0$. It follows from the first equation of the vaccination model (2.1) that

$$\frac{dS}{dt} = \Pi + \omega_v V(t) - (\lambda + \xi_v + \mu)S(t) \geq \Pi - (\lambda + \xi_v + \mu)S(t),$$

which can be re-written as:

$$\frac{d}{dt}\left[S(t)exp\Big\{\int_0^t \lambda(u)du + (\xi_v + \mu)t\Big\}\right] \geq \Pi\, exp\Big\{\int_0^t \lambda(u)du + (\xi_v + \mu)t\Big\}.$$

Hence,

$$S(t_1)exp\Big\{\int_0^{t_1} \lambda(u)du + (\xi_v + \mu)t_1\Big\} - S(0) \geq \Pi \int_0^{t_1} exp\Big\{\int_0^x \lambda(\nu)d\nu + (\psi_L + \mu)x\Big\}dx,$$

so that

$$S(t_1) \geq exp\Big\{-\int_0^{t_1} \lambda(u)du - (\xi_v + \mu)t_1\Big\}\left[S(0) + \Pi\, exp\Big\{\int_0^x \lambda(\nu)d\nu + (\xi_v + \mu)x\Big\}dx\right] > 0,$$

Similarly, it can be shown that all the remaining state variables of the vaccination model (2.1) are non-negative (for all non-negative initial conditions) for $t \geq 0$. Consequently, all the solutions of the vaccination model (2.1), with non-negative initial conditions, remain non-negative for all time $t > 0$. □

Theorem 2.2.2. *Consider the vaccination model* (2.1) *with non-negative initial conditions. The region* Ω *is positively-invariant and attracts all solutions of the model* (2.1)*.*

Proof. Adding all the equations of the model (2.1) gives (Safdar *et al.*, 2023; Safdar and Gumel, 2023):

$$\dot{N} = \Pi - \mu N - \delta_p I_p - \delta_s I_s - \delta_a I_a - \delta_h I_h. \tag{2.3}$$

Since all the parameters of the (2.1) are non-negative, it follows from (2.3) that:

$$\dot{N} \leq \Pi - \mu N. \tag{2.4}$$

Hence, if $N(t) > \dfrac{\Pi}{\mu}$, then $\dot{N} < 0$. Furthermore, by applying a standard comparison theorem (Lakshmikantham and Vatsala, 1999; Gumel *et al.*, 2021b; Safdar *et al.*, 2023) on (2.4), the following inequality holds:

$$N(t) \leq N(0)e^{-\mu t} + \frac{\Pi}{\mu}\left(1 - e^{-\mu t}\right).$$

Hence, if $N(0) \leq \dfrac{\Pi}{\mu}$, then $N(t) \leq \dfrac{\Pi}{\mu}$. If $N(0) > \dfrac{\Pi}{\mu}$ (which means that $N(0)$ is outside Ω) then $N(t) > \dfrac{\Pi}{\mu}$, for all $t > 0$ but with $\lim_{t\to\infty} N(t)$ (and this type of solution trajectory strives to enter the region Ω) (Gumel *et al.*, 2021b). Therefore, every solution of the vaccination model (2.1) with initial conditions in Ω remains in Ω for all time t. In other words, the region Ω is positively-invariant and attracts all initial solutions of the vaccination model (2.1) (Safdar *et al.*, 2023; Safdar and Gumel, 2023). □

The epidemiological consequence of Theorem 2.2.2 is that it is sufficient to consider the dynamics of the flow generated by the vaccination model (2.1) in the invariant and bounded region Ω (since the model (2.1) is well-posed epidemiologically and mathematically in the feasible region Ω (Hethcote, 2000)). The existence and asymptotic stability properties of the equilibria of the model (2.1) will now be explored (Safdar and Gumel, 2023).

2.3 Existence and Asymptotic Stability of Equilibria

In this section, the vaccination model (2.1) will be rigorously analyzed to explore the conditions for the existence and asymptotic stability of its equilibria.

2.3.1 Disease-Free Equilibrium

The vaccination model (2.1) has a unique disease-free equilibrium (DFE) given by (Safdar and Gumel, 2023):

$$\begin{aligned}\mathcal{E}_0 &= \left(S^*, V^*, E^*, I_p^*, I_s^*, I_a^*, I_h^*, R_n^*, R_{nv}^*\right) \\ &= \left(\frac{\Pi\left(\mu+\omega_v\right)}{\mu\left(\mu+\xi_v+\omega_v\right)}, \frac{\Pi\xi_v}{\mu\left(\mu+\xi_v+\omega_v\right)}, 0, 0, 0, 0, 0, 0, 0\right).\end{aligned}$$

Local asymptotic stability of DFE

The asymptotic stability property of the DFE ($\mathcal{E}_0$) will be explored using the *next generation operator method* (van den Driessche and Watmough, 2002; Diekmann *et al.*, 1990). Specifically, using the notation in (van den Driessche and Watmough, 2002), it follows that the associated non-negative matrix of new infection terms (F) and the M-matrix of the linear transition terms (V) are given, respectively, by (Safdar *et al.*, 2023; Safdar and Gumel, 2023):

$$F = \begin{bmatrix} 0 & f_{11} & f_{12} & f_{13} & f_{14} \\ 0 & 0 & 0 & 0 & 0 \\ 0 & 0 & 0 & 0 & 0 \\ 0 & 0 & 0 & 0 & 0 \\ 0 & 0 & 0 & 0 & 0 \end{bmatrix} \quad \text{and} \quad V = \begin{bmatrix} K_1 & 0 & 0 & 0 & 0 \\ -\sigma_E & K_2 & 0 & 0 & 0 \\ 0 & -r\sigma_p & K_3 & 0 & 0 \\ 0 & -(1-r)\sigma_p & 0 & K_4 & 0 \\ 0 & 0 & -\phi_s & 0 & K_5 \end{bmatrix}, \tag{2.5}$$

where,

$f_{11} = \beta_p \left[\frac{S^* + (1-\varepsilon_v)V^*}{N^*}\right]$, $f_{12} = \beta_s \left[\frac{S^* + (1-\varepsilon_v)V^*}{N^*}\right]$, $f_{13} = \beta_a \left[\frac{S^* + (1-\varepsilon_v)V^*}{N^*}\right]$,

$f_{14} = \beta_h \left[\frac{S^* + (1-\varepsilon_v)V^*}{N^*}\right]$, $K_1 = \sigma_E + \mu$, $K_2 = \sigma_p + \mu + \delta_p$, $K_3 = \phi_s + \gamma_s + \mu + \delta_s$,

$K_4 = \gamma_a + \mu + \delta_a$, and $K_5 = \gamma_h + \mu + \delta_h$.

Let f_v represent the proportion of wholly-susceptible individuals that are fully-vaccinated at disease-free equilibrium. In other words,

$$f_v = \frac{V^*}{N^*} = \frac{\xi_v}{\mu + \xi_v + \omega_v}. \tag{2.6}$$

It follows, based on the computation of the next generation matrices above (van den Driessche and Watmough, 2002; Diekmann *et al.*, 1990), that the *vaccination reproduction number* (or the *control reproduction number*) of the vaccination model (2.1), denoted by $\mathbb{R}_{cv}$, is given by (where, ρ is the spectral radius) (Safdar and Gumel, 2023):

$$\mathbb{R}_{cv} = \rho(FV^{-1}) = \mathbb{R}_0 \left(1 - \varepsilon_v \frac{V^*}{N^*}\right) = \mathbb{R}_0 \left(1 - \varepsilon_v f_v\right), \tag{2.7}$$

where, f_v is as defined in Equation (2.6) and

$$\mathbb{R}_0 = \mathbb{R}_{cv}|_{\varepsilon_v = V = 0}, \tag{2.8}$$

is the *basic reproduction number* of the vaccination model (2.1). It can be shown (by applying the next generation operator method on the model (2.1) in the absence of vaccination) that (Safdar and Gumel, 2023):

$$\mathbb{R}_0 = \mathbb{R}_{0p} + \mathbb{R}_{0s} + \mathbb{R}_{0a} + \mathbb{R}_{0h}, \tag{2.9}$$

where,

$$\mathbb{R}_{0p} = \beta_p \left(\frac{S^*}{N^*}\right) \left(\frac{\sigma_E}{\sigma_E + \mu}\right) \left(\frac{1}{\sigma_p + \delta_p + \mu}\right),$$

$$\mathbb{R}_{0s} = \beta_s \left(\frac{S^*}{N^*}\right) \left(\frac{\sigma_E}{\sigma_E + \mu}\right) \left(\frac{r\sigma_p}{\sigma_p + \delta_p + \mu}\right) \left(\frac{1}{\phi_s + \gamma_s + \delta_s + \mu}\right),$$

$$\mathbb{R}_{0a} = \beta_a \left(\frac{S^*}{N^*}\right) \left(\frac{\sigma_E}{\sigma_E + \mu}\right) \left(\frac{(1-r)\sigma_p}{\sigma_p + \delta_p + \mu}\right) \left(\frac{1}{\gamma_a + \delta_a + \mu}\right),$$

and,

$$\mathbb{R}_{0h} = \beta_h \left(\frac{S^*}{N^*}\right) \left(\frac{\sigma_E}{\sigma_E + \mu}\right) \left(\frac{r\sigma_p}{\sigma_p + \delta_p + \mu}\right) \left(\frac{\phi_s}{\phi_s + \gamma_s + \delta_s + \mu}\right) \left(\frac{1}{\gamma_h + \delta_h + \mu}\right),$$

are the constituent reproduction numbers for the transmission of the disease by infectious individuals in the pre-symptomatic, symptomatic, asymptomatic and hospitalized classes, respectively. It is worth stating that, while the basic reproduction number ($\mathbb{R}_0$) measures the average number of new SARS-CoV-2 cases generated by a typical infectious individual if introduced in a completely-susceptible population, the control reproduction number ($\mathbb{R}_{cv}$) measures the average number of new SARS-CoV-2 cases generated by a typical infectious individual introduced into a population where a certain proportion of the wholly-susceptible population is fully-vaccinated (with any of the three aforementioned FDA-approved vaccines) (Safdar and Gumel, 2023).

The asymptotic stability result below follows from Theorem 2 of (van den Driessche and Watmough, 2002):

Theorem 2.3.1. *The disease-free equilibrium* ($\mathcal{E}_0$) *of the vaccination model* (2.1) *is locally-asymptotically stable (LAS) if* $\mathbb{R}_{cv} < 1$*, and unstable if* $\mathbb{R}_{cv} > 1$.

The epidemiological implication of Theorem 2.3.1 is that a small influx of SARS-CoV-2 cases will not generate a large outbreak in the community if the control reproduction number ($\mathbb{R}_{cv}$) is brought to, and maintained at, a value less than unity (Safdar *et al.*, 2023; Safdar and Gumel, 2023). In other words, the vaccination program implemented in the United States can lead to the effective control of the SARS-CoV-2 pandemic if it can result in reducing (and maintaining) the control reproduction number to a value less than one, provided the initial number of infectious individuals introduced into the population is small enough (Safdar and Gumel, 2023).

Existence of backward bifurcation

Certain epidemiological mechanisms associated with the spread and control of infectious diseases are known to induce *backward bifurcation*, a dynamic phenomenon characterised by the co-existence of two stable attractors (namely the stable disease-free equilibrium and a stable endemic equilibrium) when the associated reproduction number of the model is less than one (Safdar and Gumel, 2023; Gumel, 2012; Iboi *et al.*, 2018; Iboi and Gumel, 2018; Garba *et al.*, 2008; Garba and Gumel, 2010; Blayneh *et al.*, 2010). The epidemiological implication of the presence of a backward bifurcation in the transmission dynamics of an infectious disease is that bringing (and maintaining) the reproduction number of the model to a value less than one, while necessary, may not be sufficient to lead to the elimination of the disease (Safdar and Gumel, 2023; Gumel, 2012; Iboi *et al.*, 2018; Iboi and Gumel, 2018). One common cause of backward bifurcation in disease transmission models is the use of an imperfect vaccine (Gumel, 2012; Elbasha and Gumel, 2006; Elbasha *et al.*, 2011). Since the vaccination model (2.1) uses an imperfect vaccine, it is instructive to explore the likelihood (or derive the conditions for the occurrence) of a backward bifurcation in its transmission dynamics. This is done below. In particular, we claim the following result (Safdar and Gumel, 2023):

Theorem 2.3.2. *The vaccination model* (2.1) *undergoes a backward bifurcation at* $\mathbb{R}_{cv} = 1$ *whenever the associated bifurcation coefficients (denoted by* a *and* b *and given by Equations* (A.6) *and* (A.7) *in Appendix A), are positive (or, equivalently, when Inequality* (A.10) *holds).*

The proof of Theorem 2.3.2, based on using the center manifold theory (Safdar and Gumel, 2023; Carr, 2012; van den Driessche and Watmough, 2002; Gumel and Song, 2008; Castillo-Chavez and Song, 2004; Dushoff *et al.*, 1998), is given in Appendix A.

Figure 2.3 depicts the associated backward bifurcation diagram for the vaccination model (2.1). It should be mentioned that, for computational convenience (in generating the bifurcation diagrams), we set, without loss of generality, the eigenvectors v_1 and v_3 in Equation (A.2) (given in Appendix A) to one. Similarly, we set the eigenvectors w_1, w_7 and w_9 in Equation (A.3) to unity (Safdar and Gumel, 2023).

The epidemiological implication of Theorem 2.3.2 is that the ability of the intervention and mitigation programs implemented (vaccination and face mask usage in this case) to bring (and maintain) the control reproduction number, $\mathbb{R}_{cv}$, to a value less than one, while necessary, is no longer sufficient for the elimination of the SARS-CoV-2 pandemic in the community. Such control (within the bistability region in Figure 2.3) is now dependent on the size of the initial sub-populations of the model. Specifically, initial conditions of the model (2.1) that lie below the stable manifold of the saddle point (the separatrix which separates the basin of attraction of the stable endemic equilibrium and that of the stable disease-free equilibrium) will converge to the disease-free equilibrium, while those that lie above the separatrix will converge to an endemic equilibrium point (Safdar and Gumel, 2023). It follows from Figure 2.3 that, in order to be outside the backward bifurcation region, the intervention and mitigation measures implemented in the community would need to be ramped up to further reduce the control reproduction number below one (and outside the bistability region). Thus, the presence of a backward bifurcation in the transmission dynamics of a disease makes its effective control more difficult (since it imposes greater requirement in terms of the efficacy and coverage of interventions) (Safdar and Gumel, 2023; Gumel and Song, 2008; Gumel, 2012).

To ensure that the effective control of the disease (or its elimination) is independent of the initial sizes of the sub-populations of the model, it is necessary that the disease-

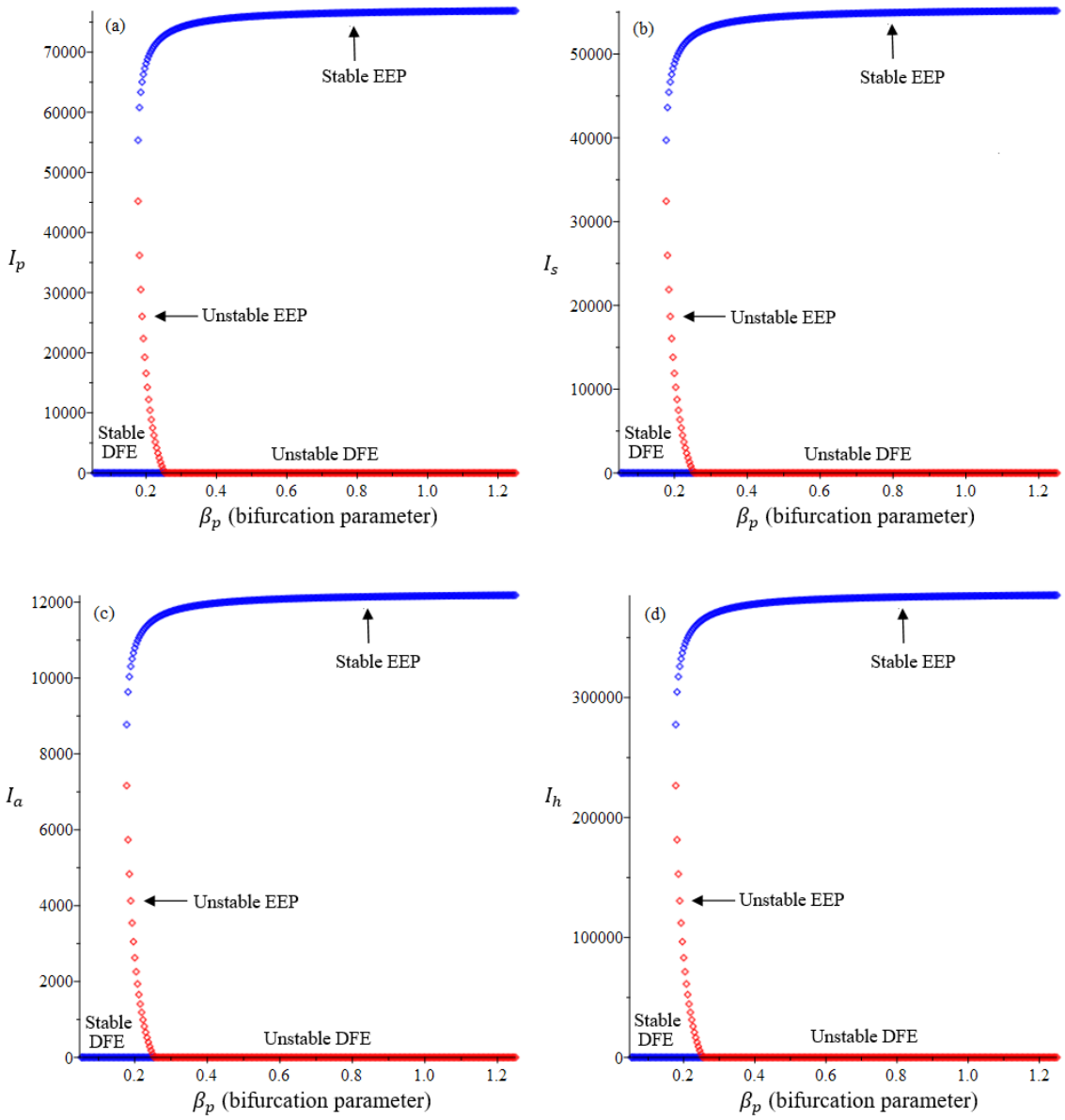

Figure 2.3: Backward Bifurcation Diagram for the Vaccination Model (2.1), Showing the the Profiles of the Population of (a) Pre-symptomatically-infectious Individuals (I_p), (b) Symptomatic Individuals (I_s), (c) Asymptomatically-infectious Individuals (I_a) and (d) Hospitalized Individuals (I_h), as a Function of the Bifurcation Parameter β_p. Parameter Values Used Are: $\Pi = 20,000, \omega_v = 0.00004, \mu = 0.001, \xi_v = 0.002, \varepsilon_v = 0.8, \varepsilon_n = 0.08, \varepsilon_{nv} = 0.08, \sigma_E = 0.2, \sigma_p = 0.98, \phi_s = 0.95, \gamma_s = 0.12, \gamma_a = 0.12, \gamma_h = 0.12, \delta_p = 0.0095, \delta_a = 0.0095, \delta_s = 0.015, \delta_h = 0.015, r = 0.9921, d_1 = 1.5, d_2 = 0.75, d_3 = 1$. With This Arbitrary Set of Parameter Values, the Values of the Associated Backward Bifurcation Coefficients (Denoted by a and b, and given in Appendix A) Are $a = 6.3833 \times 10^{-6} > 0$ and $b = 0.17481 > 0$, Respectively. Furthermore, $\beta_p^* = 0.24010$ and $\mathbb{R}_{cv} = 1$. Apart from the efficacies (i.e., $\varepsilon_v, \varepsilon_n$ and ε_{nv}), Scaling Factors (i.e., d_1, d_2 and d_3) and the Proportion "r" , which are dimensionless, all the other parameters have unit of *per* day (Safdar and Gumel, 2023).

free equilibrium is proved to be globally-asymptotically stable when the reproduction number of the model is less than one. This is explored in Section 2.3.1 below, for two special cases of the vaccination model (2.1) (Safdar and Gumel, 2023).

Global asymptotic stability of DFE: special cases

In this section, the result in Theorem 2.3.1 are extended to prove the global asymptotic stability of the DFE for two special cases of the vaccination model (2.1), as follows (Safdar *et al.*, 2023; Safdar and Gumel, 2023).

Special case 1:

Consider, first of all, the special case of the model (2.1) where the vaccines administered in the population are assumed to offer perfect protective efficacy against the original strain of the pandemic. That is, consider the model (2.1) with $\varepsilon_v = 1$. This assumption is plausible, for instance, in the case of the Pfizer or Moderna vaccine (with each being almost 95% effective against the original SARS-CoV-2 strain) (Pearson, 2021; Mancuso *et al.*, 2021). Furthermore, for mathematical tractability, it is assumed, for this special case, that natural immunity is perfect against re-infection (so that $\varepsilon_n = \varepsilon_{nv} = 1$). For this special case of the vaccination model (2.1), it can be seen that the associated next generation matrix of new infection terms, denoted by $\tilde{F}$, is given by (note that, for this special case, the next generation matrix of linear transition terms, V, remains the same, as defined by Equation (2.5). Furthermore, $N^* = \Pi/\mu$) (Safdar and Gumel, 2023):

$$\tilde{F} = \begin{bmatrix} 0 & \beta_p\left(\frac{S^*}{N^*}\right) & \beta_s\left(\frac{S^*}{N^*}\right) & \beta_a\left(\frac{S^*}{N^*}\right) & \beta_h\left(\frac{S^*}{N^*}\right) \\ 0 & 0 & 0 & 0 & 0 \\ 0 & 0 & 0 & 0 & 0 \\ 0 & 0 & 0 & 0 & 0 \\ 0 & 0 & 0 & 0 & 0 \end{bmatrix}. \tag{2.10}$$

The control reproduction number of this special case of the basic model, denoted by $\tilde{\mathbb{R}}_{cv}$, is given by:

$$\tilde{\mathbb{R}}_{cv} = \rho(\tilde{F}V^{-1}) = \mathbb{R}_{cv}|_{\varepsilon_v=1}. \tag{2.11}$$

We claim the following result (Safdar and Gumel, 2023):

Theorem 2.3.3. *Consider the special case of the vaccination model* (2.1) *with* $\varepsilon_v = \varepsilon_n = \varepsilon_{nv} = 1$ *and* $\tilde{\mathbb{R}}_{cv} \leq 1 - f_v < 1$ *(with* f_v *as defined in Eqaution* (2.6)*). The disease-free equilibrium of the special case of the model* ($\mathcal{E}_0$) *is globally-asymptotically stable in* Ω *whenever* $\tilde{\mathbb{R}}_{cv} < 1$.

The proof of Theorem 2.3.3, based on using Lyapunov function (Gumel *et al.*, 2021a; Brozak *et al.*, 2021; Iboi *et al.*, 2020a), is given in Appendix B. The result of Theorem 2.3.3 is numerically illustrated in Figure 2.4, where all initial conditions of the special case of the model converged to the disease-free equilibrium when the associated control reproduction number, $\tilde{\mathbb{R}}_{cv}$, is less than one (Safdar and Gumel, 2023). The epidemiological implication of Theorem 2.3.3 is that, for the special case of the vaccination model (2.1) with $\varepsilon_v = \varepsilon_n = \varepsilon_{nv} = 1$, the COVID-19 pandemic can be eliminated in the United States if the threshold quantity, $\tilde{\mathbb{R}}_{cv}$, can be brought to (and maintained at) a value less than one. In other words, for the aforementioned special case of the model, having $\tilde{\mathbb{R}}_{cv} < 1$ is necessary and sufficient for the effective control

(or elimination) of the pandemic in the United States. Hence, implementing a vaccination program that can bring (and maintain) $\tilde{\mathbb{R}}_{cv}$ to a value less than one will result in the elimination of the pandemic in the United States (Safdar and Gumel, 2023).

It is worth mentioning that substituting $\varepsilon_v = \varepsilon_n = \varepsilon_{nv} = 1$ into the expressions for

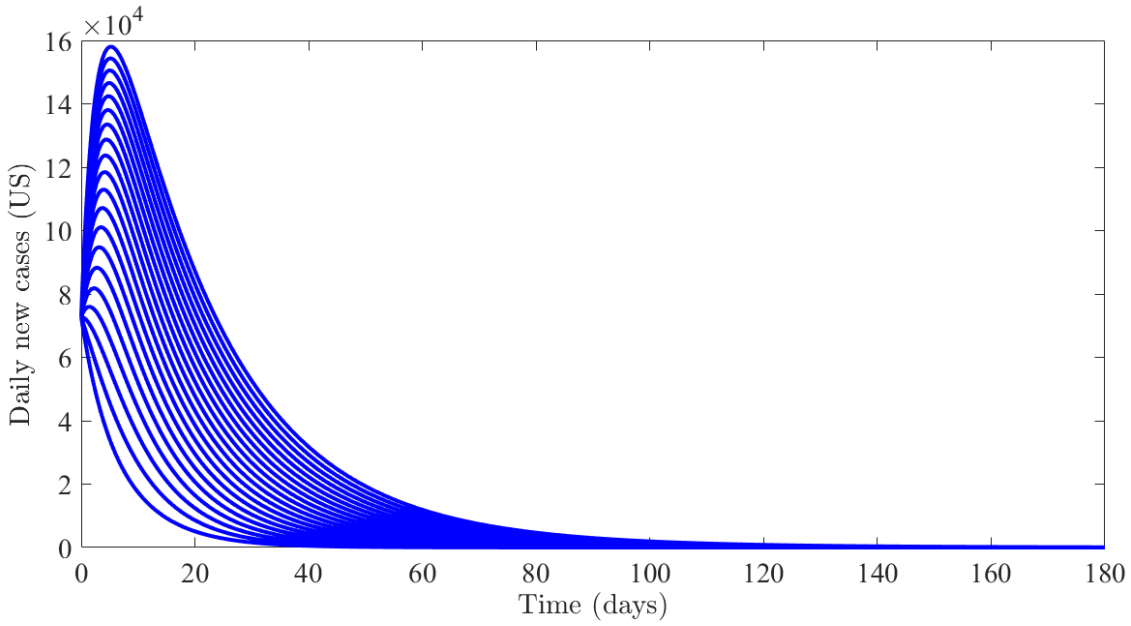

Figure 2.4: Simulations of the Special Case of the Vaccination Model (2.1), for the Average Number of Daily New Cases in the United States as a Function of Time (in Days), Showing Convergence of Initial Conditions to the Disease-free Equilibrium (DFE) When $\tilde{\mathbb{R}}_{cv} < 1$. The Values of the Parameters Used In These Simulations Are as given by Their Baseline Values given in Tables 2.3 and 2.4, with $\beta_a = 0.1542$ Day^{-1}. With This Set of Parameter Values, $\tilde{\mathbb{R}}_{cv} = 0.3824 < 1$ (Safdar and Gumel, 2023).

the backward bifurcation coefficients (a and b) in Appendix A, and simplifying, shows that $a = -2.7089 \times 10^{-14} < 0$ and $b = 3.1 \times 10^{-9} > 0$, as tabulated in Table 2.5. Thus, it follows from Item (i) of Theorem 4.1 in (Castillo-Chavez and Song, 2004) that, unlike the full model (2.1), the special case of the model with $\varepsilon_v = \varepsilon_n = \varepsilon_{nv} = 1$ will not undergo backward bifurcation at $\tilde{\mathbb{R}}_{cv} = 1$ (this is in line with the global asymptotic stability result proved for the disease-free equilibrium of the special case

of the model in Theorem 2.3.3) (Safdar and Gumel, 2023). In fact, this special case of the model undergoes a forward bifurcation at $\tilde{\mathbb{R}}_{cv} = 1$ (as depicted in Figure 2.5), and no endemic equilibrium exists when $\tilde{\mathbb{R}}_{cv} < 1$. Hence, this study shows identifies a sufficient condition for the emergence of the dynamic behavior of backward bifurcation in the transmission dynamics of SARS-CoV-2, namely the imperfect nature of the vaccine-derived and natural immunity (to prevent the acquisition of SARS-CoV-2 infection by vaccinated susceptible individuals, and the re-infection of recovered individuals) (Safdar and Gumel, 2023).

Table 2.5 shows that when the baseline values of the efficacies of the vaccine-derived immunity ($\varepsilon_v = 0.85$), natural immunity ($\varepsilon_n = 0.85$) and natural and vaccine-derived immunity ($\varepsilon_{nv} = 0.95$), given in Table 2.3, are substituted into the expressions for the associated backward bifurcation coefficients (a and b in Appendix A), the values of these coefficients become $a = 3.41948 \times 10^{-7} > 0$ and $b = 0.09911 > 0$, respectively (see Table 2.5). In other words, it follows from Item (i) of Theorem 4.1 in (Castillo-Chavez and Song, 2004) that backward bifurcation will occur if the baseline values of the parameters of the model (2.1), tabulated in Table 2.3, are used (Safdar and Gumel, 2023). Thus, this study shows that backward bifurcation is, indeed, a realistic feature in the transmission dynamics of SARS-CoV-2 in a population that uses imperfect vaccines and where natural (and combined natural and vaccine-derived) immunity do not offer perfect protection against re-infection. Table 2.5 further shows that the likelihood of a backward bifurcation occurring increases as the values of the parameters related to the vaccine-derived (ε_v) and natural immunity (ε_n and ε_{nv}) increase towards one (note that the likelihood of backward bifurcation decreases with decreasing values of the bifurcation coefficients, a and b; and backward bifurcation does not occur when the coefficient a further decreases to values less than zero, in line with Item (i) of Theorem 4.1 in (Castillo-Chavez and Song, 2004)). In other

words, this study shows that the phenomenon of backward bifurcation is more likely to occur in the community if vaccines with lower protective efficacy are used and if the efficacy of natural and combined natural and vaccine-derived immunity to prevent re-infection in the community are low (Safdar and Gumel, 2023).

Immunity efficacy	**Value of bifurcation coefficient,** a	**Value of bifurcation coefficient,** b	**Value of** β_p^*
$\varepsilon_v = 0.50, \varepsilon_n = 0.50, \varepsilon_{nv} = 0.50$	$9.72721 \times 10^{-7} > 0$	$0.03303 > 0$	0.21395
$\varepsilon_v = 0.85, \varepsilon_n = 0.85, \varepsilon_{nv} = 0.95$	$3.41948 \times 10^{-7} > 0$	$0.09911 > 0$	0.23200
$\varepsilon_v = 0.90, \varepsilon_n = 0.90, \varepsilon_{nv} = 0.95$	$2.33118 \times 10^{-7} > 0$	$0.06607 > 0$	0.23450
$\varepsilon_v = 0.95, \varepsilon_n = 0.95, \varepsilon_{nv} = 0.95$	$1.19874 \times 10^{-7} > 0$	$0.03307 > 0$	0.23750
$\varepsilon_v = 1.00, \varepsilon_n = 1.00, \varepsilon_{nv} = 1.00$	$-2.7231 \times 10^{-14} < 0$	$3.1 \times 10^{-9} > 0$	0.24010

Table 2.5: Effect of Efficacies of Vaccine-derived (ε_v), Natural (ε_n) and Combined Natural and Vaccine-derived (ε_{nv}) on the Likelihood of the Occurrence of Backward Bifurcation in the Vaccination Model (2.1), as Measured by the Values of the Associated Backward Bifurcation Coefficients, a and b (given in Appendix A and the Values of β_p^*. Parameter Values (Chosen Arbitrarily for Illustrative Purposes) Used in Generating This Table Are: $\Pi = 20,000, \omega_v = 0.00037, \mu = 0.000034, \xi_v = 0.0004277, \sigma_E = 0.2, \sigma_p = 0.5, \phi_s = 0.15, \gamma_s = 0.2, \gamma_a = 0.125, \gamma_h = 0.12, \delta_p = 0, \delta_a = 0, \delta_s = 0.0000498, \delta_h = 0.00005, r = 0.152, d_1 = 1.5, d_2 = 0.75, d_3 = 1, \beta_s = d_1 \times \beta_p, \beta_a = d_2 \times \beta_p, \beta_h = d_3 \times \beta_p$ and Various Values of ε_v, ε_n and ε_{nv}. This Set of Parameter Values Is Used to Compute the Corresponding Values of the Bifurcation Parameter, β_p^*. Furthermore, for This Set of Parameter Values, $\tilde{\mathbb{R}}_{cv} = 1$. Apart from the Efficacies (i.e., $\varepsilon_v, \varepsilon_n$ and ε_{nv}), Scaling Factors (i.e., d_1, d_2 and d_3) and the Proportion "r", Which Are Dimensionless, All the Other Parameters Have Unit of *per* Day (Safdar and Gumel, 2023).

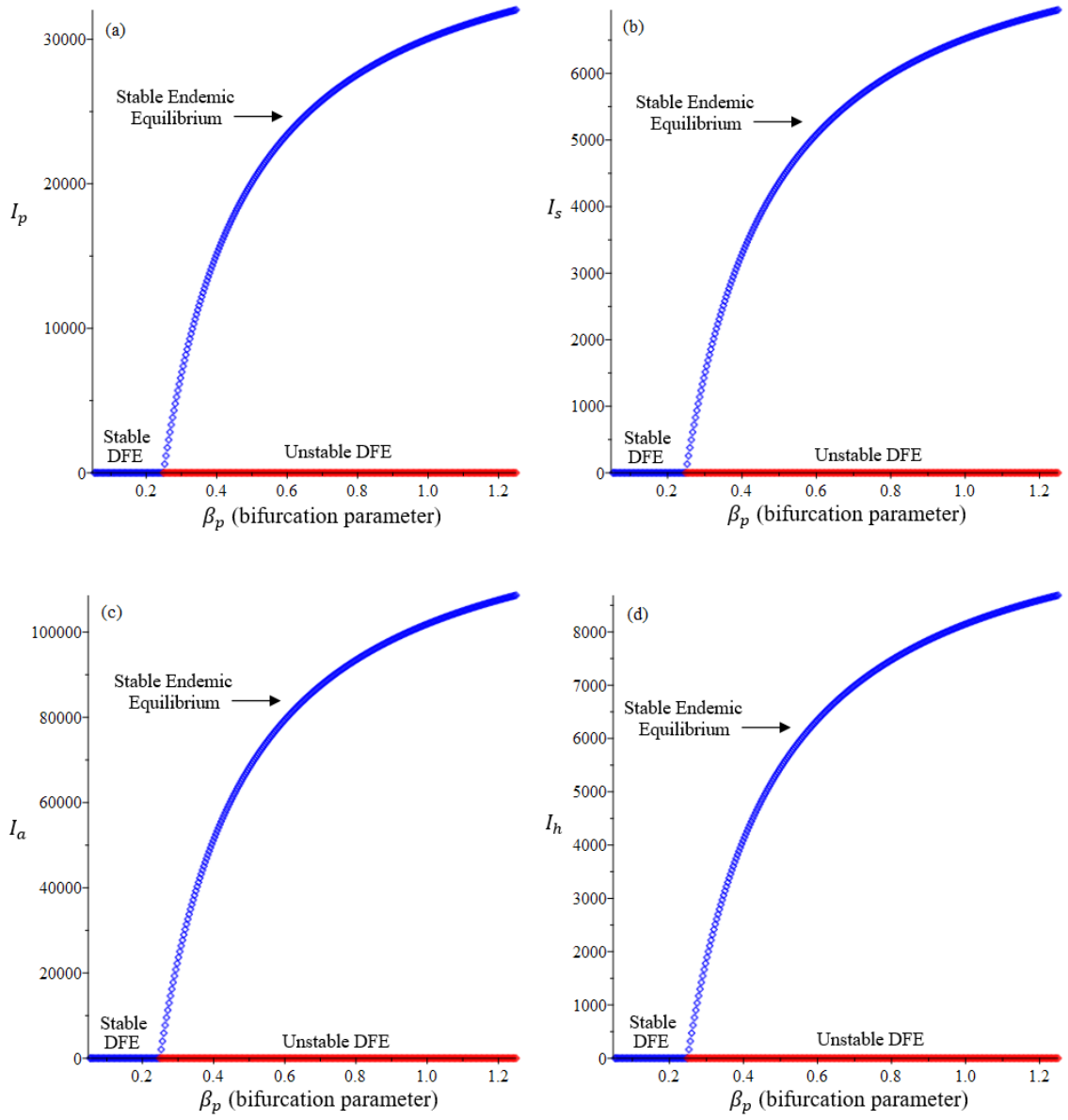

Figure 2.5: Forward Bifurcation Diagram for the Vaccination Model (2.1), Showing the the Profiles of the Population of (a) Pre-symptomatically-infectious Individuals (I_p), (b) Symptomatic Individuals (I_s), (c) Asymptomatically-infectious Individuals (I_a) and (d) Hospitalized Individuals (I_h), as a Function of the Bifurcation Parameter β_p. Parameter Values Used Are: $\Pi = 20000, \omega_v = 0.00037, \beta_p = 0.24010, \beta_s = 0.36022, \beta_a = 0.18011, \beta_h = 0.24010, \mu = 0.000034, \xi_v = 0.0004277, \varepsilon_v = 1, \varepsilon_n = 1, \varepsilon_{nv} = 1, \sigma_E = 0.2, \sigma_p = 0.5, \phi_s = 0.15, \gamma_s = 0.2, \gamma_a = 0.125, \gamma_h = 0.12, \delta_p = 0, \delta_a = 0, \delta_s = 0.0000498, \delta_h = 0.00005, r = 0.152, d_1 = 1.5, d_2 = 0.75, d_3 = 1$. With This Arbitrary Set of Parameter Values, the Values of the Associated Backward Bifurcation Coefficients (Denoted by a and b, and given in Appendix A Are $a = -2.7231 \times 10^{-14} > 0$ and $b = 3.1 \times 10^{-9} > 0$, Respectively. Furthermore, $\beta_p^* = 0.24010$ and $\tilde{\mathbb{R}}_{cv} = 1$. Apart from the Efficacies (i.e., $\varepsilon_v, \varepsilon_n$ and ε_{nv}), Scaling Factors (i.e., d_1, d_2 and d_3) and the Proportion "r", Which Are Dimensionless, All the Other Parameters Have Unit of *per* Day (Safdar and Gumel, 2023).

Special case 2:

The global asymptotic stability of the disease-free equilibrium of the vaccination model (2.1) can also be established for another special case of the model in the absence of disease-induced mortality and recovered individuals do not acquire SARS-CoV-2 re-infection. That is, we consider the special case of the vaccination model (2.1) with $\delta_p = \delta_s = \delta_a = \delta_h = 0$ and $\varepsilon_n = \varepsilon_{nv} = 1$. The assumption for having negligible disease-induced mortality is reasonable owing to the fact that (a) this study focuses on the SARS-CoV-2 dynamics in the United States during the period when Omicron is the predominant variant (i.e., starting from November 28, 2021) and (b) Omicron is far less fatal than the SARS-CoV-2 variants that preceded it (particularly Delta) (Safdar *et al.*, 2023; Ngonghala *et al.*, 2023; Safdar and Gumel, 2023).

Setting $\delta_p = \delta_s = \delta_a = \delta_h = 0$ into the vaccination model (2.1), and adding all the resulting equations, shows that $\dfrac{dN}{dt} = \Pi - \mu N$, from which it follows that $N(t) \to \dfrac{\Pi}{\mu}$ as $t \to \infty$. From now on, the total population at time t, $N(t)$, will be replaced by its limiting value, $N^* = \Pi/\mu$ (i.e., the standard incidence formulation for the infection rate is now replaced by a mass action incidence). Consider the following feasible region for this (second) special case of the vaccination model (2.1) (Safdar and Gumel, 2023):

$$\Omega_{**} = \{(S, V, E, I_p, I_s, I_a, I_h, R_n, R_{nv}) \in \Omega : S \leq S^*, V \leq V^*\}. \tag{2.12}$$

It can be shown that the region Ω_{**} is positively-invariant and attracting with respect to this second special case of the vaccination model (2.1) (see Appendix C for the proof). Furthermore, it is convenient to define the following threshold quantity (Safdar and Gumel, 2023):

$$\hat{\mathbb{R}}_{cv} = \mathbb{R}_{cv}|_{\delta_p=\delta_s=\delta_a=\delta_h=0}. \tag{2.13}$$

We claim the following result (Safdar and Gumel, 2023):

Theorem 2.3.4. *Consider the special case of the vaccination model* (2.1) *in the absence of disease-induced mortality (i.e.,* $\delta_p = \delta_s = \delta_a = \delta_h = 0$*) and no re-infection of recovered individuals (i.e.,* $\varepsilon_n = \varepsilon_{nv} = 1$*). The disease-free equilibrium of this special case of the model* $(\mathcal{E}_0)$ *is globally-asymptotically stable in* Ω_{**} *whenever* $\hat{\mathbb{R}}_{cv} < 1$.

The proof of Theorem 2.3.4, based on using a comparison theorem, is given in Appendix C.

2.3.2 Existence and Stability of Endemic Equilibria: Special Case

In this section, the possible existence and asymptotic stability of endemic (positive) equilibria (i.e., equilibria where at least one of the infected components is positive) of the vaccination model (2.1) will be explored for a special case. Specifically, the special case of the model (2.1) is considered where protective efficacy of the vaccines against primary infection and re-infection is 100% (i.e., $\varepsilon_v = \varepsilon_n = \varepsilon_{nv} = 1$), no waning of vaccine-derived immunity (i.e., $\omega_v = 0$) and no disease-induced mortality (i.e., $\delta_p = \delta_s = \delta_a = \delta_h = 0$). For this special case of the vaccination model (2.1), the associated vaccination reproduction number is defined as follows (Safdar and Gumel, 2023):

$$\tilde{\mathbb{R}}_v = \mathbb{R}_{cv}|_{\delta_p=\delta_s=\delta_a=\delta_h=0,\ \varepsilon_v=1}. \tag{2.14}$$

Existence

Let $E_1 = (S^{**}, V^{**}, E^{**}, I_p^{**}, I_s^{**}, I_a^{**}, I_h^{**}, R_n^{**}, R_{nv}^{**})$ represents any arbitrary (positive) endemic equilibrium point (EEP) of the vaccination model (2.1), with $N^{**} = S^{**} + V^{**} + E^{**} + I_p^{**} + I_s^{**} + I_a^{**} + I_h^{**} + R_n^{**} + R_{nv}^{**}$. Consider the vaccination model (2.1) with $\varepsilon_v = \varepsilon_n = \varepsilon_{nv} = 1$ and $\omega_v = \delta_p = \delta_s = \delta_a = \delta_h = 0$ and $\tilde{\mathbb{R}}_v > 1$. Solving the equations of this special case of the vaccination model at steady-state, and simplifying, gives the following steady-state expressions (Safdar and Gumel, 2023):

$$\begin{aligned} S^{**} &= \frac{\Pi}{\lambda^{**} + c_1}, \quad V^{**} = \frac{\xi_v S^{**}}{c_2}, \quad E^{**} = \frac{\lambda^{**} S^{**}}{c_3}, \quad I_p^{**} = \frac{\sigma_E \lambda^{**} S^{**}}{c_3 c_4}, \\ I_s^{**} &= \frac{r\sigma_p \sigma_E \lambda^{**} S^{**}}{c_3 c_4 c_5}, \quad I_a^{**} = \frac{(1-r)\sigma_p \sigma_E \lambda^{**} S^{**}}{c_3 c_4 c_6}, \\ I_h^{**} &= \frac{\phi_s r \sigma_p \sigma_E \lambda^{**} S^{**}}{c_3 c_4 c_5 c_7}, \quad R_n^{**} = \frac{\sigma_E \lambda^{**} S^{**} P_1}{c_3}, \quad R_{nv}^{**} = \frac{\xi_v \sigma_E \lambda^{**} S^{**} P_1}{\mu c_3}, \end{aligned} \tag{2.15}$$

where,

$$\begin{aligned} c_1 &= \xi_v + \mu, c_2 = \omega_v + \mu, c_3 = \sigma_E + \mu, c_4 = \sigma_p + \mu, c_5 = \phi_s + \gamma_s + \mu, c_6 = \gamma_a + \mu, \\ c_7 &= \gamma_h + \mu, P_1 = \frac{r\sigma_p}{c_5} + \frac{(1-r)\sigma_p}{c_6} + \frac{\phi_s r \sigma_p}{c_5 c_7}, \\ P_2 &= 1 + P_1 + \frac{\xi_v}{c_2} + \frac{1}{c_3} + \frac{\sigma_E}{c_3 c_4}\left\{1 + \frac{r\sigma_p}{c_5} + \frac{(1-r)\sigma_p}{c_6} + \frac{r\phi_s\sigma_p}{c_5 c_6}\right\} + P_1 \sigma_E \left(\frac{1}{c_3} + \frac{\xi_v}{\mu c_3}\right), \end{aligned}$$

with,

$$\lambda^{**} = \frac{(\beta_p I_p^{**} + \beta_s I_s^{**} + \beta_a I_a^{**} + \beta_h I_h^{**})}{N^{**}}. \tag{2.16}$$

It follows, by substituting the expressions for I_p^{**}, I_s^{**}, I_a^{**} and I_h^{**} from Equation (2.15) into Equation (2.16) and extensive algebraic algebraic manipulations, that (Safdar and Gumel, 2023):

$$\lambda^{**} = \frac{(\tilde{\mathbb{R}}_v - 1)}{P_2}, \tag{2.17}$$

from which it follows that $\lambda^{**} > 0$ whenever $\tilde{\mathbb{R}}_v > 1$. Hence, the special case of the model has a unique endemic equilibrium point (EEP) whenever $\tilde{\mathbb{R}}_v > 1$. The components of this unique endemic equilibrium point can be obtained by substituting Equation (2.17) into the expressions for $S^{**}, V^{**}, E^{**}, I_p^{**}, I_s^{**}, I_a^{**}, I_h^{**}, R_n^{**}$ and R_{nv}^{**}, given in Equation (2.15). Thus, we have proved the following result (Safdar and Gumel, 2023):

Theorem 2.3.5. *The special case of the vaccination model* (2.1)*, with* $\varepsilon_v = \varepsilon_n = \varepsilon_{nv} = 1$ *and* $\omega_v = \delta_p = \delta_s = \delta_a = \delta_h = 0$*, has a unique endemic (positive) equilibrium, given by* E_1*, whenever* $\tilde{\mathbb{R}}_v > 1$.

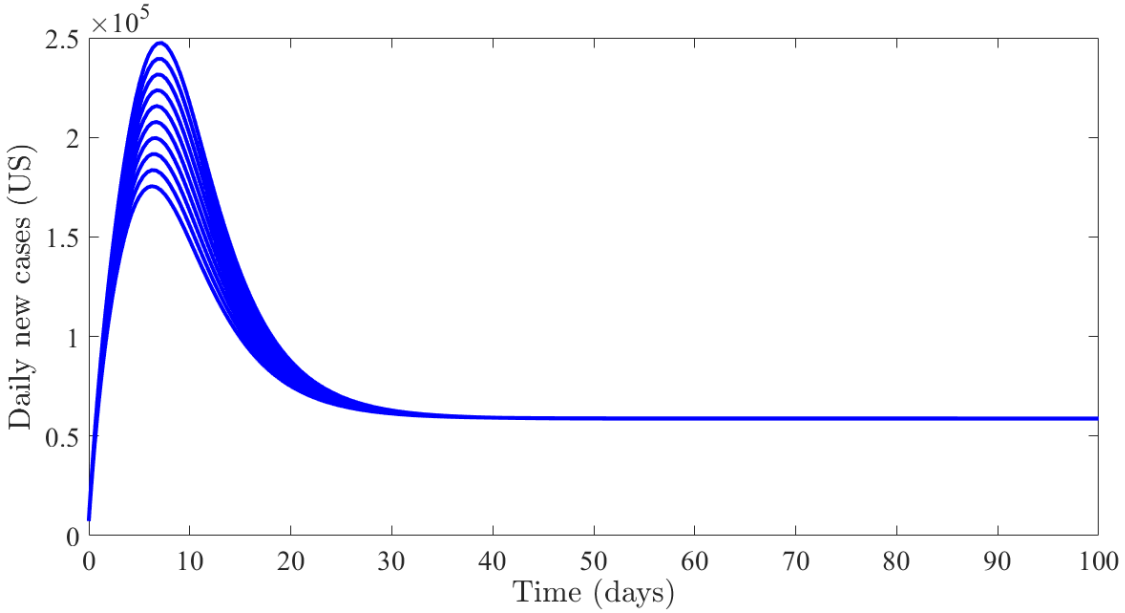

Figure 2.6: Simulations of the Special Case of the Vaccination Model (2.1), for the Number of Daily New Cases in the United States as a Function of Time, Showing Convergence of Initial Conditions to the Unique Endemic Equilibrium When $\tilde{\mathbb{R}}_v > 1$. The Values of the Parameters Used in These Simulations Are as given by Their Baseline Values given in Tables 2.3 and 2.4, with $\Pi = 12000$ Day^{-1}, $\beta_p = 0.9909$ Day^{-1}, $\beta_s = 0.9986$ Day^{-1}, $\beta_a = 0.9942$ Day^{-1}, $\beta_h = 0.9989$ Day^{-1} and $\gamma_h = 0.02$ Day^{-1} (so That, $\tilde{\mathbb{R}}_v = 2.7444 > 1$) (Safdar and Gumel, 2023).

Local asymptotic stability

The local asymptotic property of the unique endemic equilibrium of the special case of the model (2.1) (which exists whenever $\tilde{\mathbb{R}}_v > 1$, as shown in Theorem 2.3.5) will now be explored. We claim the following result (Safdar and Gumel, 2023):

Theorem 2.3.6. *The unique endemic equilibrium point ($\tilde{E}_1$) of the special case of the vaccination model* (2.1)*, with $\varepsilon_v = \varepsilon_n = \varepsilon_{nv} = 1$ and $\omega_v = \delta_p = \delta_s = \delta_a = \delta_h = 0$ (which exists when $\tilde{\mathbb{R}}_v > 1$), is locally-asymptotically stable whenever $\tilde{\mathbb{R}}_v > 1$.*

The proof of Theorem 2.3.6, based on using a Krasnoselskii sub-linearity argument (Hethcote and Thieme, 1985; Safi and Gumel, 2010; Melesse and Gumel, 2010; Esteva *et al.*, 2009), is given in Appendix D. The epidemiological implication of Theorem 2.3.6 is that, for the special case of the vaccination model (2.1) with $\varepsilon_v = \varepsilon_n = \varepsilon_{nv} = 1$ and $\omega_v = \delta_p = \delta_s = \delta_a = \delta_h = 0$, the disease will persist in the population (when the associated reproduction $\tilde{\mathbb{R}}_v$ exceeds one) if the initial sizes of the sub-populations of the model are in the basin of attraction of the endemic equilibrium. The epidemiological implication of Theorems 2.3.5 and 2.3.6 is that, for the special case of the vaccination model (with $\varepsilon_v = \varepsilon_n = \varepsilon_{nv} = 1$ and $\omega_v = \delta_p = \delta_s = \delta_a = \delta_h = 0$), the disease will persist, if the initial population sizes are in the basin of attraction of the unique endemic equilibrium, provided the value of the associated reproduction threshold ($\tilde{\mathbb{R}}_v$) exceeds unity. Figure 2.6 depicts a time series of initial solutions of the special case of the model for the case where $\tilde{\mathbb{R}}_v > 1$ showing convergence of all the initial solutions to the unique endemic equilibrium, in line with Theorem 2.3.6 (Safdar and Gumel, 2023).

2.3.3 Vaccine-Induced Herd Immunity Threshold

Herd immunity, which is a measure of the minimum percentage of the number of susceptible individuals in a community that need to be protected against the infection in order to eliminate community transmission of an infectious disease, can be attained through two main ways, namely natural immunity route (following natural recovery from infection with the disease) or by vaccination (which is widely considered to be the safest and the fastest way) (Safdar and Gumel, 2023; Anderson, 1992; Anderson and May, 1985). For vaccine-preventable diseases, such as COVID-19, it is not practically possible to vaccinate every susceptible individual in the community due to various reasons, such as infants, individuals who are pregnant, breastfeeding women, individuals with certain underlying medical conditions, or those who are unwilling to be vaccinated for COVID-19 due to some other reasons (Iboi *et al.*, 2020b; Safdar *et al.*, 2023; Safdar and Gumel, 2023). Thus, it is critical to know what minimum proportion of the susceptible population that need to be vaccinated in order to protect those that cannot be vaccinated (so that vaccine-induced herd immunity is achieved in the population). Specifically, we let $\frac{V^*}{N^*}$ be the proportion of vaccinated susceptible individuals at the disease-free steady-state (Safdar and Gumel, 2023).

To compute the herd immunity threshold associated with the vaccination model (2.1), we set the vaccination reproduction number ($\mathbb{R}_{cv}$; defined in Equation (2.7)) to one and solve for f_v. This gives:

$$f_v = \frac{1}{\varepsilon_v}\left[\left(1-\frac{1}{\mathbb{R}_0}\right)\right] = f_v^c \quad (\text{for } \mathbb{R}_0 > 1). \tag{2.18}$$

It follows from Equation (2.18) that $\mathbb{R}_{cv} < (>)1$ if $f_v > (<) f_v^c$. Furthermore, $\mathbb{R}_{cv} = 1$ whenever $f_v = f_v^c$. This result is summarized below (Safdar and Gumel, 2023):

Theorem 2.3.7. *Vaccine-induced herd immunity (i.e., COVID-19 elimination) can*

be achieved in the United States, using any of the FDA-approved anti-COVID vaccines, if the vaccine-derived immunity resulted in $f_v > f_v^c$ *(i.e., if* $\mathbb{R}_{cv} < 1$*). If* $f_v < f_v^c$ *(i.e., if* $\mathbb{R}_{cv} > 1$*), then the vaccination program will fail to eliminate the pandemic.*

Epidemiologically-speaking, Theorem 2.3.7 implies that the use of any of the approved COVID-19 vaccines can lead to the elimination of the pandemic in the United States if the proportion of susceptible individuals fully-vaccinated at steady-state reached or exceeded the aforementioned critical threshold value. In other words, the SARS-CoV-2 pandemic will be eliminated in the United States if $f_v > f_v^c$. On the contrary, the vaccination program will fail to eliminate the pandemic if the proportion vaccinated at the disease-free equilibrium falls below the aforementioned critical herd immunity threshold (Safdar and Gumel, 2023).

Figure 2.7 depicts a contour plot of the *vaccine reproduction number* ($\mathbb{R}_{cv}$), as a function of vaccine efficacy (ε_v) and vaccine coverage (f_v) at the disease-free steady-state. For these simulations, the value of each of the parameters of the model is maintained at baseline as tabulated in Tables 2.3 and 2.4. As expected, this figure shows a decrease in the value of $\mathbb{R}_{cv}$ with increasing efficacy and coverage of the vaccine. Furthermore, the contour plot shows that for the case where the overall average protective efficacy of the three vaccines is set at 85% (as tabulated in Table 2.3), at least 62% of the wholly-susceptible population needs to be fully-vaccinated at steady-state to bring the *vaccination reproduction number* ($\mathbb{R}_{cv}$) below one (Figure 2.7). However, if the average vaccine efficacy of the three vaccines drops to 60% (which is plausible, since data shows that the efficacy of the three vaccines against Omicron is much lower than against other variants (Safdar and Gumel, 2023; Sidik, 2022; Safdar *et al.*, 2023; Tseng *et al.*, 2022; Chemaitelly *et al.*, 2022)), then the requirement for the achieving the vaccine-derived herd immunity threshold in the United States drastically increases

to 87%. In other words, based on the results depicted in Figure 2.7, shows that the prospects of achieving vaccine-derived herd immunity in the United States, using the aforementioned three vaccines (Pfizer, Moderna and Johnson & Johnson vaccine), are promising provided the average vaccine efficacy against the predominant Omicron variant is high enough (even if the vaccine coverage is moderate) (Safdar and Gumel, 2023).

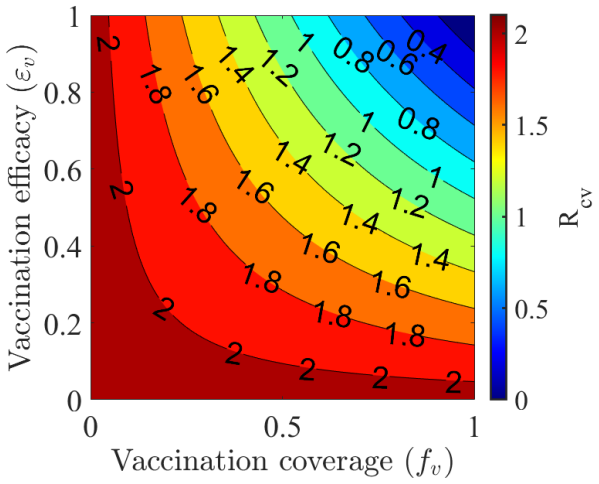

Figure 2.7: Contour Plot of the Vaccine Reproduction Number ($\mathbb{R}_{cv}$) of the Model (2.1), as a Function of Vaccine Coverage (f_v) at Steady-state and Vaccine Efficacy (ε_v), for the United States. The Values of the Parameters Used in These Simulations Are as given by Their Baseline Values given in Tables 2.3 and 2.4 (Safdar and Gumel, 2023).

2.3.4 Global Parameter Sensitivity Analysis

The vaccination model (2.1) contains 22 parameters. Although baseline values of these parameters are given mostly based on published study (as tabulated in Tables 2.3 and 2.4), uncertainties are expected to arise in the estimate of these parameter values. It is, therefore, crucial to assess the impact of these uncertainties on the outcome of the model simulations. It is also important to determine which of the 22 parameters have the most influence on the dynamics of the model (with respect to

a certain chosen response function) (Safdar and Gumel, 2023). In this section, we will use Latin Hypercube Sampling technique and partial rank correlation coefficients (PRCCs) to quantify those parameters that have the highest impact on the value of the chosen response function (Safdar and Gumel, 2023; Marino *et al.*, 2008; Blower and Dowlatabadi, 1994; McLeod *et al.*, 2006). Parameter sensitivity analysis is a quantitative measure for determining the extent to which a chosen response function changes with respect to variations in the input variables (i.e., parameters of the model) (Safdar and Gumel, 2023; Gumel *et al.*, 2021a; Marino *et al.*, 2008; Mancuso *et al.*, 2021). For the purpose of this chapter, the *vaccination reproduction number* of the model ($\mathbb{R}_{cv}$) is chosen as the response function. It should be mentioned that, since the values of 4 of the 22 parameters of the vaccination model (namely the demographic parameters Π and μ, and the disease-induced mortality rates of pre-symptomatic and asymptomatic individuals, δ_p and δ_a) are reliably known (from census data and due to the assumptions we made in Section 2.2 about the values of δ_a and δ_p), they are excluded from the sensitivity analysis. In other words, the sensitivity analysis will be based on the remaining 18 parameters of the vaccination model (2.1) (Safdar and Gumel, 2023).

The process of carrying out the sensitivity analysis entails defining a range (lower and upper bound) and distribution for each parameter of the model, and then splitting each parameter range into 1,000 equal sub-intervals (Safdar and Gumel, 2023; Gumel *et al.*, 2021a; Mancuso *et al.*, 2021). In this study, the range for each of the parameters of the model considered in the sensitivity analysis is obtained by taking 20% to the left and right of its respective baseline value given in Table 2.6 (Gumel *et al.*, 2021a). Furthermore, it is assumed, for statistical tractability, that all parameters in the response function obey the uniform distribution (Gumel *et al.*, 2021a; Mancuso

Parameter	**Baseline Value**	**Range**	**PRCC: $\mathbb{R}_{cv}$**
β_p	0.2309 day^{-1}	$0.18472 - 0.27708$	0.815*
β_s	9.998×10^{-4} day^{-1}	$0.00079 - 0.00119$	0.0153
β_a	0.5429 day^{-1}	$0.43436 - 0.65155$	0.981*
β_h	4.998×10^{-5} day^{-1}	$3.9 \times 10^{-5} - 5.9 \times 10^{-5}$	-0.0223
σ_E	0.2000 day^{-1}	$0.16000 - 0.24000$	0.0094
σ_p	0.5000 day^{-1}	$0.40000 - 0.60000$	-0.820*
r	0.095 (dimensionless)	$0.07600 - 0.11400$	-0.4670
γ_s	0.1000 day^{-1}	$0.08000 - 0.12000$	-0.852*
γ_a	0.2000 day^{-1}	$0.16000 - 0.24000$	0.0240
γ_h	0.1250 day^{-1}	$0.10000 - 0.15000$	-0.0355
ω_v	0.0037 day^{-1}	$0.00291 - 0.00437$	0.0252
δ_s	4.980×10^{-5} day^{-1}	$3.9 \times 10^{-5} - 5.9 \times 10^{-5}$	0.0051
δ_h	5.0×10^{-5} day^{-1}	$4.0 \times 10^{-5} - 6.0 \times 10^{-5}$	0.0016
ξ_v	1.9×10^{-5} day^{-1}	$1.5 \times 10^{-5} - 2.2 \times 10^{-5}$	0.0105
ϕ_s	0.2000 day^{-1}	$0.16000 - 0.24000$	-0.956*
ε_v	0.8500 (dimensionless)	$0.68000 - 1.02000$	-0.0478
ε_n	0.8500 (dimensionless)	$0.68000 - 1.02000$	-0.0285
ε_{nv}	0.9500 (dimensionless)	$0.76000 - 1.14000$	-0.0153

Table 2.6: Table of PRCC Values of the Parameters in the Expression for the Vaccination Reproduction Number, $\mathbb{R}_{cv}$, of the Vaccination Model (2.1). PRCC Values above 0.5 in Magnitude Are Highlighted with a $*$, Implying That These Parameters Are Highly-correlated with the Response Function (i.e., They Significantly Impact the Value of the Response Function, $\mathbb{R}_{cv}$). Apart from the Efficacies (i.e., $\varepsilon_v, \varepsilon_n$ and ε_{nv}) and the Proportion "r", Which Are Dimensionless, All the Other Parameters and Their Ranges Have Unit of *per* Day (Safdar and Gumel, 2023).

et al., 2021). Sets of parameter values are sampled (or drawn) from this space (i.e., parameter ranges) without replacement and used to form a 1000×18 matrix (or hypercube). Each row of this matrix is used to compute the response function ($\mathbb{R}_{cv}$) and the PRCC values are then computed to assess the contributions of uncertainty and variability in individual parameters to uncertainty and variability in the *vaccine reproduction number* (Gumel *et al.*, 2021a). Parameters with high PRCC values close to -1 or +1 are said to be highly-correlated with the response function (Safdar and Gumel, 2023; Gumel *et al.*, 2021a; Marino *et al.*, 2008). Those with negative (positive) PRCC values are said to be negatively (positively) correlated with the response function ($\mathbb{R}_{cv}$) (Safdar and Gumel, 2023; Gumel *et al.*, 2021a).

Figure 2.8 shows the PRCC values of the 18 parameters of the vaccination model (2.1), with respect to the chosen response function ($\mathbb{R}_{cv}$), computed on Day 43 of the onset of the Omicron variant in the United States (i.e., the PRCC values were computed on January 9, 2022). This date was chosen (to compute a snapshot of the PRCC values) because it corresponds to the time when the model predicted a peak of the daily new cases (see the blue curve in Figure 2.2). The PRCC values are also tabulated in Table 2.6. It can be seen from Figure 2.8 that the top five parameters that have the most influence on the response function ($\mathbb{R}_{cv}$) are (Safdar and Gumel, 2023):

(i) The effective contact rate for pre-symptomatically-infectious individuals (β_p).

(ii) The effective contact rate for asymptomatically-infectious individuals (β_a).

(iii) Progression rate of pre-symptomatic individuals (σ_p).

(iv) Recovery rate of symptomatic individuals (γ_s).

(v) Hospitalization rate of the individuals with clinical symptoms (ϕ_s).

Hence, it follows from the parameter sensitivity analysis that implementing public health intervention and mitigation strategies that target reducing the effective contact rates for pre-symptomatic and asymptomatic individuals (β_p and β_a) will be very effective in reducing the response function $\mathbb{R}_{cv}$ (and, consequently, reduce the burden of the pandemic in the United States). The parameters β_p and β_a can be reduced by implementing control strategies such as social-distancing, community lockdowns, use of face masks in public, quarantine of suspected cases and isolation of those with clinical symptoms of the disease (Safdar and Gumel, 2023; Gao *et al.*, 2023). Furthermore, strategies that increase the progression rate of pre-symptomatic individuals (σ_p), recovery rates of the individuals in the symptomatic class (γ_s), as well as increase the detection and hospitalization of symptomatic cases (ϕ_s) will reduce the COVID-19 burden in the community. The progression rate of pre-symptomatic individuals (σ_p) can be increased by contact-tracing of confirmed SARS-CoV-2 cases. The parameters γ_s and ϕ_s can be increased by implementing control strategies such as the treatment of confirmed SARS-CoV-2 cases and the rapid detection (*via* the use of effective and large scale random diagnostic testing) and hospitalization of symptomatic cases (Safdar and Gumel, 2023; Gao *et al.*, 2023).

In conclusion, this study identifies five parameters ($\beta_p, \beta_a, \sigma_p, \gamma_a$ and ϕ_s) that have the greatest influence on the value of the vaccination reproduction number ($\mathbb{R}_{cv}$), which governs the persistence or effective control of the pandemic in the United States. It is worth stating that this result is consistent with some of the results reported in the SARS-CoV-2 modeling literature, such as those in Safdar and Gumel (2023); Safdar *et al.* (2023); Gumel *et al.* (2021a); Moghadas *et al.* (2020); Ngonghala *et al.* (2020b) which suggest that pre-symptomatic and asymptomatic individuals are the main drivers of the COVID-19 pandemic. Hence, to effectively control the SARS-CoV-2 pandemic, the public health control and mitigation strategies should be focused on

effectively targeting the five identified parameters (Safdar and Gumel, 2023).

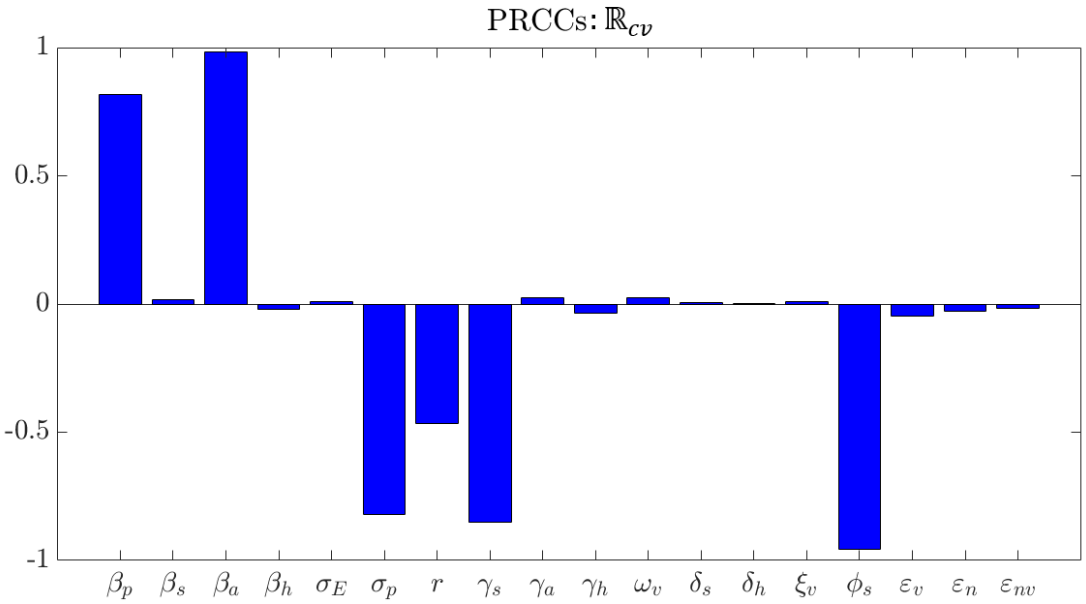

Figure 2.8: Partial Rank Correlation Coefficients (PRCCs) of the Parameters of the Vaccination Model (2.1) with Respect to the Response Function ($\mathbb{R}_{cv}$). Snapshot of the PRCC Plot Generated on Day 43 of the Onset of the Omicron Variant in the United States (i.e., When the Model Predicted a Peak of the Daily New Cases, as Shown by the Blue Curve in Figure 2.2). Parameter Values Used in These Simulations Are as given by the Baseline Values, and Their Corresponding Ranges, Tabulated in Table 2.6 (Safdar and Gumel, 2023).

2.4 Numerical Simulations

Having rigorously analysed the qualitative dynamics of the vaccination model (2.1) and carrying our detailed global sensitivity analysis of its parameters, the vaccination model will now be numerically-simulated to assess the population-level impact of control and mitigation strategies against the SARS-CoV-2 pandemic in the United States. The main focus of these simulations is to assess the impacts of face mask usage in public (as a singular intervention) and the combined impact of face mask usage with vaccination (using any of the three vaccines, Pfizer, Moderna and Johnson & Johnson, being administered in the United States) on limiting or curtailing the burden

of the COVID-19 pandemic in the United States (Safdar and Gumel, 2023). Unless otherwise stated, the simulations of the vaccination model (2.1) will be carried out using the baseline values of the fixed and fitted parameters given in Tables 2.3 and 2.4.

2.4.1 Effect of Masking as a Singular Control and Mitigation Intervention

The use of face masks in public has played a very significant dual role of preventing people from getting infected with COVID-19 (*inward efficacy* or respiratory protection), in addition to preventing those infected with COVID-19 from infecting others (*source control*) (Eikenberry *et al.*, 2020). As currently formulated, the vaccination model (2.1) does not explicitly account for the impact of face mask usage in public. In order to incorporate the usage of masking into the vaccination model, we re-scale the community contact rate parameters (β_p, β_s, β_a and β_h) by a measure of face masks effectiveness in prevention acquisition or transmission of infection. In particular, we carried out the following parameter re-scaling (where, the symbol $\rightarrow$ means "replaced by") in the model (2.1) (Safdar and Gumel, 2023):

$$\beta_p \rightarrow \beta_p(1-\varepsilon_m c_m), \beta_s \rightarrow \beta_s(1-\varepsilon_m c_m), \beta_a \rightarrow \beta_a(1-\varepsilon_m c_m) \quad \text{and} \quad \beta_a \rightarrow \beta_h(1-\varepsilon_m c_m), \tag{2.19}$$

where, $0 \leq \varepsilon_m \leq 1$ is the efficacy of the face mask to prevent transmission or acquisition of infection and $0 \leq c_m \leq 1$ is the compliance in face masks usage in the community. For the aforementioned masking scenario, the associated *masking reproduction number*, denoted by $\mathbb{R}_{cm}$, is given by (where, $\mathbb{R}_{cv}$ is as defined in Equation (2.7), but with the re-scaling (2.19) used in place of the infection rates) (Safdar and Gumel, 2023):

$$\mathbb{R}_{cm} = (1 - \varepsilon_m c_m)\mathbb{R}_{cv}. \tag{2.20}$$

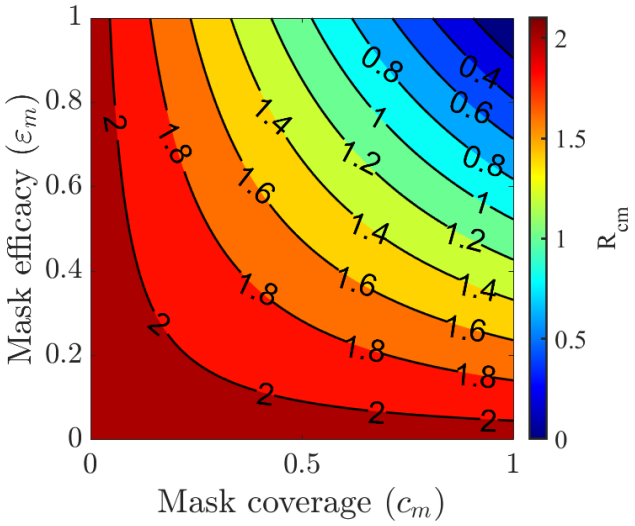

Figure 2.9: Simulations of the Re-scaled Version of the Vaccination Model (2.1) to Assess the Effect of Face Mask Usage as a Singular Public Health Control and Mitigation Intervention (I.E., No Vaccination). Contour Plots of the Masking Reproduction Number ($\mathbb{R}_{cm}$) of the Re-scaled Version of the Model (2.1), as a Function of Mask Coverage (c_m) and Efficacy (ε_m), for the United States. The Other Parameter Values Used in These Simulations Are as given by Their Respective Baseline Values in Tables 2.3 and 2.4, with the Vaccine-related Parameters and State-variable (ε_v, ω_v and $v(t)$) Set to Zero (Safdar and Gumel, 2023).

The simulation results obtained, shown by the contour plots depicted in Figure 2.9, show a marked decrease in the masking reproduction number ($\mathbb{R}_{cm}$) with increasing mask efficacy and compliance in mask usage. Using moderately efficacious face mask in the community, such as a face mask with efficacy 70% (e.g., the surgical mask with proper fitting), the simulation results show that at least 75% of the populace need to be consistently wearing face mask in public to reduce (and maintain) the masking reproduction number ($\mathbb{R}_{cm}$) to a value less than unity (it is worth recalling that bringing the masking reproduction number of the re-scaled version of the vaccination model (2.1) to a value less than unity is a necessary and sufficient condition for the elimination of the disease, in line with Theorems 2.3.1, 2.3.3 and 2.3.4 for the global asymptotic stability of the disease-free equilibrium of the model) (Safdar and Gumel,

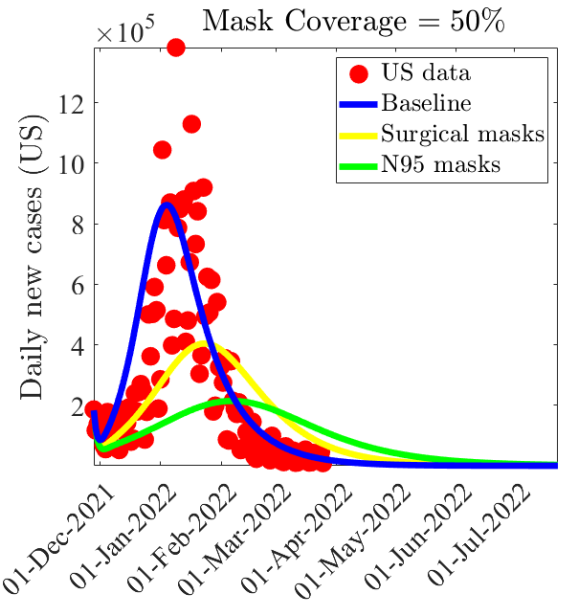

Figure 2.10: Simulations of the Re-scaled Version of the Vaccination Model, given by (2.1) with the Re-scaling (2.19), to Assess the Effect of Face Mask Usage as a Singular Public Health Control and Mitigation Intervention (i.e., No Vaccination) on the Average Daily New Cases of SARS-CoV-2 in the United States. The Other Parameter Values Used in These Simulations Are as given by Their Respective Baseline Values in Tables 2.3 and 2.4, with the Vaccine-related Parameters and State-variable (ε_v, ω_v and $v(t)$) Set to Zero (Safdar and Gumel, 2023).

2023). In other words, this study shows that the use of face mask as a singular intervention can lead to the effective control (or elimination) of the SARS-CoV-2 pandemic if at least 75% of the populace consistently wear a face mask of moderate efficacy (e.g., the surgical mask). If masks of higher efficacy (e.g., N95 mask or equivalent) is favored instead, our simulations show that such elimination can be achieved if 55% of the populace consistently wear these masks in public. Hence, the community-wide masking coverage needed to eliminate the disease decreasing with increasing efficacy of the face mask type favored or prioritized in the community (Safdar and Gumel, 2023).

The re-scaled version of the vaccination model (2.1) (given by (2.1) with the re-scaling (2.19)) is further simulated to assess the impact of face mask usage as a singular pub-

lic health control and mitigation intervention (i.e., in the absence of vaccination) on the daily new cases in the United States. To assess the singular impact of face mask usage, these simulations are carried out for the special case of the re-scaled version of the model with no vaccination (i.e., all the vaccine-related parameters and state-variable of the re-scaled model are set to zero). Furthermore, for these simulations, we set the face mask coverage in the community to be 50% (i.e., $c_m = 0.5$) and consider the scenario where only two mask types, namely surgical (with estimated efficacy of 70%, so that $\varepsilon_v = 0.7$) and N95 masks or equivalent (with estimated efficacy of 95%, so that $\varepsilon_v = 0.95$) are prioritized in the community (Safdar and Gumel, 2023). The simulation results for the two mask types, depicted in Figure 2.10, show a significant decrease in the average daily new cases at the peak recorded under the baseline scenario (i.e., compare the peaks for the yellow and green curves with the peak of the blue curve, which represents the baseline scenario; note that, for the data used in these simulations, the peak for the baseline scenario occurred on January 3, 2022). For instance, under this scenario (in the absence of vaccination), if surgical masks are prioritized (and with 50% coverage), about 53% of the daily cases recorded at the peak under the baseline scenario will have been prevented (Figure 2.10, compare the peaks of the blue and gold curves). Furthermore, if N95 masks or equivalent are prioritized (with the same 50% coverage), about 75% of the daily new cases recorded at the peak of the baseline scenario would have been averted (compare peaks of green and blue curves in Figure 2.10) (Safdar and Gumel, 2023).

In summary, this study shows that the prospect of eliminating the SARS-CoV-2 pandemic using masking as a singular public health control and mitigation strategy is promising, provided masks of moderate or high efficacy (with moderate to high coverage) are prioritized. Specifically, this study showed, based on the current observed data used in our simulations (i.e., based on the SARS-CoV-2 case data for the period

November 28, 2021 to March 23, 2022 used to parameterize the model) i.e., from the contour plot (Figure 2.9), that the SARS-CoV-2 pandemic can be eliminated in the United States (i.e., suppressed from taking off) if approximately half the populace were consistently wearing N95 mask (or equivalent) in public (if surgical masks were prioritized, the coverage level needed to achieve such elimination increases to 75%) (Safdar and Gumel, 2023). Although it may not be practical to expect humans to always be wearing face masks in public, implementing masking as a singular strategy is important for many reasons, including: (a) disease burden (i.e., severe disease, hospitalization and death) can be significantly reduced and (b) buying time (by suppressing the burden of the disease, and saving lives) before a safe and effective vaccine becomes available. For this data set, if masking was started on Day 1 of the onset of Omicron (i.e., November 28, 2021), these simulations showed that up to $53\% - 75\%$ of the daily new cases recorded at the peak (this corresponds to $225000 - 425200$) will have been prevented (Safdar and Gumel, 2023).

2.4.2 Assessing the Combined Impact of Vaccination and Masks on Herd Immunity Threshold

The re-scaled version of the vaccination model (2.1) is simulated (using the baseline values of the fixed, fitted and assumed parameter values in Tables 2.3 and 2.4), to assess the combined impact of vaccination (at baseline) and masking, on the dynamics of COVID-19 in the United States. Figure 2.11 depicts contour plots of the masking reproduction number ($\mathbb{R}_{cm}$) of the modified version of model (2.1), as a function of the average vaccine efficacy (ε_v) of the three vaccines (namely; Pfizer, Moderna and Johnson & Johnson vaccine) against the acquisition of infection with Omicron and the fraction of the United States population fully-vaccinated at steady-state (f_v) (Safdar and Gumel, 2023). Numerical simulations are carried out for the scenario when the

baseline face mask usage in the community is increased by 20%, for various face mask types. Figure 2.11(a) shows that if fabric or cloth masks (with low masking efficacy, i.e., $\varepsilon_m = 0.30$) are prioritized, the herd immunity requirement corresponding to 62% now reduces to 58%. However, if moderately effective procedure or surgical masks (with $\varepsilon_m = 0.70$) are prioritized, the herd immunity requirement significantly reduces to 52% (Figure 2.11(b)). Furthermore, the vaccine-derived herd immunity threshold reduces drastically from 62% to 48% if highly effective N95 masks (with $\varepsilon_m = 0.95$) are prioritized (Figure 2.11(c)). In summary, the contour plots in Figures 2.11(a)$-$(c) show that the proportion of the individuals who need to be fully-vaccinated to achieve herd immunity in the United States reduces with increasing coverage of face masks in the community (from the baseline face mask usage). Furthermore, the level of reduction achieved depends on the quality of the face masks used (specifically, greater reduction in herd immunity level needed to eliminate the disease is achieved if the high-quality N95 masks are prioritized, in comparison to the scenario where the cloth masks or moderately effective surgical masks are prioritized) (Safdar and Gumel, 2023).

2.4.3 Assessing the Combined Impact of Vaccination and Masks on Daily New Cases

The re-scaled version of the vaccination model (2.1) is further simulated, (using the baseline values of the fixed, fitted and assumed parameter values in Tables 2.3 and 2.4) to assess the combined impacts of mask coverage (c_m), mask type (cloth masks with masking efficacy of 30%, i.e., $\varepsilon_m = 0.30$, surgical masks with masking efficacy of 70%, i.e., $\varepsilon_m = 0.70$ and N95 respirators with masking efficacy of 95%, i.e., $\varepsilon_m = 0.95$) and vaccination (with average vaccine efficacy at the baseline level) on the daily number of new COVID-19 cases in the United States. For the scenario when the mask coverage

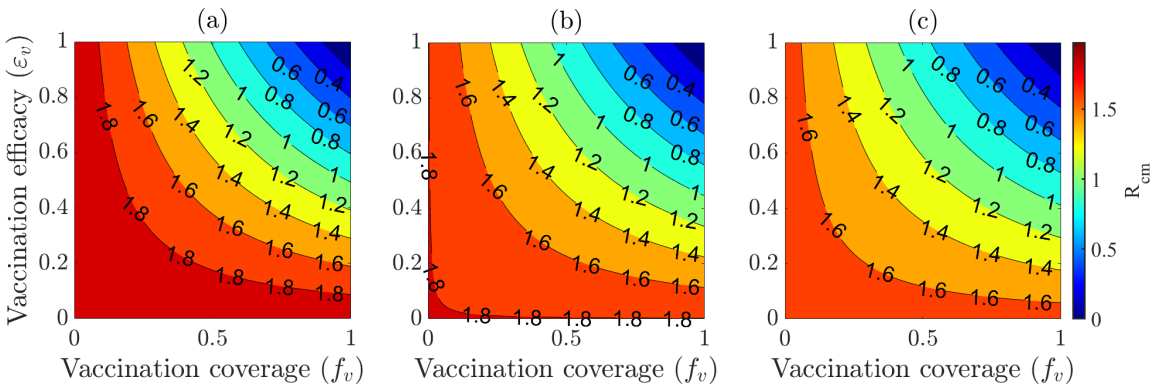

Figure 2.11: $(a)-(c)$ Contour Plots of the Face Mask Reproduction Number ($\mathbb{R}_{cm}$), as a Function of Vaccine Efficacy (ε_v) and the Fraction Vaccinated at the Steady-state (f_v) for the Case When (a) Cloth Mask Is Prioritized and the Mask Coverage Is Increased by 20% from the Baseline, (b) Surgical Mask Is Prioritized and the Coverage in Its Usage Is Increased by 20% from the Baseline, (c) N95 Mask Is Prioritized and the Coverage in Its Usage Is Increased by 20% from the Baseline. The Values of All Other Parameters Used in the Simulations Are as given by The Baseline Values in Tables 2.3 and 2.4 (Safdar and Gumel, 2023).

increases by 10% from its baseline value, the results obtained depicted in Figure 2.12(a), show that using the ineffective cloth masks will result to a 4.08% reduction in the average number of new daily cases at the peak from the baseline (by comparing the magenta and blue curves in Figure 2.12(a)). The reduction in the average number of peak daily new cases is more significant if face masks of higher quality are prioritized (Safdar and Gumel, 2023). Specifically, if the moderately-effective surgical masks are prioritized, the simulation show that up to 9.79% reduction in peak level of the daily new cases at the peak, in comparison to the peak baseline level (by comparing the gold curve and blue curve in Figure 2.12(a)). The reduction increases significantly to 13.49% if the highly-effective N95 masks are prioritized (compare the blue and green curves in Figure 2.12(a)). These reductions are more dramatic for the scenario when the mask coverage increases by 20% from its baseline value. The results obtained, depicted in Figure 2.12(b), show that using the ineffective cloth masks will result to a 8.35% reduction in the average daily new cases at the peak, in comparison to the

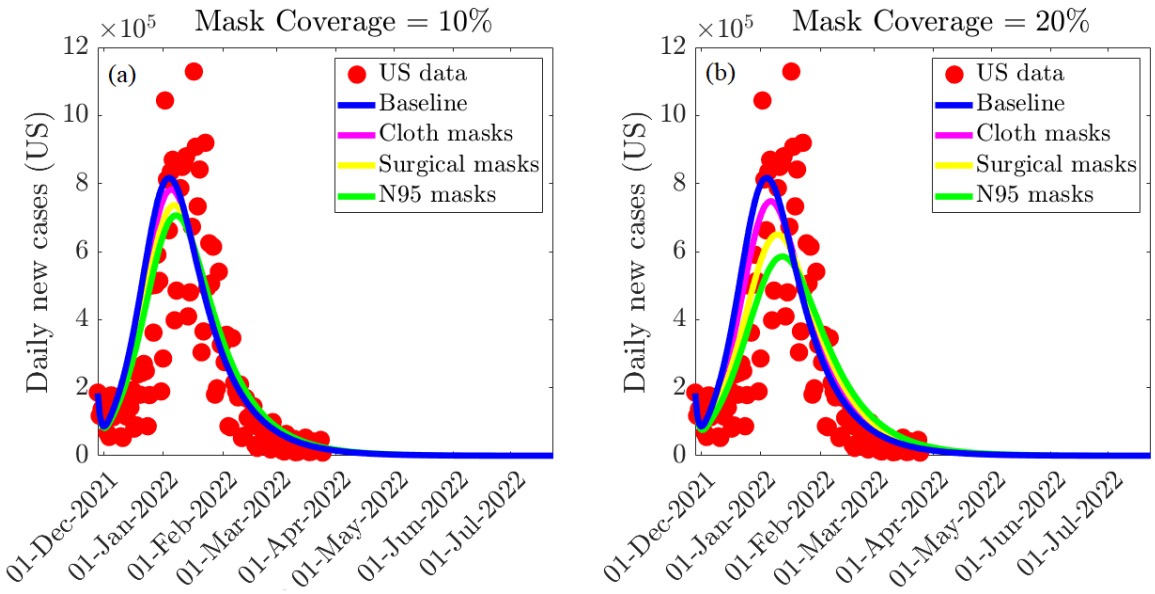

Figure 2.12: Simulations of the Model (2.1), Showing the Incremental Impact of Mask Coverage (c_m), Mask Type (Cloth Masks, with $\varepsilon_m = 0.3$; Surgical Masks, with $\varepsilon_m = 0.7$; And N95 Respirators, with $\varepsilon_m = 0.95$) on the Daily New COVID-19 Cases in the United States, as a Function Of Time. In Figure 2.12(a), the Mask Coverage (c_m) Is Increased by 10% and in Figure 2.12(b), the Mask Coverage (c_m) Is Increased by 20%, from Their Respective Baseline Values. The Values of the Other Parameters Used in These Simulations Are as given in Tables 2.3 and 2.4 (Safdar and Gumel, 2023).

baseline (compare the magenta and blue curves in Figure 2.12(b)). The reduction in the average daily new cases at the peak is more notable if moderately-effective surgical masks are prioritized, the simulation show that up to 20.37% reduction in peak daily new cases can be achieved, in comparison to the baseline (compare the gold curve and blue curve in Figure 2.12(b)). This reduction in the average daily new cases at the peak is more drastic, about 28.25% (in comparison to the baseline) if the highly-effective N95 masks are prioritized (compare the green and blue curves in Figure 2.12(b)) (Safdar and Gumel, 2023). In summary, the simulations in Figures 2.12(a) – (b) show that the reduction in the average number of daily new cases at the peak (from the baseline) is significant if the face mask coverage in the community is increased (from the baseline coverage level). Furthermore, the reduction in the

average number of peak daily cases also depends on the quality of the face masks used (specifically, drastic reduction in peak daily new cases is noted if the high-quality N95 masks are prioritized, in comparison to the scenario where the cloth masks or moderately effective surgical masks are prioritized) (Safdar and Gumel, 2023).

2.5 Discussion and Conclusions

This chapter is based on the use of mathematical modeling approaches, coupled with rigorous analysis and computation, to address the problem of the spread and control of the novel 2019 coronavirus pandemic (COVID-19) in the United States. Specifically, a mathematical model, which takes the form of a deterministic system of nonlinear differential equations, is developed and used to assess the population-level impact of three of the four FDA-approved anti-COVID vaccines (Pfizer, Moderna and Johnson & Johnson vaccines) on the transmission dynamics and control of the COVID-19 pandemic in the United States. The impact of face mask use strategy, implemented as a singular intervention strategy or in combination with the vaccination program, is also assessed (Safdar and Gumel, 2023).

The model was rigorously analysed (using techniques, tools and theories from nonlinear dynamical systems) to study its qualitative dynamical features. Furthermore, the model was parameterized by fitting it to the observed new daily COVID-19 case data for the United States for the period from November, 28, 2021 to March 23, 2023 (this period was chosen to coincide with the time the Omicron variant first emerged in the United States). The model was specifically fitted using the segment of the data from November, 28, 2021 to February 23, 2022, and use the remaining segment of the data (i.e., the segment from February 24, 2022 to March 23, 2022) to cross validate the model (Safdar and Gumel, 2023). The cross-validation showed that the vaccination model predicts the case data for the time period from February 24, 2022 to March

23, 2022 reasonably well.

The rigorous qualitative analysis of the vaccination model revealed that its unique disease-free equilibrium is locally-asymptotically stable whenever the associated *control reproduction number* of the model (denoted by $\mathbb{R}_{cv}$) is less than one. It was also shown, using the theory of center manifold (La Salle, 1976; Carr, 2012)), that the model undergoes the phenomenon of *backward bifurcation* when the control reproduction number of the model is less than 1 under certain conditions. The epidemiological implication of the backward bifurcation phenomenon is that the usual epidemiological requirement of having the control reproduction number of the model being less than 1, while necessary, is no longer sufficient for the elimination of the disease (Safdar and Gumel, 2023). In the presence of a backward bifurcation situation, more control resources need to be invested to further reduce the control reproduction number. Two main sufficient conditions were identified for the presence of backward bifurcation in the vaccination model presented, namely (a) imperfect vaccine-derived, natural and combined vaccine-derived and natural immunity to protect against the acquisition of infection (of vaccinated susceptible individuals) and re-infection (of recovered vaccinated or unvaccinated individuals) and (b) disease-induced mortality and re-infection of recovered individuals. In other words, the phenomenon of backward bifurcation does not occur when (i) the vaccine-derived and natural immunity (including the combined vaccine-derived and natural immunity) are perfect (i.e., when $\varepsilon_v = \varepsilon_n = \varepsilon_{nv} = 1$) and (ii) when the disease-induced mortality is negligible (i.e., $\delta_p = \delta_s = \delta_a = \delta_h = 0$) and recovered individuals do not acquire re-infection (i.e., $\varepsilon_n = \varepsilon_{nv} = 1$). In any of these two scenarios where backward bifurcation does not occur, we proved the global asymptotic stability of the disease-free equilibrium when the associated control reproduction number is less than one (in this case, the model undergoes a forward bifurcation at the bifurcation point, where the associated con-

trol reproduction number equals one) (Safdar and Gumel, 2023). The epidemiological implication of the global asymptotic stability result for the disease-free equilibrium of the model (for the aforementioned special cases of the model where backward bifurcation does not occur) is that the SARS-CoV-2 pandemic can be eliminated in the United States if the the associated control reproduction number can be brought to (and maintained at) a value less than one (in other words, in this case, bringing and maintaining the associated control reproduction number to a value less than one is necessary and sufficient for the elimination of the pandemic in the United States) (Safdar and Gumel, 2023).

It is also showed that the model has a unique and locally-asymptotically stable endemic equilibrium for a special case (where the vaccine is assumed to offer perfect protective efficacy against the acquisition of infection, no re-infection, no waning of vaccine-derived immunity and disease-induced mortality is negligible) whenever the associated control reproduction number exceeds one. The epidemiological implication of this result is that, for this special case of the model, the disease will persist in the population whenever the associated reproduction number is greater than one. An explicit expression for the vaccine-induced herd immunity threshold for the United States was derived. It was shown, using current data for new daily COVID-19 cases in the United States, that, for the case where the three FDA-approved vaccines offer average protective efficacy against the Omicron variant of about 85%, vaccine-derived herd immunity will be achieved in the United States if at least 62% of the populace is fully-vaccinated (Safdar and Gumel, 2023). However, if the average cross-protection efficacy provided by the vaccines reduces slightly (e.g., to 60%), about 87% of the population needs to be fully-vaccinated with either of the aforementioned vaccines to

achieve the vaccine-derived herd immunity (Safdar and Gumel, 2023).

Furthermore, using global sensitivity analysis, we identified the parameters of the model that have the most influence on the control reproduction number of the model, $\mathbb{R}_{cv}$ (hence, disease burden in the community). Specifically, the top five PRCC-ranked parameters identified, to be the effective contact rate for pre-symptomatically-infectious individuals (β_p), asymptomatically-infectious individuals (β_a), the progression rate of pre-symptomatic individuals (σ_p), the recovery rate of symptomatic individuals (γ_s) and the hospitalization rate of the individuals with clinical symptoms (ϕ_s) (Safdar and Gumel, 2023). The numerical PRCC values indicate that reduction of the infection rate of pre-symptomatic and asymptomatic individuals results in the reduction of $\mathbb{R}_{cv}$. The parameters β_p and β_a can be reduced by implementing control strategies, such as social-distancing, community lockdowns, use of face masks in public, quarantine and isolation of the confirmed cases of COVID-19. Furthermore, by increasing the progression rate of pre-symptomatic individuals, recovery rate of symptomatic individuals, and the increase in the detection and hospitalization of symptomatic cases will ultimately reduce $\mathbb{R}_{cv}$. The progression rate of the pre-symptomatic individuals (σ_p) can be increased by implementing non-pharmaceutical control invention, such as contact tracing. The parameters γ_s and ϕ_s can be increased by implementing control strategies, such as treatment of the COVID-19 infected individuals and the detection and hospitalization of symptomatic cases by large scale blanket testing in the community (Safdar and Gumel, 2023).

The model was adapted and used to assess the population-level impact of using face mask in the community as a singular intervention strategy (i.e., in the absence of vaccination) and also in combination with the vaccination program. It is also assessed exclusively the impact of face masks as a singular public health control and

mitigation intervention (i.e., with the vaccine-related parameters and state-variable set to zero) on the herd immunity requirement and on the average daily new cases in the United States. Under this scenario (i.e., with no vaccination), it is shown that the prospect of COVID-19 elimination in the United States is enhanced if almost half of the populace is consistently wearing N95 mask (if surgical masks were prioritized, the coverage level needed to achieve such elimination increases to 75%). Further, we simulate the model for the same scenario (i.e., in the absence of vaccination) to assess the impact of masking on the peak daily new cases. Our simulations showed a significant decrease in the peak daily new cases (i.e., up to 53%) if the implementation of moderately-effective surgical masks (with 50% coverage) was started on Day 1 of the onset of Omicron (i.e., end of November, 2021). Marked reductions in the peak daily new cases were recorded (i.e., up to 75%) if N95 masks were prioritized for the same scenario (i.e., if masking was started on Day 1 of the onset of Omicron and its coverage is increased by 50% from the baseline) (Safdar and Gumel, 2023).

The re-scaled version of the vaccination model was also used to assess the population-level impact of vaccination (at the baseline) combined with face mask usage for various mask types. For the scenario when the baseline face mask usage in the community is increased by 20% and moderately-effective surgical mask are prioritized, the simulations showed that at least 52% of the populace need to be fully vaccinated in order to achieve vaccine-derived herd immunity. However, if highly-efficacious face masks are prioritized (such as N95 mask), the numerical simulations showed that the requirement for achieving the vaccine-derived herd immunity is reduced significantly to 48%. Furthermore, for the same scenario (i.e., baseline face mask usage is increased by 20%), the simulations show that if the highly efficacious N95 masks are prioritized then the average number of daily new cases at the peak are significantly reduced from the baseline by about 28% (Safdar and Gumel, 2023). In summary, the

theoretical and numerical simulation results generated from this chapter showed that the prospects for the effective control and elimination of the COVID-19 pandemic in the United States is significantly improved if vaccination is combined with a face mask strategy (that prioritizes moderately effective and high-quality masks), particularly if the average efficacy of the three of the four FDA-approved vaccines being administered in the United States (namely Pfizer, Moderna and Johnson & Johnson vaccine) is high (i.e., $\approx 85\%$) (Safdar and Gumel, 2023).

It should be mentioned that in this chapter, the model presented is relatively a basic model for vaccination against the SARS-CoV-2 pandemic to illustrate the epidemiological concepts and features being highlighted. The model can be extended to incorporate other important features associated with the vaccination and SARS-CoV-2 immunity, such as allowing for waning of natural and the combined natural and vaccine-derived immunity, boosting of immunity (especially vaccine-derived) (Safdar *et al.*, 2023; Ngonghala *et al.*, 2023) and the effect of human behavior changes with respect to control and mitigation interventions (particularly adherence to vaccination and/or face mask usage) (Ngonghala *et al.*, 2021b).

Chapter 3

IMPACTS OF BOOSTING AND WANING OF IMMUNITY

3.1 Introduction

Numerous public health interventions, notably the use of three of the four FDA-approved safe and very effective anti-COVID vaccines (namely, the Pfizer-BioNTech, Moderna and Johnson & Johnson vaccines), and nonpharmaceutical interventions (such as the use of face mask, community lockdowns and social-distancing) have played a major role in effectively curtailing the COVID-19 pandemic in the United States (U.S. Food and Drug Administration and others, 2009, 2021b; Pfizer, 2020; Eikenberry *et al.*, 2020; Ngonghala *et al.*, 2020b; Bourouiba, 2020; Iboi *et al.*, 2020a; Ngonghala *et al.*, 2023; Safdar *et al.*, 2023). However, Despite the rapid development and deployment of the effective vaccines, COVID-19 cases and mortality continued to rise in the United States for most part of 2021 (and even during the early parts of 2022). This is largely due to the emergence of SARS-CoV-2 variants of concern (VoC), notably the Alpha, Beta, Gamma, Delta and Omicron variants (Ngonghala *et al.*, 2023; Mahase, 2021; Gómez-Carballa *et al.*, 2021; Karim and Karim, 2021; Duong, 2021; Koyama *et al.*, 2020; Rahimi and Abadi, 2022). Specifically, the emergence of the Omicron variant (B.1.1.529), in November of 2021, has dramatically changed the trajectory of the pandemic in the United States and globally(Del Rio *et al.*, 2022). Omicron was believed to be at least three times more contagious than Delta (Del Rio *et al.*, 2022; Callaway *et al.*, 2021) (*albeit* Delta remains the deadliest of all the SARS-CoV-2 variants that emerged (HAGEN, 2022; Hanan, 2022)). A sub-variant of Omicron, BA.2 was first identified in the United States from a sample

collected on December 14, 2021, in New Jersey (Centers for Disease Control and Prevention, 2022). It is believed to be more contagious than the original Omicron variant (i.e., BA.1) (Rahimi and Abadi, 2022; Katella, 2022). From November 28, 2021 to the end of 2021, the United States was recording over one million new cases of SARS-CoV-2 daily (and caused by the Omicron variant (Katella, 2023)). Furthermore, multiple subvariants of Omicron (including BA.5, BQ.1, and BQ.1.1) were identified as the variants of concern in the United States during the year 2022 (Katella, 2023; Centers for Disease Control and Prevention, 2023b). However, in late January of 2023, a new Omicron subvariant called XBB.1.5 was identified as the most dominant subvariant of the SARS-CoV-2 virus, causing about 50% of the infections in the United States (Katella, 2023; Centers for Disease Control and Prevention, 2023b).

Various empirical studies have shown that the protective efficacy of each of the aforementioned vaccines wane over time (Gumel *et al.*, 2021b; Ngonghala *et al.*, 2021b, 2023), necessitating the FDA to approve the administration of booster vaccines for each of the three vaccines. Specifically, the FDA approved a booster dose for all persons aged 18 years and older during the period August to November 2021 (Fast *et al.*, 2021). In late March 2022, the FDA authorized a second booster shot of COVID-19 vaccines for vulnerable populations in the United States (i.e., for people 50 years of age and older, and for individuals with certain immuno-compromising conditions who are at higher risk of severe disease, hospitalization and death) (Hause *et al.*, 2022). A second booster dose is equivalent to a fourth dose for people who received a Pfizer-BioNTech or Moderna mRNA vaccine series or a third dose for those who received the single-dose Johnson & Johnson vaccine. In August of 2022, the FDA authorized the most updated booster doses (i.e., bivalent boosters) which protect against both the original SARS-CoV-2 variant and the Omicron variants BA.4 and BA.5 (Centers for Disease Control and Prevention and others, 2022). It was available from September

2, 2022 and was administered to adults (i.e., 18 years and older) (Centers for Disease Control and Prevention and others, 2022).

Despite the deployment of the aforementioned three highly-efficacious vaccines (which were originally developed to combat against the original SARS-CoV-2 strain), COVID-19 continues to be a public health challenge (causing more new cases and mortality, *albeit* at significantly reduced burden, in comparison to the period during the peaks of the pandemic in the United States). Consequently, the vaccination program is complemented with other intervention and mitigation strategies, such as the use of face masks (Eikenberry *et al.*, 2020; Ngonghala *et al.*, 2020a, 2021b) and antiviral treatment (Jayk Bernal *et al.*, 2021), aimed at effectively combating or eliminating the pandemic in the United States.

The objective of this chapter is to design, analyse and parameterize a vaccination model that accounts for the main limitations itemized in Chapter 2. Specifically, the impact of waning and boosting of both the vaccine-derived and natural immunity, on the dynamics of the Omicron variant of SARS-CoV-2 in the United States, will be assessed. To achieve the objective of this chapter, the basic model developed in Chapter 2 will be extended to account for the boosting and waning of the aforementioned immunity types. Data corresponding to the period starting from the onset of the Omicron variant (November 2021) will be used to parameterize the model. The rest of this chapter is organized as follows. The model is formulated in Section 3.2. The basic qualitative features of the model are also derived. The model is rigorously analysed, with respect to the existence and asymptotic stability of its disease-free equilibrium, in Section 3.3. Expressions for vaccine-derived herd immunity thresholds are also derived. The model is fitted with observed daily new case COVID-19 data in Section 3.4. The methodology for implementing the data fitting process and

estimating the unknown parameters of the model is also described. Numerical simulations of the model are carried out in Section 3.5.

3.2 Model Formulation

To formulate the model for the transmission dynamics of SARS-CoV-2 in the presence of boosting and waning of both vaccine-derived and natural immunity, we split the total population at time t, denoted by $N(t)$, into mutually exclusive compartments of unvaccinated susceptible individuals ($S(t)$), fully-vaccinated susceptible individuals with high vaccine-derived immunity ($V_1(t)$), vaccinated susceptible individuals with moderate vaccine-derived immunity ($V_2(t)$) (Rella *et al.*, 2021), vaccinated susceptible individuals with low vaccine-derived immunity ($V_3(t)$), exposed individuals (i.e., newly-infected individuals who are not yet infectious; $E(t)$), pre-symptomatic infectious individuals ($I_p(t)$), symptomatically-infectious individuals ($I_s(t)$), asymptomatically-infectious individuals ($I_a(t)$), hospitalized individuals ($I_h(t)$), recovered individuals with high infection-acquired natural immunity ($R_{n1}(t)$), recovered individuals with moderate infection-acquired natural immunity ($R_{n2}(t)$), recovered individuals with low infection acquired natural immunity ($R_{n3}(t)$), recovered individuals with high infection-acquired natural and vaccine-derived immunity ($R_{nv1}(t)$), recovered individuals with moderate infection-acquired natural and vaccine-derived immunity ($R_{nv2}(t)$) and recovered individuals with low infection-acquired natural and vaccine-derived immunity ($R_{nv3}(t)$). Thus,

$$N(t) \;=\; S(t) + E(t) + \sum_{i=1}^{3} [V_i(t) + R_{n_i}(t) + R_{nv_i}(t)] + \sum_{\{j=p,s,a,h\}} I_j(t).$$

Numerous clinical studies show that the vaccine-derived immunity against SARS-CoV-2 begin to wane after nine months of the receipt of the full vaccine doses (Ngonghala *et al.*, 2023; Gumel *et al.*, 2021b; Curley, 2021). Consequently, in our model for-

mulation, individuals in the V_1 class (who enjoy high level of the protective efficacy of the vaccine) are those that are within nine months of receipt of full vaccine doses. Furthermore, individuals in the V_2 class are those who have received the full doses between 9 months to a year ago (hence, the vaccine efficacy is moderate). Finally, individuals in the V_3 class are assumed to have received the full vaccine doses from a year to two years ago (and the vaccine efficacy is low). This study allows for the waning and boosting of vaccine-derived and natural immunity (boosting of natural immunity is assumed to occur due to treatment or the use of other immune-boosting supplements (Mrityunjaya *et al.*, 2020; Alagawany *et al.*, 2021)). The model is given by the following deterministic system of nonlinear differential equations (a streamlined/abbreviated flow diagram of the model is depicted in Figure 3.1, and the state variables and parameters of the model are described in Tables 3.1 and 3.2, respectively) (Safdar *et al.*, 2023):

$$
\begin{cases}
\dot{S} &= \Pi + \omega_{v_3} V_3 + \omega_{n_3} R_{n_3} + \omega_{nv_3} R_{nv_3} - (\lambda + \xi_v + \mu) S, \\
\dot{V}_1 &= \xi_v S + \rho_{v_2} V_2 - [(1-\varepsilon_{v_1})\lambda + \omega_{v_1} + \mu] V_1, \\
\dot{V}_2 &= \omega_{v_1} V_1 + \rho_{v_3} V_3 - [(1-\varepsilon_{v_2})\lambda + \omega_{v_2} + \rho_{v_2} + \mu] V_2, \\
\dot{V}_3 &= \omega_{v_2} V_2 - [(1-\varepsilon_{v_3})\lambda + \omega_{v_3} + \rho_{v_3} + \mu] V_3, \\
\dot{E} &= \lambda S + \lambda \sum_{i=1}^{3} [(1-\varepsilon_{v_i}) V_i(t) + (1-\varepsilon_{n_i}) R_{n_i}(t) + (1-\varepsilon_{nv_i}) R_{nv_i}(t)] \\
&- (\sigma_E + \mu) E, \\
\dot{I}_p &= \sigma_E E - (\sigma_p + \gamma_p + \mu + \delta_p) I_p, \\
\dot{I}_s &= r\sigma_p I_p - (\phi_s + \gamma_s + \mu + \delta_s) I_s, \\
\dot{I}_a &= (1-r)\sigma_p I_p - (\gamma_a + \mu + \delta_a) I_a, \\
\dot{I}_h &= \phi_s I_s - (\gamma_h + \mu + \delta_h) I_h, \\
\dot{R}_{n_1} &= \sum_{j=\{p,s,a,h\}} \gamma_j I_j + \rho_{n_2} R_{n_2} - [(1-\varepsilon_{n_1})\lambda + \xi_v + \omega_{n_1} + \mu] R_{n_1}, \\
\dot{R}_{n_2} &= \omega_{n_1} R_{n_1} + \rho_{n_3} R_{n_3} - [(1-\varepsilon_{n_2})\lambda + \xi_v + \omega_{n_2} + \rho_{n_2} + \mu] R_{n_2}, \\
\dot{R}_{n_3} &= \omega_{n_2} R_{n_2} - [(1-\varepsilon_{n_3})\lambda + \xi_v + \omega_{n_3} + \rho_{n_3} + \mu] R_{n_3}, \\
\dot{R}_{nv_1} &= \xi_v R_{n_1} + \rho_{nv_2} R_{nv_2} - [(1-\varepsilon_{nv_1})\lambda + \omega_{nv_1} + \mu] R_{nv_1}, \\
\dot{R}_{nv_2} &= \xi_v R_{n_2} + \omega_{nv_1} R_{nv_1} + \rho_{nv_3} R_{nv_3} - [(1-\varepsilon_{nv_2})\lambda + \omega_{nv_2} + \rho_{nv_2} + \mu] R_{nv_2}, \\
\dot{R}_{nv_3} &= \xi_v R_{n_3} + \omega_{nv_2} R_{nv_2} - [(1-\varepsilon_{nv_3})\lambda + \omega_{nv_3} + \rho_{nv_3} + \mu] R_{nv_3},
\end{cases}
\tag{3.1}
$$

where,

$$
\lambda = (\beta) \left(\frac{\eta_p I_p + \eta_s I_s + \eta_a I_a + \eta_h I_h}{N} \right), \tag{3.2}
$$

is the infection rate. In (3.2), β is the effective contact rate for individuals and η_j (with $j = \{p, s, a, h\}$) is the modification parameter for the heterogeneity in the infectiousness of infected individuals in the presymptomatic (I_p), symptomatic (I_s),

asymptomatic (I_a) and hospitalized (I_h) class, respectively.

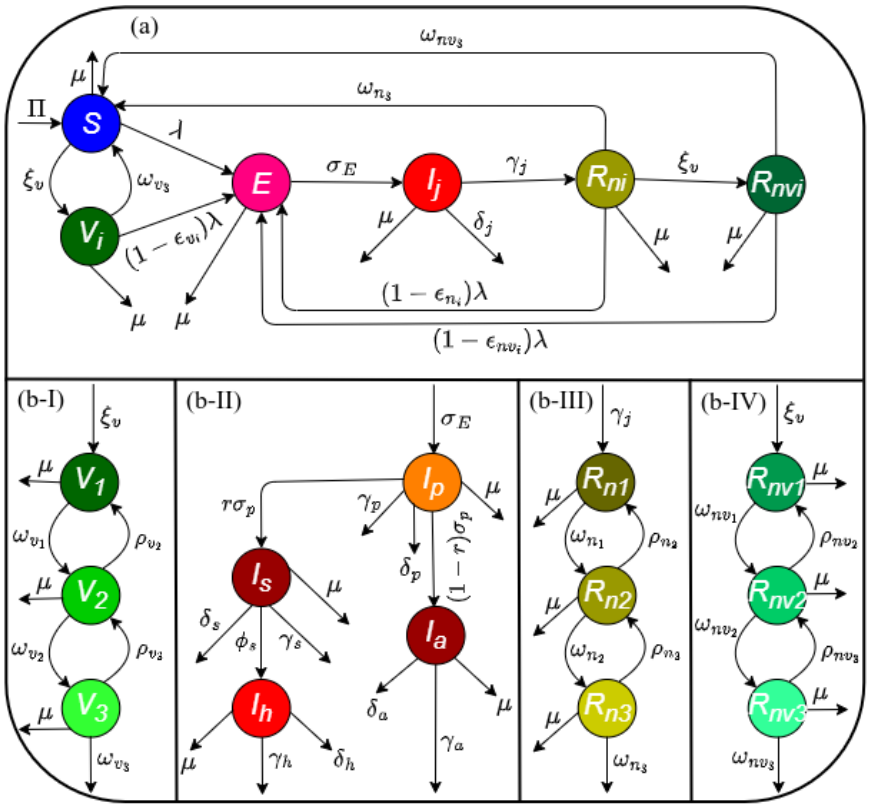

Figure 3.1: (a) Streamlined Flow Diagram of the Model (3.1). (b-I)−(b-IV) Depict Sub-flow Diagrams of the Model Illustrating the Transitions Within the Compartments for Fully Vaccinated (V_i) with High, Moderate and Low Vaccine-derived Immunity, Infectious (I_j), Recovered with High, Moderate and Low Natural Immunity (R_{n_i}) and Recovered with Both Natural and Vaccine-derived Immunity at High, Moderate and Low Levels (R_{nv_i}) Individuals, Respectively (for $i = 1, 2, 3$ and $j = \{p, s, a, h\}$). The Streamlined Flow Diagram Is Drawn to Simplify and Enhance the Readability of the General Structure of the Model (the Full Version of the Flow Diagram of the Model Is given in Appendix E) (Safdar *et al.*, 2023).

In the model (3.1), Π is the recruitment of individuals into the population, ω_{v_i} $(i = 1, 2, 3)$ is the vaccine waning rate for vaccinated individuals in stage V_i, ω_{n_i} is the waning natural immunity for recovered individuals in stage R_{n_i}, ω_{nv_i} is the waning rate of both vaccine-derived and natural immunity for individuals in stage R_{nv_i}, λ is the infection rate (defined in Equation (3.2)), ξ_v is the *per capita* vaccination rate and

μ is the natural death rate. Vaccinated individuals in V_2 and V_3 classes receive booster doses at the rate ρ_{vi} $(i = 2, 3)$ and revert to the higher efficacy vaccination stage V_1 and V_2, respectively. Similarly, recovered individuals in the R_{n2} and R_{n3} classes receive immune booster at a rate ρ_{n2} and ρ_{n3}, respectively (and revert, respectively, to stages R_{n1} and R_{n2}). Individuals in R_{nv2} and R_{nv3} (that have both the vaccine-derived and natural immunity) receive a booster at a rate ρ_{nv2} and ρ_{nv3}, respectively (and revert to R_{nv1} and R_{nv2}, respectively).

The parameter ε_{vi} is the average protective efficacy of the vaccine for vaccinated susceptible individuals in stage $V_i\,(i = 1, \cdots, 3)$, while $\varepsilon_{n_i}\,(i = 1, \cdots, 3)$ is the average efficacy of natural immunity to prevent recovered individuals (in the R_{ni} class) from acquiring future SARS-CoV-2 infection and $\varepsilon_{nv_i}\,(i = 1, \cdots, 3)$ is the average efficacy of natural and vaccine-derived immunity to prevent future SARS-CoV-2 infection of recovered individuals (in the R_{nv_i}, $i = 1, 2, 3$, classes). Exposed individuals progress to the pre-symptomatic stage at the rate σ_E, and pre-symptomatic individuals progress to either become symptomatically-infectious, at a rate $r\sigma_p$ (where, $0 \leq r \leq 1$ is the proportion of these individuals that show clinical symptoms), or become asymptomatically-infectious, at the rate $(1 - r)\sigma_p$. Symptomatic individuals are hospitalized at a rate ϕ_s, and infectious individuals in stage I_j recover at a rate γ_j (with $j = \{p, s, a, h\}$). Finally, disease-induced mortality occur in the I_j, I_s, I_a and I_h classes at a rate $\delta_j\,(j = \{p, s, a, h\})$. Some of the main assumptions made in the formulation of the model (3.1) are (Safdar *et al.*, 2023):

(a) A well-mixed population: individuals are indistinguishable, and every member of the population is equally likely to mix with every other member of the population.

(b) Vaccinated susceptible individuals (in the V_1, V_2 and V_3 classes) are assumed

to have received the full required doses (i.e., two doses for Pfizer or Moderna vaccine, one dose for the Johnson & Johnson vaccine), and that enough time has elapsed for the body to develop the full vaccine-derived immunity (which is typically two weeks after receiving the booster dose (Andrews *et al.*, 2022a; Thompson, 2022)).

(c) The three SARS-CoV-2 vaccines that received FDA's Emergency Use Authorization (Pfizer, Moderna and Johnson & Johnson) are imperfect (U.S. Food and Drug Administration and others, 2009; Food and Drug Administration and others, 2020; U.S. Food and Drug Administration and others, 2021b). That is, the vaccines offer partial protective immunity (with average efficacy $0 < \varepsilon_{v_i} < 1$), which wanes over time (at a rate ω_{v_i}), for $i = 1, \cdots, 3$ (Curley, 2021; Gumel *et al.*, 2021b). In other words, vaccinated individuals can experience breakthrough infection (Oliver *et al.*, 2020; U.S. Food and Drug Administration and others, 2021a).

(d) We assume the gradual waning of both vaccine-derived and natural immunity over time, resulting, ultimately, in reverting to the wholly-susceptible class S (Gumel *et al.*, 2021b). Moreover, the overall transitions from V_1 to S, R_{n_1} to S and R_{nv_1} to S hold gamma distribution (Childs *et al.*, 2022).

(e) Vaccination is only offered to wholly-susceptible individuals or those who recovered naturally from COVID-19 infection but their natural immunity has waned completely or those recovered individuals who had acquired natural plus vaccine-derived immunity after recovering from COVID-19 infection but the immunity has completely waned over time. In other words, individuals who are currently infected are not vaccinated.

(f) Immunity level can be increased or strengthened, by using immunity boosters (Centers for Disease Control and Prevention and others, 2021; Pacific and Hasan, 2021; Mrityunjaya *et al.*, 2020; Alagawany *et al.*, 2021), for the individuals in the V_i, R_{n_i} and R_{nv_i} $(i = 1, \cdots, 3)$ classes.

State variable	**Description**
S	Population of unvaccinated (wholly) susceptible individuals
V_1	Population of vaccinated susceptible individuals with high vaccine-derived immunity
V_2	Population of vaccinated susceptible individuals with moderate vaccine-derived immunity
V_3	Population of vaccinated susceptible individuals with low vaccine-derived immunity
E	Population of exposed (newly-infected individuals)
I_p	Population of pre-symptomatic infectious individuals
I_s	Population of infectious individuals with clinical symptoms of the disease
I_a	Population of asymptomatically-infectious individuals
I_h	Population of hospitalized individuals
R_{n_1}	Population of recovered individuals with high natural immunity
R_{n_2}	Population of recovered individuals with moderate natural immunity
R_{n_3}	Population of recovered individuals with low natural immunity
R_{nv_1}	Population of recovered individuals with high natural and vaccine-derived immunity
R_{nv_2}	Population of recovered individuals with moderate natural and vaccine-derived immunity
R_{nv_3}	Population of recovered individuals with low natural and vaccine-derived immunity

Table 3.1: Description of the State Variables of the Model (3.1) (Safdar *et al.*, 2023).

The model (3.1) extends numerous COVID-19 vaccination models in the literature,

such as those in Alagoz *et al.* (2021); Ramos *et al.* (2021); Shoukat *et al.* (2022); Gumel *et al.* (2021b,a); Mancuso *et al.* (2021), by, *inter alia*:

(a) Incorporating the gradual waning of vaccine-derived, natural and natural plus vaccine-derived immunity (gradual waning of immunity was not considered in Ngonghala *et al.* (2021b, 2023); Gumel *et al.* (2021b,a)).

(b) Accounting for the administration of booster doses in the population (this was not considered in Mancuso *et al.* (2021); Gumel *et al.* (2021b); Ramos *et al.* (2021); Gonzalez-Parra *et al.* (2021); Shoukat *et al.* (2022); Alagoz *et al.* (2021); Gumel *et al.* (2021a)).

(c) Including two recovered populations to explicitly account for (and differentiate) recovered individuals with natural immunity and those with both natural and vaccine-derived immunity (this was not considered in Gumel *et al.* (2021a); Ngonghala *et al.* (2023); Gumel *et al.* (2021b))

(d) Incorporating the reinfection and loss of immunity of the recovered individuals (this was not considered in Gumel *et al.* (2021b); Mancuso *et al.* (2021); Gumel *et al.* (2021a)).

Parameter	**Description**
Π	Recruitment rate
β	Effective contact rate
$\eta_j\,(j=\{p,s,a,h\})$	Modification parameter for the infectiousness of the individuals in I_p, I_s, I_a, and I_h classes, respectively
ξ_v	Vaccination rate
μ	Natural death rate
r	Proportion of individuals who show clinical symptoms of the disease
$\omega_{v_i}(i=1,2,3)$	Waning rate of vaccinated individuals in stage V_i

$\omega_{n_i}(i=1,2,3)$	Waning rate of natural immunity for individuals in stage R_{n_i}
$\omega_{nv_i}(i=1,2,3)$	Waning rate of natural plus vaccine-derived immunity in individuals in stage R_{nv_i}
$\rho_{v_2}(\rho_{v_3})$	Boosting rate of vaccine-derived immunity for individuals in stage $V_2(V_3)$
$\rho_{n_2}(\rho_{n_3})$	Boosting rate of natural immunity for individuals in $R_{n_2}(R_{n_3})$ stage
$\rho_{nv_2}(\rho_{nv_3})$	Boosting rate of vaccine-derived and natural immunity of those in stage $R_{nv_2}(R_{nv_3})$
$\varepsilon_{v_i}(i=1,2,3)$	Vaccine efficacy for individuals in V_1, V_2 and V_3 class, respectively
$\varepsilon_{n_i}(i=1,2,3)$	Efficacy of natural immunity to prevent infection of recovered individuals in R_{n_1}, R_{n_2} and R_{n_3}
$\varepsilon_{nv_i}(i=1,2,3)$	Efficacy of natural and vaccine derived immunity to prevent infection of recovered individuals in R_{nv_1}, R_{nv_2} and R_{nv_3} stage
σ_E	Progression rate from exposed individuals to pre-symptomatic stage
σ_p	Progression rate of pre-symptomatic individuals to either symptomatic or asymptomatic class
$\gamma_j\,(j=\{p,s,a,h\})$	Recovery rate for individuals in the I_p, I_s, I_a and I_h class, respectively
ϕ_s	Hospitalization rate of individuals with clinical symptoms of the disease
$\delta_j\,(j=\{p,s,a,h\})$	Disease-induced mortality rate for individuals in the I_p, I_s, I_a and I_h class, respectively

Table 3.2: Description of the Parameters of the Model (3.1)(Safdar *et al.*, 2023).

3.2.1 Basic Qualitative Properties of the Model

The basic qualitative properties of the model (3.1) are explored in this section. Specifically, the positivity and boundedness of the solutions of the model are established. First of all, since the model (3.1) monitors the temporal dynamics of human popula-

tions, all its parameters are non-negative. Consider the following biologically-feasible region for the model (3.1):

$$\Omega = \left\{ (S, V_1, V_2, V_3, E, I_p, I_s, I_a, I_h, R_{n_1}, R_{n_2}, R_{n_3}, R_{nv_1}, R_{nv_2}, R_{nv_3}) \in \mathbb{R}^{15}_{+} : N(t) \leq \frac{\Pi}{\mu} \right\},$$

where, $N(t)$ is the total population. Furthermore, let

$$X(0) = (S(0), V_i(0), E(0), I_p(0), I_s(0), I_a(0), I_h(0), R_{ni}(0), R_{nvi}(0))^T,$$

with $i = 1, 2, 3$, be the vector of initial solutions of the model (3.1). We claim the following result.

Theorem 3.2.1. *Let the initial data for the model* (3.1) *be* $S(0) > 0, V_i(0) \geq 0, E(0) \geq 0, I_p(0) \geq 0, I_s(0) \geq 0, I_a(0) \geq 0, I_h(0) \geq 0, R_{ni}(0) \geq 0, R_{nvi}(0) \geq 0$, *with* $i = 1, 2, 3$. *Then the solutions of the model* (3.1) *with positive initial data, will remain positive for all time* $t > 0$.

Proof. Let $t_1 = sup\{t > 0 : S(t) > 0, V_1(0) > 0, V_2(0) > 0, V_3(0) > 0, E(0) > 0, I_p(0) > 0, I_s(0) > 0, I_a(0) > 0, I_h(0) > 0, R_{n_1}(0) > 0, R_{n_2}(0) > 0, R_{n_3}(0) > 0, R_{nv_1}(0) > 0, R_{nv_2}(0) > 0, R_{nv_3}(0) > 0 \in [0, t]\}$. Thus, $t_1 > 0$. It follows from the first equation of the model (3.1) that

$$\frac{dS}{dt} = \Pi + \omega_{v_3} V_3(t) + \omega_{n_3} R_{n_3}(t) + \omega_{nv_3} R_{nv_3}(t) - (\lambda + \xi_v + \mu) S(t) \geq \Pi - (\lambda + \xi_v + \mu) S(t),$$

which can be re-written as:

$$\frac{d}{dt}\left[S(t) exp\Big\{ \int_0^t \lambda(u)du + (\xi_v + \mu)t \Big\} \right] \geq \Pi\, exp\Big\{ \int_0^t \lambda(u)du + (\xi_v + \mu)t \Big\}.$$

Hence,

$$S(t_1) exp\Big\{ \int_0^{t_1} \lambda(u)du + (\xi_v + \mu)t_1 \Big\} - S(0) \geq \Pi \int_0^{t_1} exp\Big\{ \int_0^x \lambda(\nu)d\nu + (\psi_L + \mu)x \Big\} dx,$$

so that

$$S(t_1) \geq exp\Big\{ - \int_0^{t_1} \lambda(u)du - (\xi_v + \mu)t_1 \Big\} \left[S(0) + \Pi\, exp\Big\{ \int_0^x \lambda(\nu)d\nu + (\xi_v + \mu)x \Big\} dx \right] > 0,$$

Similarly, it can be shown that all the remaining state variables of the vaccination model (3.1) are non-negative (for all non-negative initial conditions) for $t > 0$. Consequently, all the solutions of the vaccination model (3.1), with non-negative initial conditions, remain non-negative for all time $t > 0$. □

Theorem 3.2.2. *Consider the model* (3.1) *with non-negative initial data,* $X(0)$*. The region* Ω *is positively-invariant and bounded with respect to the model* (3.1)*.*

Proof. Adding all the equations of the model (3.1) gives

$$\dot{N} = \Pi - \mu N - \delta_p I_p - \delta_s I_s - \delta_a I_a - \delta_h I_h. \tag{3.3}$$

It follows (noting the non-negativity of the parameters of the model (3.1)) from (3.3) that

$$\dot{N} \leq \Pi - \mu N. \tag{3.4}$$

Hence, if $N > \frac{\Pi}{\mu}$, then $\dot{N} < 0$. Thus, it follows, by applying a standard comparison theorem (Lakshmikantham *et al.*, 1989; Gumel *et al.*, 2021b; Safdar *et al.*, 2023) on (3.4), that:

$$N(t) \leq N(0)e^{-\mu t} + \frac{\Pi}{\mu}\left(1 - e^{-\mu t}\right).$$

Furthermore, if $N(0) \leq \frac{\Pi}{\mu}$, then $N(t) \leq \frac{\Pi}{\mu}$. Thus, the solutions of the model (3.1) are bounded. Therefore, every solution of the model (3.1) with initial conditions in Ω remains in Ω for all time t. In other words, the region Ω is positively-invariant and attracts all initial solutions of the model (3.1). Hence, it is sufficient to consider the dynamics of the flow generated by (3.1) in Ω (where, the model is epidemiologically- and mathematically well-posed) (Safdar *et al.*, 2023). □

3.3 Asymptotic Stability of DFE

The consequence of Theorem 3.2.2 is that it is sufficient to consider the dynamics of the flow generated by the system given in (3.1) in Ω, since the vaccination-waning-boosting model (3.1) is epidemiologically and mathematically well-posed (Hethcote, 2000) there.

3.3.1 Local asymptotic stability

The disease-free equilibrium of the model (3.1) is given by:

$$\mathcal{E}_0 = \left(S^*, V_1^*, V_2^*, V_3^*, E^*, I_p^*, I_s^*, I_a^*, I_h^*, R_{n_1}^*, R_{n_2}^*, R_{n_3}^*, R_{nv_1}^*, R_{nv_2}^*, R_{nv_3}^*\right), \tag{3.5}$$

where,

$$\begin{aligned} S^* &= \frac{\Pi\left[\mu\rho_{v_2}A_1 + A_2\left(\mu\rho_{v_3} + A_3A_4\right)\right]}{D_1}, \\ V_1^* &= \frac{\Pi\xi_v\left[\rho_{v_2}A_1 + \mu\rho_{v_3} + A_3A_4\right]}{D_2}, \\ V_2^* &= \frac{\Pi\xi_v\omega_{v_1}A_1}{D_2}, \\ V_3^* &= \frac{\Pi\xi_v\omega_{v_1}\omega_{v_2}}{D_2}, \end{aligned} \tag{3.6}$$

with,

$$\begin{aligned} A_1 &= \mu + \rho_{v_3} + \omega_{v_3}, A_2 = \mu + \omega_{v_1}, A_3 = \mu + \omega_{v_2}, A_4 = \mu + \omega_{v_3}, \\ B_1 &= \mu + \xi_v, B_2 = \mu + \rho_{v_3} + \omega_{v_2}, B_3 = \mu + \rho_{v_3}, B_4 = \mu + \rho_{v_2} + \omega_{v_1}, \\ B_5 &= \mu + \xi_v + \omega_{v_1}, \\ D_1 &= \mu[\xi_v\left(\left(A_2\right)\left(B_2\right) + \rho_{v_2}\left(A_1\right) + \omega_{v_3}\left(\mu + \omega_{v_1} + \omega_{v_2}\right)\right) + \mu\rho_{v_2}(A_1) \\ &+ \left(A_2\right)\left(\mu\rho_{v_3} + \left(A_3\right)\left(A_4\right)\right)], \\ D_2 &= \mu\left(B_1\right)\left[\left(A_2\right)\left(B_2\right) + \rho_{v_2}\left(B_3\right)\right] + \mu\omega_{v_3}\left[\left(B_1\right)\left(B_4\right) + \omega_{v_2}\left(B_5\right)\right], \end{aligned}$$

and all other components (for the infected and recovered compartments of the model) take the value zero.

Here, too, the asymptotic stability property of the DFE ($\mathcal{E}_0$) will be explored using

the *next generation operator method* (van den Driessche and Watmough, 2002; Diekmann *et al.*, 1990). It can be shown that the associated non-negative matrix of new infection terms (F) and the M-matrix of the linear transition terms (V) are given, respectively, by (Safdar *et al.*, 2023):

$$F = \begin{bmatrix} 0 & f_1 & f_2 & f_3 & f_4 \\ 0 & 0 & 0 & 0 & 0 \\ 0 & 0 & 0 & 0 & 0 \\ 0 & 0 & 0 & 0 & 0 \\ 0 & 0 & 0 & 0 & 0 \end{bmatrix} \quad \text{and} \quad V = \begin{bmatrix} K_1 & 0 & 0 & 0 & 0 \\ -\sigma_E & K_2 & 0 & 0 & 0 \\ 0 & -r\sigma_p & K_3 & 0 & 0 \\ 0 & -(1-r)\sigma_p & 0 & K_4 & 0 \\ 0 & 0 & -\phi & 0 & K_5 \end{bmatrix}, \quad (3.7)$$

where,

$$f_1 = \beta\,\eta_p \left(\frac{S^* + A^*}{N^*}\right), f_2 = \beta\,\eta_s \left(\frac{S^* + A^*}{N^*}\right), f_3 = \beta\,\eta_a \left(\frac{S^* + A^*}{N^*}\right),$$

$$f_4 = \beta\,\eta_h \left(\frac{S^* + A^*}{N^*}\right),$$

with (noting that $N^* = \Pi/\mu$),

$$A^* = (1-\varepsilon_{v_1})V_1^* + (1-\varepsilon_{v_2})V_2^* + (1-\varepsilon_{v_3})V_3^*, K_1 = \sigma_E + \mu, K_2 = \sigma_p + \gamma_p + \mu + \delta_p,$$

$$K_3 = \phi_s + \gamma_s + \mu + \delta_s, K_4 = \gamma_a + \mu + \delta_a \text{ and } K_5 = \gamma_h + \mu + \delta_h.$$

Let (where, ρ is the spectral radius):

$$\mathbb{R}_v = \rho(FV^{-1}) = \left\{ \frac{\beta\sigma_E\,(S^* + A^*)\,K}{(N^*)\left(\prod_{q=1}^{5} K_q\right)} \right\}, \quad (3.8)$$

where,

$$K = K_3K_4K_5\eta_p + K_3K_5\eta_a\sigma_p(1-r) + K_4K_5\eta_s r\sigma_p + K_4\eta_h\phi_s r\sigma_p. \quad (3.9)$$

The result below follows from Theorem 2 of (van den Driessche and Watmough, 2002).

Theorem 3.3.1. *The disease-free equilibrium* ($\mathcal{E}_0$) *of the model* (3.1) *is locally-asymptotically stable if* $\mathbb{R}_v < 1$*, and unstable if* $\mathbb{R}_v > 1$*.*

The threshold quantity $\mathbb{R}_v$ is the *vaccination reproduction number* of the model (3.1), which measures the average number of new COVID-19 cases generated by a single infectious individual introduced into a population where, a certain proportion is vaccinated. Here, too, the epidemiological consequence of Theorem (3.3.1) is that a small influx of COVID-19 cases will not generate a large outbreak in the community if the vaccination reproduction number ($\mathbb{R}_v$) is maintained at a value less than unity. It is worth noting that in the absence of vaccination and other public health interventions, the vaccination reproduction number ($\mathbb{R}_v$) reduces to the basic reproduction number (denoted by $\mathbb{R}_0$). That is,

$$\mathbb{R}_0 = \mathbb{R}_v|_{V_1^*=V_2^*=V_3^*=0} = \left\{ \frac{\beta\sigma_E K}{\prod_{q=1}^{5} K_q} \right\}.$$

3.3.2 Global asymptotic stability: special cases

In this section, we will explore the global asymptotic stability of the disease-free equilibrium of the model (3.1) for two special cases, as described below.

Special case 1:

Consider the special case of the model (3.1) where, the vaccine being used in the community offers 100% protective efficacy against primary infection and re-infection (i.e., $\varepsilon_{v_i} = \varepsilon_{n_i} = \varepsilon_{nv_i} = 1$; for $i = 1, 2, 3$).

For the aforementioned special case of the model, it can be seen that the associated next generation matrix of new infection terms, denoted by $\tilde{F}$, is given by (that, for

this special case, the next generation matrix of linear transition terms, V, remains the same, as given in (3.7). Furthermore, $N^* = \Pi/\mu$) Safdar *et al.* (2023):

$$\tilde{F} = \begin{bmatrix} 0 & \beta\eta_p\left(\frac{S^*}{N^*}\right) & \beta\eta_s\left(\frac{S^*}{N^*}\right) & \beta\eta_a\left(\frac{S^*}{N^*}\right) & \beta\eta_h\left(\frac{S^*}{N^*}\right) \\ 0 & 0 & 0 & 0 & 0 \\ 0 & 0 & 0 & 0 & 0 \\ 0 & 0 & 0 & 0 & 0 \\ 0 & 0 & 0 & 0 & 0 \end{bmatrix}.$$

The control reproduction number of this special case of the model (3.1), denoted by $\tilde{\mathbb{R}}_v$, is given by:

$$\tilde{\mathbb{R}}_v = \rho(\tilde{F}V^{-1}) = \mathbb{R}_v|_{\varepsilon_v=1} = \left\{ \frac{\beta\sigma_E S^* K}{(N^*)\left(\prod_{q=1}^{5} K_q\right)} \right\} \text{ (with } K \text{ as defined in Equation (3.9)).} \tag{3.10}$$

We claim the following result:

Theorem 3.3.2. *Consider the special case of the model* (3.1) *with* $\varepsilon_{v_i} = \varepsilon_{n_i} = \varepsilon_{nv_i} = 1$ *and* $\tilde{\mathbb{R}}_v \leq 1 - \sum_{i=1}^{3} f_{v_i} < 1$ *for* $i = 1, 2, 3$ *(with* f_{v_i} *as defined in Equation* (3.11)*). The disease-free equilibrium of the special case of the model* ($\mathcal{E}_0$) *is globally-asymptotically stable in* Ω *whenever* $\tilde{\mathbb{R}}_v < 1$.

The proof of Theorem 3.3.2, based on using linear Lyapunov function (Gumel *et al.*, 2021a; Brozak *et al.*, 2021; Iboi *et al.*, 2020a), is given in Appendix F. Epidemiologically-speaking, Theorem 3.3.2 shows that, for the special case of the model (3.1) with $\varepsilon_{v_i} = \varepsilon_{n_i} = \varepsilon_{nv_i} = 1$ (for $i = 1, 2, 3$), the disease can be eliminated from the community if the threshold quantity, $\tilde{\mathbb{R}}_v$, can be brought to (and maintained at) a value less

than unity.

Special case 2:

The global asymptotic stability of the disease-free equilibrium of the model (3.1) can also be established for another special case which entails setting the parameters related to disease-induced mortality (i.e., $\delta_p, \delta_s, \delta_a$ and $\delta_h = 0$) and re-infection (i.e., ε_{n_i} and $\varepsilon_{nv_i} = 1$; with $i = 1, 2, 3$) to zero. Setting $\delta_p = \delta_s = \delta_a = \delta_h = 0$ in the model (3.1), and adding all the equations of the model, shows that $\dfrac{dN}{dt} = \Pi - \mu N$, from which it follows that $N(t) \to \dfrac{\Pi}{\mu}$ as $t \to \infty$. From now on, we replace $N(t)$ with its limiting value, $N^* = \Pi/\mu$ in the model (i.e., the standard incidence formulation for the infection rate is now replaced by a mass action incidence). We claim the following result:

Theorem 3.3.3. *Consider the special case of the model* (3.1) *in the absence of disease-induced mortality (i.e.,* $\delta_p = \delta_s = \delta_a = \delta_h = 0$*) and no re-infection of recovered individuals (i.e.,* $\varepsilon_{n_i} = \varepsilon_{nv_i} = 1$*, with* $i = 1, 2, 3$*). The disease-free equilibrium of this special case of the model* ($\mathcal{E}_0$) *is globally-asymptotically stable in* Ω_{**} *whenever* $\hat{\mathbb{R}}_v < 1$.

The proof of Theorem 3.3.3, based on using a comparison theorem, is given in Appendix G (Safdar *et al.*, 2023).

3.3.3 Vaccine-induced herd immunity threshold

The concept and importance of vaccine-induced (or vaccine-derived) herd immunity threshold has been discussed in detail in Section 2.3.3 (for the case of a model with a single vaccination class). Since vaccine-waning-boosting model (3.1) has three vaccination classes (V_1, V_2 and V_3), accounting for the three levels of vaccine-derived immunity (high, moderate and low), but we will compute the vaccine-derived herd

immunity threshold for the United States with respect to the wholly-susceptible individuals who are fully vaccinated and moved to V_1 class (as it represents the actual fraction of individuals who initially received the full vaccine doses of any of the aforementioned vaccines). Specifically, we let (Safdar *et al.*, 2023)

$$f_{v_1} = \frac{V_1^*}{N^*}, f_{v_2} = \frac{V_2^*}{N^*}, f_{v_3} = \frac{V_3^*}{N^*}, \text{ with } N^* = \frac{\Pi}{\mu}. \tag{3.11}$$

Here, f_{v_1} represents the proportion of susceptible members of the population that have been fully-vaccinated (using any of the three FDA-approved vaccines considered in this dissertation), while f_{v_k} (with $k = 2, 3$) represents the proportion of individuals in the V_k class that have received the booster dose at the disease-free equilibrium ($\mathcal{E}_0$). Using the definition (3.11) in Equation (3.8) gives:

$$\mathbb{R}_v = \left\{ \frac{\beta\sigma_E[1 - (\varepsilon_{v_1} f_{v_1} + \varepsilon_{v_2} f_{v_2} + \varepsilon_{v_3} f_{v_3})]K}{\left(\prod_{q=1}^{5} K_q\right)} \right\},$$

with K as defined in Equation (3.9).

This threshold quantity can be expressed in terms of the basic reproduction number ($\mathbb{R}_0$) of the model, as:

$$\mathbb{R}_v = \left(1 - \sum_{i=1}^{3} \varepsilon_{v_i} f_{v_i}\right) \mathbb{R}_0. \tag{3.12}$$

Setting $\mathbb{R}_v = 1$ in Equation (3.12), and simplifying, gives:

$$\sum_{i=1}^{3} \varepsilon_{v_i} f_{v_i} = \left(1 - \frac{1}{\mathbb{R}_0}\right), \tag{3.13}$$

from which we can solve for the fraction fully-vaccinated (those in V_1 class), at steady-state for the vaccinated class (denoted by f_{v_1}), in terms of the basic reproduction

number, giving:

$$f_{v_1} = \frac{1}{\varepsilon_{v_1}}\left[\left(1-\frac{1}{\mathbb{R}_0}\right)-(\varepsilon_{v_2}f_{v_2}+\varepsilon_{v_3}f_{v_3})\right] = f_{v_1}^c \quad (\text{for } \mathbb{R}_0 > 1). \tag{3.14}$$

It follows from Equation (3.14) that $\mathbb{R}_v < (>)1$ if $f_{v_1} > (<) f_{v_1}^c$. Furthermore, $\mathbb{R}_v = 1$ whenever $f_{v_1} = f_{v_1}^c$. This result is summarized below (Safdar *et al.*, 2023):

Theorem 3.3.4. *Vaccine-induced herd immunity (i.e., COVID-19 elimination) can be achieved in the United States, using any of the three FDA-approved anti-COVID vaccines, if the vaccination program can lead to the vaccination of susceptible individuals resulted in $f_{v_1} > f_{v_1}^c$ (i.e., if $\mathbb{R}_v < 1$). If $f_{v_1} < f_{v_1}^c$ (i.e., if $\mathbb{R}_v > 1$), then the vaccination program will fail to eliminate the COVID-19 pandemic.*

The epidemiological implication of Theorem 3.3.4 is that the use of any of the three approved COVID-19 vaccines (considered in this dissertation) can lead to the elimination of the pandemic in the United States if the proportion of susceptible individuals fully-vaccinated and with high level of vaccine-derived immunity (i.e., those in V_1 class) at steady-state reached or exceeded the aforementioned critical threshold values. In other words, the SARS-CoV-2 pandemic is predicted to be eliminated in the United States if $f_{v_1} > f_{v_1}^c$. On the contrary, the Vaccination program will fail to eliminate the pandemic if the proportion vaccinated at the disease-free equilibrium falls below the aforementioned critical herd immunity thresholds.

It should be mentioned that since the Pfizer and Moderna vaccines offer protective efficacy of about 95% and 94%, respectively (Pearson, 2021), and the Johnson & Johnson vaccine offers a protective efficacy of about 67% (Mancuso *et al.*, 2021), we set the average vaccine protective efficacy for individuals in the V_1 class to be (Safdar *et al.*, 2023)

$$\varepsilon_{v_1} = \frac{0.95+0.94+0.67}{3} \approx 0.85. \tag{3.15}$$

It is worth mentioning that the expression (3.15), for the average vaccine protective efficacy, is a dynamic quantity that depends on the actual combinations of SARS-CoV-2 vaccines adopted in the community at time t (it should be mentioned that, in deriving the estimate for ε_{v_1} in Equation (3.15), we used the values of the respective efficacies of the three vaccines estimated in (Pearson, 2021; Mancuso *et al.*, 2021) during the period around October, 2020 to January, 2021). Table 3.5 summarizes the assumed baseline efficacy levels for average vaccine-derived and natural immunity to be used in our numerical simulations. Using the baseline values of the fixed and fitted parameters in Tables $3.3 - 3.4$, together with the baseline average vaccine-derived and natural immunity protective efficacy levels in Table 3.5, it follows from Equation (3.14) that the critical vaccine-derived herd immunity threshold for each of the vaccinated compartment is given, by $f_{v_1}^c \approx 0.72$. The value of $f_{v_1}^c$ is computed by substituting the values of f_{v_2} and f_{v_3} from Equation (3.11) (i.e., $f_{v_2} = 0.01589$ and $f_{v_3} = 0.00066$, computed using the baseline parameter values in Tables $3.3 - 3.5$). In other words, based on the parameterization of the model (3.1) with the recent case data for Omicron BA.1 variant in the United States, population-level herd immunity can be achieved in the United States if at least 72% of the wholly-susceptible individuals are fully vaccinated (i.e., 72% of individuals in the S class are fully-vaccinated and moved to the V_1 class).

Figure 3.2 depicts contour plot of the vaccination reproduction number ($\mathbb{R}_v$), as a function of average vaccination efficacy (ε_{v_1}) and coverage of fully-vaccinated individuals at steady-state (f_{v_1}). It follows from the above plot that, for the overall vaccine-protective efficacy set at 85% (as stated above), at least 72% of the wholly-susceptible population need to be vaccinated at steady-state to bring the vaccination reproduction number ($\mathbb{R}_v$) below one (Figure 3.2). Under this setting, the computed

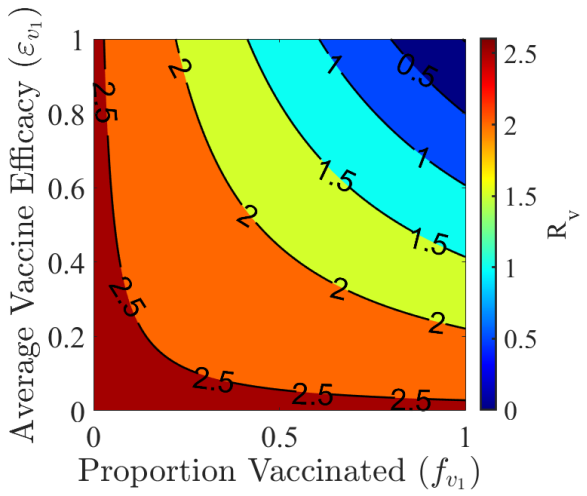

Figure 3.2: Contour Plot of the Vaccine Reproduction Number ($\mathbb{R}_v$) of the Model (3.1), as a Function of Vaccine Coverage at Steady-State (f_{v_1}) and Average Vaccine Efficacy (ε_{v_1}), for the United States. Vaccination of Wholly-susceptible Individuals ($S(t)$; f_{v_1} Is Proportion of Wholly-susceptible Individuals Who Are Fully-vaccinated at Steady-state). Parameter Values Used in These Simulations Are as given by Their Respective Baseline Values in Tables 3.3 − 3.5 (Safdar *et al.*, 2023).

value of the control reproduction number ($\mathbb{R}_v$), obtained using the baseline parameter values in Tables 3.3 − 3.5, is $\mathbb{R}_v \approx 0.97$. Similarly, the computed value of the basic reproduction number ($\mathbb{R}_0$) is $\mathbb{R}_0 \approx 2.59$. In summary, the results depicted in Figure 3.2 show that population-level herd immunity can be achieved in the United States *via* the implementation a vaccination program (based on using any of the three aforementioned approved vaccines) that emphasizes the full vaccination of a sizable proportion of the susceptible pool (at least 72%). Overall, our study shows that, for the case where the average protective immunity offered by the vaccines for fully-vaccinated individuals in the V_1 class is 85%, vaccine-derived herd immunity can be achieved in the United States if at least 72% of the susceptible population is fully-vaccinated (with any of the three aforementioned FDA-approved anti-COVID vaccines) (Safdar *et al.*, 2023).

It should be mentioned that for the case when the high level of the vaccine-induced

efficacy for individuals in the V_1 class is decreased to 65%, for instance (while the vaccine protective efficacy for individuals in the V_2 and V_3 classes remain at the baseline level), our simulations showed that at least 93% of the wholly-susceptible population need to be fully-vaccinated. Thus, this study shows that lower protective efficacy of the vaccine (for fully-vaccinated individuals) incurs higher requirement for the vaccination coverage of the susceptible population to achieve herd immunity. Vaccinating 93% of the wholly-susceptible population is, of course, not realistically feasible in large populations, such as the United States. Hence, it is imperative that highly efficacious vaccines are developed and used. In other words, using vaccines with higher protective efficacy (e.g., vaccines with 85% protective efficacy, as computed in Equation (3.15)) incurs lower, and realistically attainable, requirement for the vaccination coverage (about 72%). As of March 12, 2023, data from the CDC shows that about 69% of the United States population is fully-vaccinated (Centers for Disease Control and Prevention, 2023a). Thus, this chapters shows that the prospect of achieving vaccine-derived herd immunity using any of the three vaccines considered in this dissertation (i.e., Pfizer vaccine, Moderna vaccine, and Johnson & Johnson vaccine) is promising if the coverage is moderate enough, provided the average vaccine efficacy offered by the aforementioned three vaccines is high enough.

3.4 Data Fitting and Parameter Estimation

In this section, the model (3.1) was fitted by using the available data for the observed daily new COVID-19 cases for the United States (for the period November 28, 2021 – February 23, 2022). The model (3.1) has several parameters, some of which are known from the literature (as tabulated in Table 3.3) and the remaining unknown parameters are obtained by fitting the model (3.1) with the daily new case data obtained from the Johns Hopkins University COVID-19 repository (Dong *et al.*, 2020).

The model was fitted using a standard nonlinear least squares approach (as described in Section 2.2.1). The unknown parameters which are estimated from the fitting are presented in Table 3.4.

The overall methodology of the data fitting procedure is same as discussed in Section 2.2.1. The results obtained, depicted in Figure 3.3, shows a very good fit for the model output (blue curve) and the observed daily new case data (red dots). The data for the second segment of the data, for the period from February 24, 2022 to March 23, 2022, was used for the cross validation of the fitted data. This also shows a very good fit for the model output (green curve) and for the remaining data points of the observed data (red dots) of Figure 3.3. This segment of the Figure 3.3 clearly shows that the model (3.1) cross validates the observed daily new case data for the period from February 23, 2022 to March 23, 2022 perfectly (solid green curve). Furthermore, we show, in this figure, the prediction of the model for the daily COVID-19 new cases for approximately a five-week period after March 24, 2022 (i.e., the region to the right of the dashed vertical black line), as illustrated by the solid magenta curve in Figure 3.3 (Safdar *et al.*, 2023).

Parameter	Value	Source
σ_E	1/5 day^{-1}	Ngonghala *et al.* (2023)
σ_p	1/2 day^{-1}	Linton *et al.* (2020)
r	0.095 (dimensionless)	Weintraub (2022)
ϕ_s	1/5 day^{-1}	Ngonghala *et al.* (2023)
γ_s	1/10 day^{-1}	Gumel *et al.* (2021b); Mancuso *et al.* (2021)
γ_a	1/5 day^{-1}	Gumel *et al.* (2021b); Mancuso *et al.* (2021)
γ_h	1/8 day^{-1}	Gumel *et al.* (2021b); Mancuso *et al.* (2021)
η_p	5/4 (dimensionless)	Gumel *et al.* (2021b)
η_s	1 (dimensionless)	Gumel *et al.* (2021b)
η_a	3/2 (dimensionless)	Gumel *et al.* (2021b)
η_h	3/4 (dimensionless)	Gumel *et al.* (2021b)
ξ_v	1.9×10^{-5} day^{-1}	Bosman *et al.* (2021)
Π	12000 day^{-1}	Gumel *et al.* (2021b)
μ	3.4×10^{-5} day^{-1}	Ngonghala *et al.* (2021b)
δ_p	0 day^{-1}	Tan *et al.* (2021)
ω_{v_1}	1/274 day^{-1}	Curley (2021)
ω_{v_2}	1/365 day^{-1}	Curley (2021)
ω_{v_3}	1/365 day^{-1}	Curley (2021)
ω_{n_1}	1/274 day^{-1}	Curley (2021)
ω_{n_2}	1/365 day^{-1}	Curley (2021)
ω_{n_3}	1/365 day^{-1}	Curley (2021)
ω_{nv_1}	1/548 day^{-1}	Assumed
ω_{nv_2}	1/730 day^{-1}	Assumed
ω_{nv_3}	1/730 day^{-1}	Assumed
ρ_{v_2}	1/14 day^{-1}	Gregory and Salenetri (2022); Thompson (2022)
ρ_{v_3}	1/14 day^{-1}	Gregory and Salenetri (2022); Thompson (2022)
ρ_{n_2}	1/14 day^{-1}	Gregory and Salenetri (2022)
ρ_{n_3}	1/14 day^{-1}	Gregory and Salenetri (2022)
δ_h	5.0×10^{-5} day^{-1}	Ngonghala *et al.* (2021b)
δ_a	0 day^{-1}	Desmon (2022)

Table 3.3: Baseline Values of the Fixed Parameters of the Model (3.1) (Safdar *et al.*, 2023).

Furthermore, in fitting the model to observed daily new case data for the United

States, the average efficacies for individuals in the V_i classes (with $i = 1, 2, 3$) were set to their respective values in Table 3.5. Specifically, the value of the average vaccine efficacy for individuals in the V_1 class (ε_{v_1}) is set at 85% based on the expression given in Equation (3.15). The estimate for the average vaccine efficacy for individuals in the V_2 class (ε_{v_2}) was adapted from the empirical studies in (Lin *et al.*, 2022; Andrews *et al.*, 2022b). First of all, these studies show variations in the timing of the attainment of the residual efficacy (after a few months of receipt of COVID-19 vaccination), which depend on the type of vaccine (Pfizer, Moderna or Johnson & Johnson). Further, the studies showed that the vaccine-derived efficacy of the Johnson & Johnson vaccine dropped from the initial 74.8% to 59.4% after five months of the receipt of the single-dose (Lin *et al.*, 2022). Similarly, the protective efficacy of the Pfizer vaccine decreased from 94.5% to 75.7% after 8 months of the receipt of the full doses of the Pfizer vaccine (Andrews *et al.*, 2022b). Finally, the efficacy of the Moderna vaccine decreased from 95.5% to 84.3% after 5 months of full vaccination (Andrews *et al.*, 2022b). Based on these estimates, we considered it plausible to set the average vaccine efficacy for individuals in the V_2 class to be 50%.

Additionally, numerous empirical studies have shown that the effectiveness of the Pfizer and Moderna vaccines against symptomatic COVID-19 is less than 20% for the Omicron variant after the administration of the second dose of the vaccine (Sidik, 2022; Tan *et al.*, 2022). Consequently, it deems reasonable to set the average vaccine-derived efficacy for individuals in the V_3 class to be about 20%. Moreover, an empirical study showed that individuals who received the second booster dose of the Pfizer or Moderna vaccine have their vaccine effectiveness against the acquisition of breakthrough infection increased from 19% to 49% (Grewal *et al.*, 2022). This is in line with the assumption in our model formulation regarding the transition of individuals

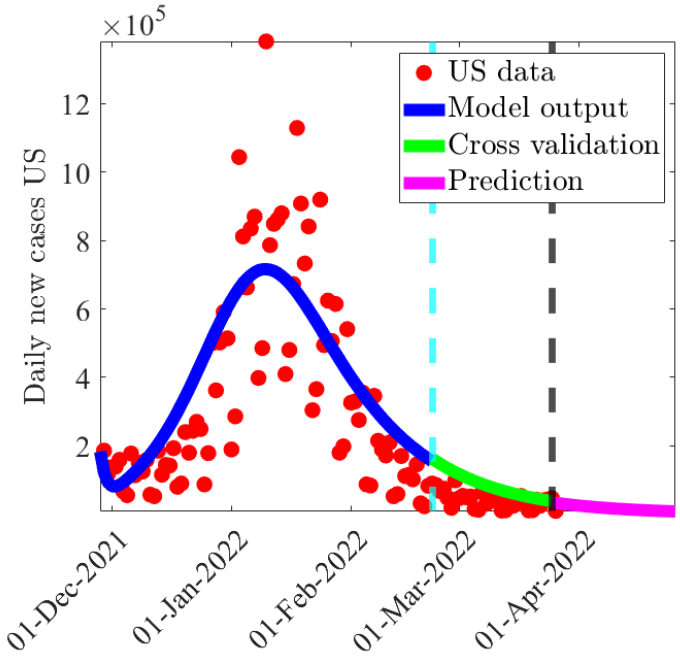

Figure 3.3: Time Series Illustration of the Least Squares Fit of the Model (3.1), Showing the Model's Output For The Daily New Cases in the United States (Blue Curve) Compared to the Observed Daily Confirmed Cases for the United States (Red Dots) from November 28, 2021 to February 23, 2022 (Segment to the Left of the Dashed Vertical Cyan Line), Using the Fixed, Estimated and Assumed Baseline Parameter Values given in Tables 3.3, 3.4 and 3.5 Respectively. The Segment from February 24, 2022 to April 30, 2022 (i.e., Solid Green and Magenta Curves or the Entire Segment to the Right of the Dashed Cyan Vertical Line) Illustrates the Performance of the Model (3.1) in Predicting the Daily New Cases in the United States (Safdar *et al.*, 2023).

from the V_3 class (where, the average efficacy was set to be 20%) to the V_2 class (where, the average vaccine efficacy is set at 50%).

3.5 Numerical Simulations

The model (3.1) will now be simulated to assess the population-level impact of waning and boosting of vaccine-derived and natural immunity on the dynamics of the Omicron variant in the United States. Unless otherwise stated, the simulations will be carried out using the baseline values of the parameters tabulated in Tables 3.3 – 3.5.

Parameter	Estimated Value	95% Confidence Interval
β	0.2551 day^{-1}	$[0.2551 - 0.2556]$ day^{-1}
ρ_{nv_2}	0.6999 day^{-1}	$[0.0769 - 0.6999]$ day^{-1}
ρ_{nv_3}	0.0989 day^{-1}	$[0.0100 - 0.0989]$ day^{-1}
δ_s	4.9989×10^{-5} day^{-1}	$[1.0 \times 10^{-6} - 4.9 \times 10^{-5}]$ day^{-1}

Table 3.4: Baseline Values of Fitted (Estimated) Parameters and Confidence Intervals (CIs) of the Model (3.1), Obtained by Fitting the Model with the Observed Daily New Case COVID-19 Data for the United States for the Period November 28th, 2021 to February 23rd, 2022 (Safdar *et al.*, 2023).

Vaccine Efficacy of V_n class	Vaccine Efficacy of R_n class	Vaccine Efficacy of R_n class
$\varepsilon_{v_1} = 0.85$	$\varepsilon_{n_1} = 0.85$	$\varepsilon_{nv_1} = 0.95$
$\varepsilon_{v_2} = 0.50$	$\varepsilon_{n_2} = 0.50$	$\varepsilon_{nv_2} = 0.50$
$\varepsilon_{v_3} = 0.20$	$\varepsilon_{n_3} = 0.20$	$\varepsilon_{nv_3} = 0.20$

Table 3.5: Assumed Baseline Levels of the Parameters for the Efficacy of the Vaccine-derived and Natural Immunity (Safdar *et al.*, 2023).

3.5.1 Assessing the impact of waning of vaccine-derived immunity: with and without boosting

To assess the impact of waning of vaccine-derived immunity for this scenario, the model (3.1) is simulated using the following three (arbitrary) levels of the parameters related to the waning of vaccine-derived immunity in the population (Safdar *et al.*, 2023):

(i) Low level of waning of vaccine-derived immunity: here, it is considered vaccine-derived immunity to wane within 48 months (i.e., we set $\omega_{v_1} = \omega_{v_2} = \omega_{v_3} = 0.0007$ *per* day) but parameters related to natural immunity and combined natural and vaccine-derived immunity are maintained at baseline level.

(ii) Baseline level of waning of vaccine-derived immunity: in this case, waning of vaccine-derived immunity is set to occur within 9 months (so that, $\omega_{v_1} = \omega_{v_2} =$

$\omega_{v_3} = 0.0037$ *per* day) but parameters related to natural immunity and combined natural and vaccine-derived immunity are maintained at baseline level.

(iii) High level of waning of vaccine-derived immunity: in this scenario, it is assumed that vaccine-derived immunity wanes within 3 months (i.e., $\omega_{v_1} = \omega_{v_2} = \omega_{v_3} = 0.0110$ *per* day), but parameters related to natural immunity and combined natural and vaccine-derived immunity are maintained at baseline level.

For these simulations, all other parameters of the model (including those that involve the waning of natural immunity, as stated above) are maintained at their baseline values (given in Tables 3.3 − 3.5). Furthermore, these simulations are carried in the absence and presence of boosting of vaccine-derived immunity (recall that boosting of vaccine-derived immunity, maintained at baseline level, is achieved *via* the administration of the required doses of any of the approved SARS-CoV-2 booster vaccines used in the United States).

The simulation results obtained, depicted in Figure 3.4. First of all, these simulations also depict the fitting of the model's output for the daily new cases with the observed COVID-19 data (used in Section 3.4) for the baseline scenario (as shown by the blue curves and the red dots in Figure 3.4). Furthermore, these simulations show that, in the absence of boosting of vaccine-derived immunity, waning of vaccine-derived immunity generally induces only a marginal impact on the average number of new daily COVID-19 cases in the United States, for each of the three waning levels considered in our simulations, in comparison to the baseline scenario. For example, under the fast waning scenario for vaccine-derived immunity (i.e., vaccine-derived immunity wanes within three months, but natural immunity is maintained at its baseline level) and no boosting of vaccine-derived immunity is implemented, the simulations show a marginal (about 2%) increase in the peak level of the daily new cases, in comparison

to the peak baseline level (this is evident by comparing the blue and magenta curves in Figure 3.4(a), and the zoomed-in version of the segments of the curves near the peaks shown in Figure 3.4(b)). For the slow waning scenario (i.e., if the vaccine-derived immunity wanes within 48 months, but natural immunity is maintained at baseline level), the increase in daily new cases at the peak (in comparison to the baseline) reduces to about 1.4% (compare the blue and green curves in Figures 3.4(a) and (b)).

In the presence of boosting of vaccine-derived immunity (at baseline level), the simulations show a significant reduction in the average number of daily new cases at the peak recorded under the above waning scenarios without boosting of vaccine-derived immunity. For instance, for the case where vaccine-derived immunity wanes within three months (but natural immunity is maintained at baseline level), boosting of vaccine-derived immunity at the baseline level significantly reduces the increase in daily new cases at the peak (by about 68%), in comparison to the corresponding case without boosting of vaccine-derived immunity (compare the blue and magenta curves in Figure 3.4(c), and the corresponding zoomed-in portions of the curves near the peaks shown in Figure 3.4(d)). Furthermore, under the slow waning scenario, boosting of vaccine-derived immunity at baseline level further increases the reduction in the peak daily new cases (compare the green and blue curves in Figures 3.4(c) and (d)).

The model (3.1) is further simulated to assess the impact of waning and boosting of vaccine-derived immunity (for the case where natural immunity is maintained at baseline) for the following two scenarios (Safdar *et al.*, 2023):

Scenario (a): Waning near the baseline level and slow boosting. Here, it is assumed that the waning of vaccine-derived immunity range between 6 to 12 months

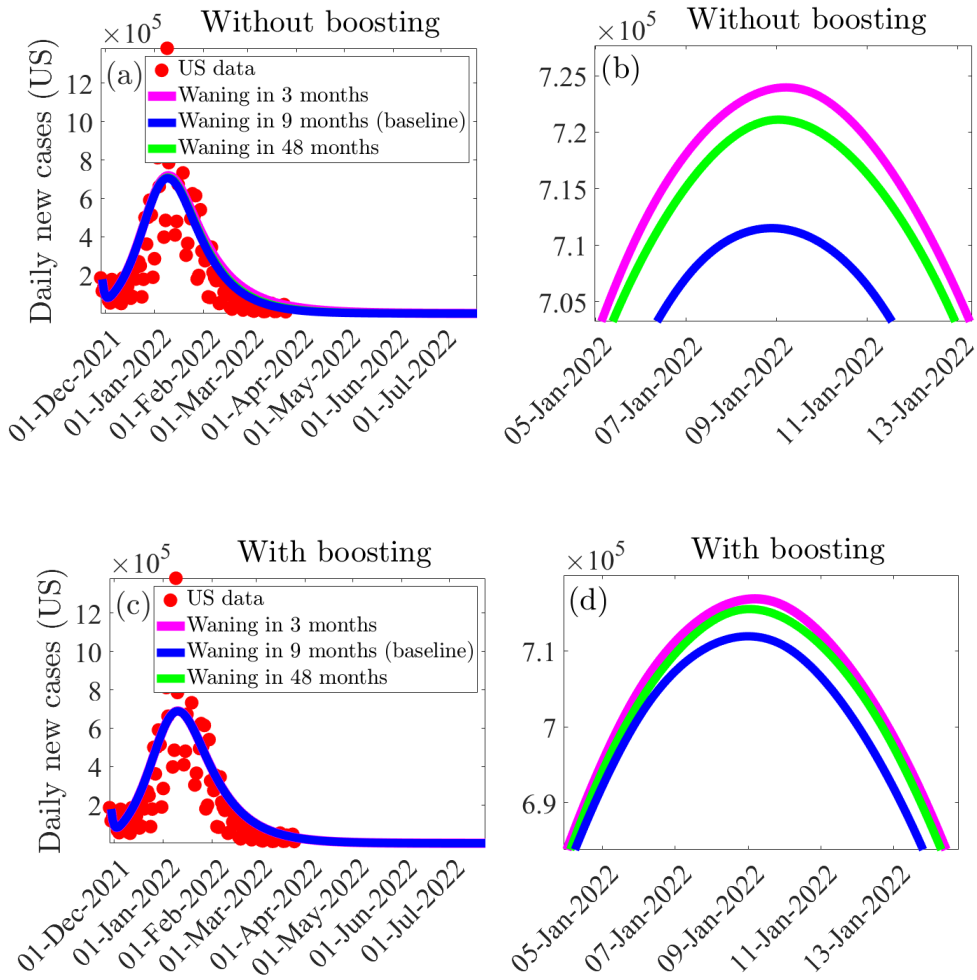

Figure 3.4: Simulations of the Model (3.1) to Assess the Population-level Impact of Waning of Vaccine-derived Immunity in the Absence and Presence of Boosting of Vaccine-derived Immunity (Maintained at Baseline Level). $(a) - (d)$: Average Number of New Daily Cases at the Peak in the Absence ((a) and (b)) and Presence ((c) and (d)) of Boosting of Vaccine-derived Immunity. Three Levels of Waning of Vaccine-derived Immunity Were Considered: Vaccine-derived Immunity Wanes in Three Months (Magenta Curves), Nine Months (Blue Curves) and Forty Eight Months (Green Curves). Zoomed-in Versions of the Portions of the Curves near the Peaks Depicted in Figures (a) and (c) Are Shown in Figures (b) and (d), Respectively. The Values of the Other Parameters of the Model Used in These Simulations Are as given in Tables 3.3 – 3.5 (Safdar *et al.*, 2023).

(i.e., near the baseline level of 9 months) and the duration of boosting of vaccine-derived immunity range from 20 days to 100 days.

Scenario (b): Waning near the baseline level and boosting near the base-

line level. Under this scenario, vaccine-derived immunity wanes within the same 6 to 12 months period (as in Scenario (a)), but boosting of vaccine-derived immunity is accelerated to be implemented within 8 to 20 days (i.e., near the baseline level of 14 days).

The results obtained are depicted in the form of heat maps for the vaccination reproduction number ($\mathbb{R}_v$) of the model (3.1), as a function of the rates of waning (ω_v) and boosting (ρ_v) of vaccine-derived immunity in Figure 3.5. This figure shows that, for the waning rate near the baseline value and slow boosting scenario (i.e., Scenario (a)), the values of the vaccination reproduction number lie in the range $\mathbb{R}_v \in [0.99, 1.44]$ (with a mean of $\mathbb{R}_v \approx 1.21$), suggesting that the disease will persist in the population (this is in line with the theoretical result given in Theorem 3.3.1). In other words, this result shows that waning at baseline level and slower boosting, in comparison to waning and boosting at baseline levels, increases the prospect for disease persistence in the population. For Scenario (b), the simulations (Figure 3.5(b)) show a marked decrease in the range of the reproduction number, with $\mathbb{R}_v \in [0.95, 1.04]$ (with a mean of $\mathbb{R}_v \approx 0.99$), suggesting possible elimination of the pandemic (in line with Theorems 2.3.1 $-$ 3.3.1). Thus, boosting of vaccine-derived (near the baseline rate) enhances the prospect for pandemic elimination.

In summary, while the simulations in this section show that waning of vaccine-derived immunity generally induces only a marginal impact in the average number of new cases at the peak of the COVID-19 pandemic, boosting of vaccine-derived immunity (maintained at its baseline level) resulted in a dramatic reduction in the average number of new cases at the peak, in comparison to the case where boosting is not implemented. Furthermore, delay in boosting of vaccine-derived immunity, in com-

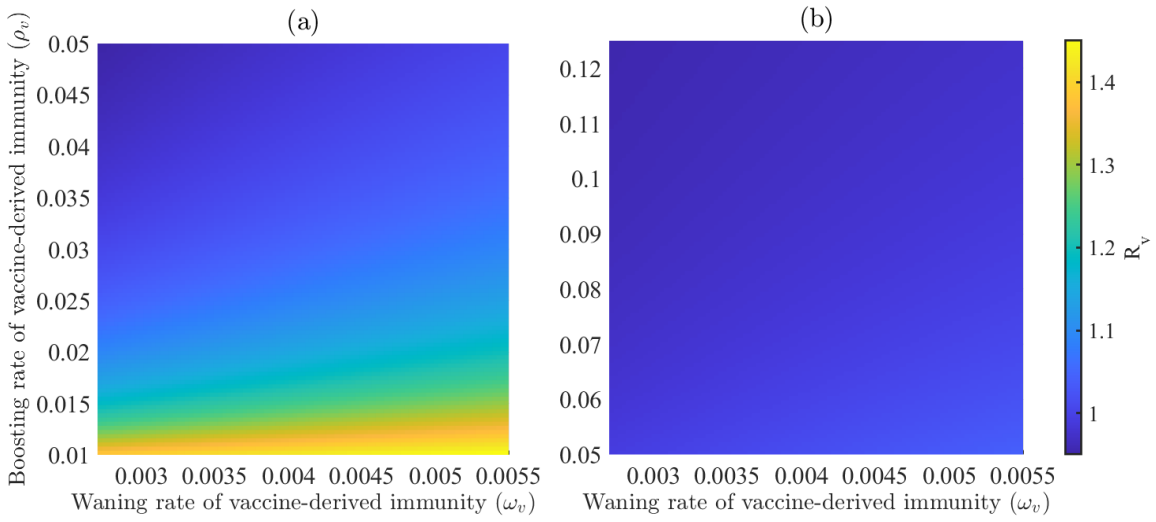

Figure 3.5: Effect of Waning and Boosting of Vaccine-derived Immunity. Heat Maps of the Vaccination Reproduction Number ($\mathbb{R}_v$), as a Function of the Rates of Waning (ω_v) and Boosting (ρ_v) of Vaccine-derived Immunity. (a) Waning of Vaccine-derived Immunity Range Between 6 to 12 Months, and Duration of Boosting of Vaccine-derived Immunity Range from 20 Days to 100 Days (Slow Boosting). (b) Waning of Vaccine-derived Immunity Range from 6 to 12 Months, While Duration of Boosting of Vaccine-derived Immunity Range from 8 to 20 Days (Fast Boosting) (Safdar *et al.*, 2023).

parison to the baseline level of boosting, could alter the trajectory of the disease from possible elimination (as measured by the vaccine reproduction number, $\mathbb{R}_v$, taking a value less than one) to persistence of the disease (as measured by the reproduction number being greater than one).

3.5.2 Assessing the effect of waning of natural immunity: with and without boosting

Natural immunity can be boosted *via* treatment or the use of other immune-boosting supplements (Mrityunjaya *et al.*, 2020; Alagawany *et al.*, 2021). To assess the impact of waning of natural immunity, the model (3.1) is simulated using the following (arbitrarily-chosen) waning levels (Safdar *et al.*, 2023):

(i) Low level of waning of natural immunity: here, too, it is considered natural immunity to wane within 48 months (i.e., we set $\omega_{n_1} = \omega_{n_2} = \omega_{n_3} = 0.0007$ *per* day), but vaccine-derived immunity and combined natural and vaccine-derived immunity are kept at baseline.

(ii) Baseline waning of natural immunity: in this case, waning of natural immunity is set to occur within 9 months (so that, $\omega_{n_1} = \omega_{n_2} = \omega_{n_3} = 0.0037$ *per* day), but vaccine-derived immunity and combined natural and vaccine-derived immunity are kept at baseline.

(iii) High level of waning of natural immunity: here, too, natural immunity is assumed to wane within 3 months (i.e., $\omega_{n_1} = \omega_{n_2} = \omega_{n_3} = 0.0110$ *per* day), but vaccine-derived immunity and combined natural and vaccine-derived immunity are kept at baseline.

For the simulations in this section, all other parameters (including those related to the waning of vaccine-derived immunity and combined waning of natural and vaccine-derived) are set to their baseline values (given in Tables 3.3 − 3.5). The simulation results obtained, depicted in Figure 3.6, also showed that waning of the natural immunity general only induces a marginal increase in the average number of new daily COVID-19 cases in the United States, in comparison to the baseline scenario (where, the waning of natural immunity is assumed to occur within 9 months). In particular, if natural immunity wanes within three months and no boosting of natural immunity is implemented, the average number of new daily cases at the peak increases by about 3.7%, in comparison to the baseline scenario (compare the blue and magenta curves in Figure 3.6(a), and the zoomed-in portions of the curves near the peaks, depicted in Figure 3.6(b)). An additional marginal increase in the average number of new daily cases at the peak is recorded under the slow waning scenario for the

natural immunity, in comparison to the baseline scenario (compare the blue and green curves in Figures 3.6(a) and (b)). However, if natural immunity is boosted (at

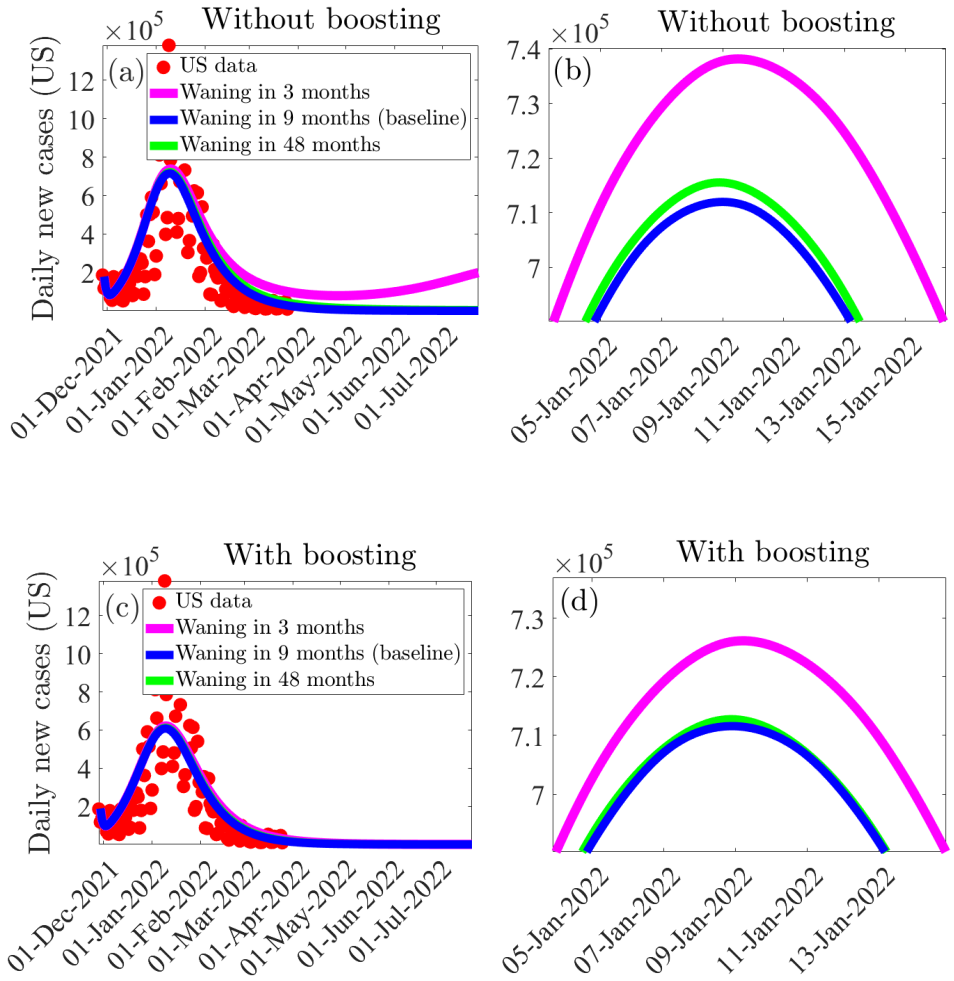

Figure 3.6: Simulations of the Model (3.1) to Assess the Population-level Impact of Waning of Natural Immunity for the Case with and Without Boosting of Natural Immunity (at the Baseline Level). $(a)-(d)$: Average Number of New Daily Cases at the Peak in the Absence ((a) and (b)) Presence ((c) and (d)) of Boosting of Natural Immunity. Three Levels of Waning of Natural Immunity Were Considered: Natural Immunity Wanes in Three Months (Magenta Curves), Nine Months (Blue Curves) and Forty Eight Months (Green Curves). Zoomed-in Versions of the Portions of the Curves near the Peaks Depicted in Figures (a) and (c) Are Shown in Figures (b) and (d), Respectively. The Values of the Other Parameters of the Model Used in These Simulations Are as given in Tables 3.3 − 3.5 (Safdar *et al.*, 2023).

baseline level), our simulations show a marked reduction in the increase in the average daily new cases recorded at the peak, in comparison to the corresponding scenario

without boosting of the natural immunity. Specifically, when natural immunity wanes within three months and boosting of natural immunity is implemented (maintained at its baseline level), the increase in the average number of new daily cases at the peak (in comparison to the baseline) reduces to about 2.1% (compare the blue and magenta curves in Figure 3.6(c), and the zoomed-in portions near the peak depicted in Figure 3.6(d)). This represents an approximately 45.3% reduction in the average daily new cases at the peak, in comparison to the corresponding scenario where natural immunity is not boosted. It should be mentioned that boosting of vaccine-derived immunity (at baseline) plays a more significant role in reducing the average number of new daily cases, in comparison to the corresponding boosting of natural immunity (this can be seen by comparing the corresponding peaks in Figures 3.4 and 3.6). In particular, while boosting of vaccine-derived immunity (at baseline) will lead to about 68% reduction in the number of new daily cases at the peak, boosting of natural immunity (at baseline) will lead to about 45% reduction in the number of new daily cases at the peak). Further significant reductions in the average number of new daily cases are recorded if the natural immunity wanes at a slower rate (compare the blue and green curves in Figures 3.6(a) and (c) or (b) and (d), without and with boosting of natural immunity).

In summary, like in the case of waning of vaccine-derived immunity discussed in Section 3.5.1, the simulations in this section show that while the waning natural immunity only causes a marginal increase in the average number of new cases at the peak, boosting natural immunity (at baseline) resulted in a significant reduction in the average number of new cases recorded at the peak, in comparison to the scenario where a strategy for boosting of natural immunity is not implemented in the community.

3.6 Discussion and Conclusions

The COVID-19 pandemic, caused by SARS-CoV-2, has made a significant impact on public health and the economy of almost every nation on earth since its emergence in December of 2019. The United States became the epicenter of the pandemic since late May, 2020 (recording the highest numbers of cumulative cases, hospitalizations and deaths). As of March 19, 2023, the virus had caused over 105 million cumulative daily new cases and over 1.1 million deaths in the United States (Worldometer., 2023; Dong *et al.*, 2020). The rapid development, deployment, and administration of several safe and highly effective vaccines contributed significantly in curbing the spread of the virus worldwide. Three of these vaccines (the Pfizer-BioNTech, Moderna and Johnson & Johnson vaccines) have been approved by the FDA for use in the United States. The effectiveness of these vaccines in combating COVID-19 has been negatively affected by the emergence of various variants of SARS-CoV-2 (e.g., the Delta and Omicron variants). In particular, the Omicron (B.1.1.529) variant was declared a variant of concern by the World Health Organization in late November, 2021 (Thakur and Kanta Ratho, 2021), due to its exceptionally high transmissibility. Although all the available vaccines were developed for the original SARS-CoV-2 virus strain, they have been able to offer some level of cross-protection against other variants of concern. Furthermore, multiple studies have shown that the efficacy of vaccine-derived immunity wanes over time (Curley, 2021; Dan *et al.*, 2021; Gumel *et al.*, 2021b; Ngonghala *et al.*, 2023). In order to overcome the waning effect of vaccine-derived immunity, booster vaccines were recommended by the CDC in November 2021 (Ferdinands *et al.*, 2022; Centers for Disease Control and Prevention and others, 2021).

In this chapter, a novel mathematical model is developed to assess the population-

level impact of the waning and boosting of vaccine-derived and natural immunity against the Omicron BA.1 variant of SARS-CoV-2 in the United States. The model was parameterized by fitting it to the observed cumulative COVID-19 case data for the United States for the period from November, 28, 2021 to February 23, 2022 (Dong *et al.*, 2020). We used the remaining segment of the available data (i.e., the segment from February 24, 2022 to March 23, 2022) to cross validate the model. This cross validation, together with simulations involving the new daily COVID-19 cases, showed a good match to the observed data.

The model was rigorously analyzed to gain qualitative insight into the dynamics and burden of the diseases. The analysis showed that the disease-free equilibrium (DFE) of the model is locally-asymptotically stable whenever the vaccination reproduction number (denoted by $\mathbb{R}_v < 1$) is below one. Using the baseline values of the fixed and estimated parameters of the model, we computed the numerical value of $\mathbb{R}_v$ during the period of the emergence and circulation of the Omicron variant (starting from late November of 2021). The computed value was $\mathbb{R}_v = 0.97$ (suggesting that Omicron was on a downward trajectory towards elimination in the United States). The numerical value of the basic reproduction number of the model (which is computed in the absence of any control measure implemented) was $\mathbb{R}_0 = 2.59$. The computed value of $\mathbb{R}_0$ falls within the estimated range of $\mathbb{R}_0$ values for Omicron presented in several modeling studies (such as those in Ngonghala *et al.* (2023); Safdar *et al.* (2023); Elliott *et al.* (2022a,b); Kim *et al.* (2022)). We showed that the disease-free equilibrium of the model is globally-asymptotically for two special cases ((a) when the vaccines offer 100% protection against acquisition of infection and no reinfection and (b) disease-induced mortality is negligible and reinfection does not occur) when the associated vaccination reproduction number is less than one. The epidemiological implication of this global asymptotic stability result is that the SARS-CoV-2 pandemic can be

eliminated if the the associated vaccination reproduction number can be brought to (and maintained at) a value less than one (in other words, having the value of this reproduction threshold less than one is necessary and sufficient for the elimination of the pandemic in the United States).

Explicit expression for the vaccine-induced herd immunity threshold was derived, and it was showed, using current data for COVID-19 cases in the United States, that, for the case where the three vaccines offer 85% average protective efficacy against the Omicron variant, vaccine-derived herd immunity will be achieved in the United States if about 72% of the wholly-susceptible population are fully vaccinated (with three FDA-approved vaccines considered in this dissertation). On the other hand, if the average protective efficacy offered by the three vaccines is reduced to a lower level, such as 65% (as against 85% above), at least 93% of the wholly-susceptible population need to be vaccinated to achieve herd immunity. Furthermore, if the average vaccine efficacy offered by the aforementioned three vaccines drops to around 50% (or drops to a much lower value, as presented by Bar-On *et al.* (2021), or as stated in several studies on the effectiveness of these vaccines against Omicron (Buchan *et al.*, 2022; Tseng *et al.*, 2022; Chemaitelly *et al.*, 2022; Sidik, 2022)), then almost 100% of the wholly-susceptible population need to be vaccinated in order to achieve vaccine-derived herd immunity in the United States. This very high level of vaccination coverage (i.e., vaccinating almost 100% of the susceptible population) is not realistically attainable, especially in large populations such as the United States. Data related to COVID-19 from the United States Centers for Disease Control and Prevention show that, as of March 9, 2023, about 69.3% of the United States population was fully-vaccinated (Centers for Disease Control and Prevention, 2023a; Center for Disaster Philanthropy, 2023). Thus, the numerical simulations suggest that, for the scenario that the three

vaccines offer the reasonably high average protective efficacy of 85% against acquisition of infection, herd immunity can realistically achieved in the United States by fully-vaccinating a moderate proportion (about 72%) of the wholly-susceptible.

We conducted extensive numerical simulations to assess the impact of waning and boosting of vaccine-derived and natural immunity for each three arbitrarily selected waning scenarios (slow, baseline, and fast). Based on these simulations, that in the absence of boosting of vaccine-derived and natural immunity, waning of vaccine-derived and natural immunity only causes a marginal increase in the average number of daily cases (at the peak), in comparison to the baseline scenario. In other words, we showed that waning of either vaccine-derived or natural immunity (or both) has only marginal impact, for each of the three waning scenarios considered in this chapter, on the dynamics of the SARS-CoV-2 pandemic (as measured in terms of increases in the average number of daily new cases recorded at the peak, in comparison to the case where baseline values of all the parameters of the model are used).

It was also showed that if fully-vaccinated individuals with moderate or low level of vaccine-derived immunity are boosted (at baseline level), the effect of waning of immunity is a lot less pronounced, in comparison to the baseline scenario (in other words, dramatic reductions in the increase in the average number of daily new cases at the peak recorded under the three waning scenarios) are achieved if both immunity types are boosted at baseline level, in comparison to the corresponding scenarios where the immunity wanes but no boosting is implemented. It is further showed that boosting of vaccine-derived immunity is more beneficial (in reducing average number of new cases) than boosting of natural immunity. Specifically, for the fast waning scenario, boosting of vaccine-derived immunity (at baseline level) resulted in an approximate 68% reduction in the average number of new daily cases at the peak, while boosting

of natural immunity resulted in about $\approx 45\%$ reduction in the number of new daily cases at the peak (in comparison to the corresponding scenarios without boosting). Furthermore, in this chapter we showed that boosting of vaccine-derived immunity (implemented near the baseline level) increased the prospects of altering the trajectory of the COVID-19 pandemic from persistence to possible elimination (even for the fast waning scenario of the vaccine derived-immunity) of the pandemic in the United States. Thus, the implementation of vaccination-boosting strategy greatly enhances the prospects of eliminating the COVID-19 pandemic in the United States.

In addition to the standard assumptions on which the model is built, some of the limitations of the model developed in this chapter include the fact that we did not explicitly account for the impact of other control interventions (notably, the use of face masks, voluntary testing and detection of SARS-CoV-2 cases, isolation of confirmed cases, etc.), which also play important roles in the battle against the COVID-19 pandemic. Further, the model developed in this chapter assumes that the population is well-mixed and does not explicitly account for a number of heterogeneities, including age and risk structure, which may be relevant to gain insight into the dynamics of the disease. Furthermore, this chapter did not account for the effects of other SARS-CoV-2 variants, including the BA.2, BA.5, BQ.1, and BQ.1.1 Omicron variants (which are more contiguous than the original BA.1 Omicron variant) (Karim and Karim, 2021; Katella, 2021; Centers for Disease Control and Prevention, 2023b; Katella, 2023). Nonetheless, this chapter shows, overall, that the prospect for the effective control and mitigation (and, consequently, elimination) of the COVID-19 pandemic in the United States is very promising using a combined vaccination-boosting strategy, provide the vaccinate and boosting coverages are moderately high enough.

REFERENCES

Centers for Disease Control and Prevention, "COVID-19 Treatments and Medications ", https://www.cdc.gov/coronavirus/2019-ncov/your-health/treatments-for-severe-illness.html, (Accessed November 07, 2022) (2022).

Mayo Clinic, "COVID-19: Who's at higher risk of serious symptoms?", https://www.mayoclinic.org/diseases-conditions/coronavirus/in-depth/coronavirus-who-is-at-risk/art-20483301, (Accessed December 18, 2022) (2022).

U.S. Department of Health & Human Services, "COVID-19 Treatments and Therapeutics ", https://www.hhs.gov/coronavirus/covid-19-treatments-therapeutics/index.html, (Accessed November 07, 2022) (2022).

U.S. Food and Drug Authority, "Coronavirus (COVID-19) Update: FDA Authorizes New Monoclonal Antibody for Treatment of COVID-19 that Retains Activity Against Omicron Variant ", https://www.fda.gov/news-events/press-announcements/coronavirus-covid-19-update-fda-authorizes-new-monoclonal-antibody-treatment-covid-19-retains, (Accessed November 07, 2022) (2022).

Aiello, A. E., G. F. Murray, V. Perez, R. M. Coulborn, B. M. Davis, M. Uddin, D. K. Shay, S. H. Waterman and A. S. Monto, "Mask use, hand hygiene, and seasonal influenza-like illness among young adults: a randomized intervention trial", The Journal of Infectious Diseases **201**, 4, 491–498 (2010).

Aiello, A. E., V. Perez, R. M. Coulborn, B. M. Davis, M. Uddin and A. S. Monto, "Facemasks, hand hygiene, and influenza among young adults: a randomized intervention trial", PLOS ONE **7**, 1, e29744 (2012).

Alagawany, M., Y. A. Attia, M. R. Farag, S. S. Elnesr, S. A. Nagadi, M. E. Shafi, A. F. Khafaga, H. Ohran, A. A. Alaqil, A. El-Hack *et al.*, "The strategy of boosting the immune system under the COVID-19 pandemic", Frontiers in Veterinary Science p. 712 (2021).

Alagoz, O., A. K. Sethi, B. W. Patterson, M. Churpek, G. Alhanaee, E. Scaria and N. Safdar, "The impact of vaccination to control COVID-19 burden in the United States: A simulation modeling approach", PLOS ONE **16**, 7, e0254456 (2021).

Alanagreh, L., F. Alzoughool and M. Atoum, "The human coronavirus disease COVID-19: its origin, characteristics, and insights into potential drugs and its mechanisms", Pathogens **9**, 5, 331 (2020).

American Society of Gene plus Cell Therapy, "Adenovirus-Based Vaccine for COVID-19", https://patienteducation.asgct.org/covid19-vaccines/adenovirus-vaccines-for-covid19, (Accessed November 05, 2022) (2021).

Anderson, R. M., "The concept of herd immunity and the design of community-based immunization programmes", Vaccine **10**, 13, 928–935 (1992).

Anderson, R. M. and R. M. May, "Vaccination and herd immunity to infectious diseases", Nature **318**, 6044, 323–329 (1985).

Andrews, N., J. Stowe, F. Kirsebom, S. Toffa, T. Rickeard, E. Gallagher, C. Gower, M. Kall, N. Groves, A.-M. O'Connell *et al.*, "COVID-19 vaccine effectiveness against the Omicron (B.1.1.529) variant", New England Journal of Medicine **386**, 16, 1532–1546 (2022a).

Andrews, N., J. Stowe, F. Kirsebom, S. Toffa, R. Sachdeva, C. Gower, M. Ramsay and J. Lopez Bernal, "Effectiveness of COVID-19 booster vaccines against COVID-19-related symptoms, hospitalization and death in England", Nature Medicine **28**, 4, 831–837 (2022b).

Anjum, N., "Twin mammals and covid-19: life and science of the suspects. preprints 2020", (2020).

Banks, H. T., M. Davidian, J. R. Samuels and K. L. Sutton, "An inverse problem statistical methodology summary", in "Mathematical and Statistical Estimation Approaches in Epidemiology", pp. 249–302 (Springer, 2009).

Bar-On, Y. M., Y. Goldberg, M. Mandel, O. Bodenheimer, L. Freedman, N. Kalkstein, B. Mizrahi, S. Alroy-Preis, N. Ash, R. Milo *et al.*, "Protection of BNT162b2 vaccine booster against COVID-19 in Israel", New England Journal of Medicine **385**, 15, 1393–1400 (2021).

Bergman, M. S., D. J. Viscusi, Z. Zhuang, A. J. Palmiero, J. B. Powell and R. E. Shaffer, "Impact of multiple consecutive donnings on filtering facepiece respirator fit", American Journal of Infection Control **40**, 4, 375–380 (2012).

Bi, Q., Y. Wu, S. Mei, C. Ye, X. Zou, Z. Zhang, X. Liu, L. Wei, S. A. Truelove, T. Zhang *et al.*, "Epidemiology and transmission of COVID-19 in Shenzhen China: Analysis of 391 cases and 1,286 of their close contacts", MedRxiv (2020).

Billingsley, A., "How Does the Immune System Fight COVID-19?", `https://www.goodrx.com/conditions/covid-19/how-the-immune-system-fights-covid-19`, (Accessed October 30, 2022) (2020).

Blayneh, K. W., A. B. Gumel, S. Lenhart and T. Clayton, "Backward bifurcation and optimal control in transmission dynamics of West Nile virus", Bulletin of Mathematical Biology **72**, 4, 1006–1028 (2010).

Blower, S. M. and H. Dowlatabadi, "Sensitivity and uncertainty analysis of complex models of disease transmission: an HIV model, as an example", International Statistical Review/Revue Internationale de Statistique **62**, 2, 229–243 (1994).

Bootsma, M. C. and N. M. Ferguson, "The effect of public health measures on the 1918 influenza pandemic in US cities", Proceedings of the National Academy of Sciences **104**, 18, 7588–7593 (2007).

Bosman, J., J. Hoffman, M. Sanger-Katz and T. Arango, "Who are the unvaccinated in America? there's no one answer", The New York Times (2021).

Bourouiba, L., "Turbulent gas clouds and respiratory pathogen emissions: Potential implications for reducing transmission of COVID-19", JAMA **323**, 18, 1837–1838 (2020).

Brozak, S. J., B. Pant, S. Safdar and A. B. Gumel, "Dynamics of COVID-19 pandemic in India and Pakistan: A metapopulation modelling approach", Infectious Disease Modelling **6**, 1173–1201 (2021).

Buchan, S. A., H. Chung, K. A. Brown, P. C. Austin, D. B. Fell, J. B. Gubbay, S. Nasreen, K. L. Schwartz, M. E. Sundaram, M. Tadrous *et al.*, "Estimated effectiveness of COVID-19 vaccines against Omicron or Delta symptomatic infection and severe outcomes", JAMA Network Open **5**, 9, e2232760–e2232760 (2022).

Callaway, E., H. Ledford *et al.*, "How bad is Omicron? what scientists know so far", Nature **600**, 7888, 197–199 (2021).

Carr, J., *Applications of centre manifold theory*, vol. 35 (Springer Science & Business Media, 2012).

Castillo-Chavez, C. and B. Song, "Dynamical models of tuberculosis and their applications", Mathematical Biosciences & Engineering **1**, 2, 361 (2004).

Center for Disaster Philanthropy, "COVID-19 Coronavirus", `https://disasterphilanthropy.org/disasters/covid-19-coronavirus/`, (Accessed March 15, 2023) (2023).

Centers for Disease Control and Prevention, "Understanding how COVID-19 vaccines work", URL `https://www.cdc.gov/coronavirus/2019-ncov/vaccines/different-vaccines/how-they-work.html`, library Catalog: https://www.cdc.gov/. Publisher: Centers for Disease Control and Prevention. (Accessed October 27, 2022) (2020).

Centers for Disease Control and Prevention, "Omicron Variant: What You Need to Know", `https://www.cdc.gov/coronavirus/2019-ncov/variants/omicron-variant.html#.`, (Accessed May 09, 2022) (2022).

Centers for Disease Control and Prevention, "COVID Data Tracker", `https://covid.cdc.gov/covid-data-tracker/#vaccinations_vacc-people-booster-percent-pop5`, (Accessed March 15, 2023) (2023a).

Centers for Disease Control and Prevention, "COVID Data Tracker", `https://covid.cdc.gov/covid-data-tracker/#variant-summary`, (Accessed March 19, 2023) (2023b).

Centers for Disease Control and Prevention and others, "CDC expands eligibility for COVID-19 booster shots to all adults", (2021).

Centers for Disease Control and Prevention and others, "Stay up to date with COVID-19 vaccines including boosters", (2022).

Centers for Disease Control and Protection, "COVID-19 Treatments and Medications", https://www.cdc.gov/coronavirus/2019-ncov/your-health/treatments-for-severe-illness.html, (Accessed October 30, 2022) (2022).

Chemaitelly, H., H. H. Ayoub, S. AlMukdad, P. Coyle, P. Tang, H. M. Yassine, H. A. Al-Khatib, M. K. Smatti, M. R. Hasan, Z. Al-Kanaani *et al.*, "Duration of mRNA vaccine protection against SARS-CoV-2 Omicron BA. 1 and BA. 2 subvariants in Qatar", Nature Communications **13**, 1, 1–12 (2022).

Childs, L., D. W. Dick, Z. Feng, J. M. Heffernan, J. Li and G. Röst, "Modeling waning and boosting of COVID-19 in Canada with vaccination", Epidemics p. 100583 (2022).

Chorba, T., "The concept of the crown and its potential role in the downfall of coronavirus", Emerging Infectious Diseases **26**, 9, 2302 (2020).

Chowell, G., "Fitting dynamic models to epidemic outbreaks with quantified uncertainty: a primer for parameter uncertainty, identifiability, and forecasts", Infectious Disease Modelling **2**, 3, 379–398 (2017).

Cohen, J. and K. Kupferschmidt, "'A very, very bad look' for remdesivir", (2020).

Cuevas, E., "An agent-based model to evaluate the COVID-19 transmission risks in facilities", Computers in Biology and Medicine **121**, 103827 (2020).

Curley, B., "How long does immunity from covid-19 vaccination last?", Healthline, (Accessed on July 25, 2021) (2021).

Dan, J. M., J. Mateus, Y. Kato, K. M. Hastie, E. D. Yu, C. E. Faliti, A. Grifoni, S. I. Ramirez, S. Haupt, A. Frazier *et al.*, "Immunological memory to SARS-CoV-2 assessed for up to 8 months after infection", Science **371**, 6529, eabf4063 (2021).

Del Rio, C., S. B. Omer and P. N. Malani, "Winter of omicron—the evolving COVID-19 pandemic", JAMA **327**, 4, 319–320 (2022).

Desmon, S., ""COVID and the Heart: It Spares No One"", https://publichealth.jhu.edu/2022/covid-and-the-heart-it-spares-no-one, (Accessed August 30, 2022) (2022).

Diekmann, O., J. A. P. Heesterbeek and J. A. Metz, "On the definition and the computation of the basic reproduction ratio R0 in models for infectious diseases in heterogeneous populations", Journal of Mathematical Biology **28**, 4, 365–382 (1990).

Dolgin, E. *et al.*, "The tangled history of mRNA vaccines", Nature **597**, 7876, 318–324 (2021).

Dong, E., H. Du and L. Gardner, "An interactive web-based dashboard to track COVID-19 in real time", The Lancet Infectious Diseases **20**, 5, 533–534 (2020).

Dunkle, L. M., K. L. Kotloff, C. L. Gay, G. Áñez, J. M. Adelglass, A. Q. Barrat Hernández, W. L. Harper, D. M. Duncanson, M. A. McArthur, D. F. Florescu *et al.*, "Efficacy and safety of NVX-CoV2373 in adults in the United States and Mexico", New England Journal of Medicine **386**, 6, 531–543 (2022).

Duong, D., "What's important to know about the new COVID-19 variants?", (2021).

Dushoff, J., W. Huang and C. Castillo-Chavez, "Backwards bifurcations and catastrophe in simple models of fatal diseases", Journal of Mathematical Biology **36**, 3, 227–248 (1998).

Eikenberry, S. E., M. Mancuso, E. Iboi, T. Phan, K. Eikenberry, Y. Kuang, E. Kostelich and A. B. Gumel, "To mask or not to mask: Modeling the potential for face mask use by the general public to curtail the COVID-19 pandemic", Infectious Disease Modelling **5**, 293–308 (2020).

Elbasha, E. H. and A. B. Gumel, "Theoretical assessment of public health impact of imperfect prophylactic HIV-1 vaccines with therapeutic benefits", Bulletin of Mathematical Biology **68**, 3, 577–614 (2006).

Elbasha, E. H., C. N. Podder and A. B. Gumel, "Analyzing the dynamics of an SIRS vaccination model with waning natural and vaccine-induced immunity", Nonlinear Analysis: Real World Applications **12**, 5, 2692–2705 (2011).

Elliott, P., O. Eales, B. Bodinier, D. Tang, H. Wang, J. Jonnerby, D. Haw, J. Elliott, M. Whitaker, C. E. Walters *et al.*, "Dynamics of a national Omicron SARS-CoV-2 epidemic during January 2022 in England", Nature Communications **13**, 1, 1–10 (2022a).

Elliott, P., O. Eales, N. Steyn, D. Tang, B. Bodinier, H. Wang, J. Elliott, M. Whitaker, C. Atchison, P. J. Diggle *et al.*, "Twin peaks: the Omicron SARS-CoV-2 BA. 1 and BA. 2 epidemics in England", Science p. eabq4411 (2022b).

Esteva, L., A. B. Gumel and C. V. De LeóN, "Qualitative study of transmission dynamics of drug-resistant malaria", Mathematical and Computer Modelling **50**, 3-4, 611–630 (2009).

Esteva, L. and C. Vargas, "Influence of vertical and mechanical transmission on the dynamics of dengue disease", Mathematical Biosciences **167**, 1, 51–64 (2000).

Fast, H. E., E. Zell, B. P. Murthy, N. Murthy, L. Meng, L. G. Scharf, C. L. Black, L. Shaw, T. Chorba and L. Q. Harris, "Booster and additional primary dose COVID-19 vaccinations among adults aged $\geq$ 65 years—United States, August 13, 2021–November 19, 2021", Morbidity and Mortality Weekly Report **70**, 50, 1735 (2021).

Ferdinands, J. M., S. Rao, B. E. Dixon, P. K. Mitchell, M. B. DeSilva, S. A. Irving, N. Lewis, K. Natarajan, E. Stenehjem, S. J. Grannis *et al.*, "Waning 2-dose and 3-dose effectiveness of mRNA vaccines against COVID-19–associated emergency department and urgent care encounters and hospitalizations among adults during

periods of Delta and Omicron variant predominance—vision network, 10 states, August 2021–January 2022", Morbidity and Mortality Weekly Report **71**, 7, 255 (2022).

Ferguson, N. M., D. Laydon, G. Nedjati-Gilani, N. Imai, K. Ainslie, M. Baguelin, S. Bhatia, A. Boonyasiri, Z. Cucunubá, G. Cuomo-Dannenburg *et al.*, "Impact of non-pharmaceutical interventions (NPIs) to reduce COVID-19 mortality and healthcare demand", London: Imperial College COVID-19 Response Team, March **16** (2020).

Firth, J. A., J. Hellewell, P. Klepac and S. Kissler, "Using a real-world network to model localized COVID-19 control strategies", Nature Medicine pp. 1–22, URL `https://doi.org/10.1038/s41591-020-1036-8` (2020).

Food, U., D. Administration *et al.*, "Vaccines and related biological products advisory committee meeting. FDA briefing document Moderna COVID-19 vaccine", Retrieved on February **5**, 2021 (2020).

Food and Drug Administration and others, "FDA briefing document, Pfizer-BioNTech COVID-19 vaccine", in "Vaccines and Related Biological Products Advisory Committee Meeting", (2020).

Food and Drug Administration and others, "Coronavirus (COVID-19) update: FDA authorizes pharmacists to prescribe Paxlovid with certain limitations. FDA", (2022).

Gao, S., P. Binod, C. W. Chukwu, T. Kwofie, S. Safdar, L. Newman, S. Choe, B. K. Datta, W. K. Attipoe, W. Zhang *et al.*, "A mathematical model to assess the impact of testing and isolation compliance on the transmission of covid-19", Infectious Disease Modelling (2023).

Garba, S. M. and A. B. Gumel, "Effect of cross-immunity on the transmission dynamics of two strains of dengue", International Journal of Computer Mathematics **87**, 10, 2361–2384 (2010).

Garba, S. M., A. B. Gumel and M. A. Bakar, "Backward bifurcations in dengue transmission dynamics", Mathematical Biosciences **215**, 1, 11–25 (2008).

Gómez-Carballa, A., J. Pardo-Seco, X. Bello, F. Martinón-Torres and A. Salas, "Superspreading in the emergence of COVID-19 variants", Trends in Genetics **37**, 12, 1069–1080 (2021).

Gonzalez-Parra, G., D. Martínez-Rodríguez and R. J. Villanueva-Micó, "Impact of a new SARS-CoV-2 variant on the population: A mathematical modeling approach", Mathematical and Computational Applications **26**, 2, 25 (2021).

Gregory, M. and M. Salenetri, ""How long does immunity from COVID-19 vaccination."", `https://www.wusa9.com/article/news/verify/how-long-does-it-take-for-the-vaccine-booster-to-get-to-full-protection/65-aa7344c2-fcd5-4c70-bbcd-046e9f697be7`, (Accessed March 22, 2022) (2022).

Grewal, R., S. A. Kitchen, L. Nguyen, S. A. Buchan, S. E. Wilson, A. P. Costa and J. C. Kwong, "Effectiveness of a fourth dose of COVID-19 mRNA vaccine against the Omicron variant among long term care residents in Ontario, Canada: test negative design study", BMJ **378** (2022).

Gumel, A., "Causes of backward bifurcations in some epidemiological models", Journal of Mathematical Analysis and Applications **395**, 1, 355–365 (2012).

Gumel, A. B., E. A. Iboi, C. N. Ngonghala and E. H. Elbasha, "A primer on using mathematics to understand COVID-19 dynamics: Modeling, analysis and simulations", Infectious Disease Modelling **6**, 148–168 (2021a).

Gumel, A. B., E. A. Iboi, C. N. Ngonghala and G. A. Ngwa, "Toward achieving a vaccine-derived herd immunity threshold for COVID-19 in the US", Frontiers in Public Health **9** (2021b).

Gumel, A. B., C. C. McCluskey and P. van den Driessche, "Mathematical study of a staged-progression hiv model with imperfect vaccine", Bulletin of Mathematical Biology **68**, 8, 2105–2128 (2006).

Gumel, A. B. and B. Song, "Existence of multiple-stable equilibria for a multi-drug-resistant model of Mycobacterium Tuberculosis", Mathematical Biosciences & Engineering **5**, 3, 437 (2008).

HAGEN, A., ""How Dangerous Is the Delta Variant (B.1.617.2)?"", `https://asm.org/Articles/2021/July/How-Dangerous-is-the-Delta-Variant-B-1-617-2`, (Accessed Oct 18, 2022) (2022).

Hale, J. K., "Ordinary differential equations", (No Title) (1969).

Hanan, M., ""Delta Has Been Brutal: How the Deadliest Covid Variant Has Affected the World"", `https://www.biospace.com/article/delta-has-been-brutal-how-the-deadliest-covid-variant-has-affected-the-world-/`, (Accessed Oct 18, 2022) (2022).

Hause, A. M., J. Baggs, P. Marquez, W. E. Abara, J. Baumblatt, P. G. Blanc, J. R. Su, B. Hugueley, C. Parker, T. R. Myers *et al.*, "Safety monitoring of COVID-19 mRNA vaccine second booster doses among adults aged $\geq$ 50 years—United States, March 29, 2022–July 10, 2022", Morbidity and Mortality Weekly Report **71**, 30, 971 (2022).

Haynes, B., N. E. Messonnier and M. S. Cetron, "First travel-related case of 2019 novel coronavirus detected in United States: press release, Tuesday, January 21, 2020", `https://stacks.cdc.gov/view/cdc/84535`, (Accessed March 15, 2023) (2020).

He, X., W. Hong, X. Pan, G. Lu and X. Wei, "SARS-CoV-2 Omicron variant: characteristics and prevention", MedComm **2**, 4, 838–845 (2021).

Hethcote, H. W., "The Mathematics of Infectious Diseases", SIAM Review **42**, 4, 599–653 (2000).

Hethcote, H. W. and H. R. Thieme, "Stability of the endemic equilibrium in epidemic models with subpopulations", Mathematical Biosciences **75**, 2, 205–227 (1985).

Iboi, E., O. O. Sharomi, C. Ngonghala and A. B. Gumel, "Mathematical modeling and analysis of COVID-19 pandemic in Nigeria", MedRxiv (2020a).

Iboi, E. A. and A. B. Gumel, "Mathematical assessment of the role of Dengvaxia vaccine on the transmission dynamics of dengue serotypes", Mathematical Biosciences **304**, 25–47 (2018).

Iboi, E. A., C. N. Ngonghala and A. B. Gumel, "Will an imperfect vaccine curtail the COVID-19 pandemic in the US?", Infectious Disease Modelling **5**, 510–524 (2020b).

Iboi, E. A., K. Okuneye, O. Sharomi and A. B. Gumel, "Comments on "A Mathematical Study to Control Visceral Leishmaniasis: An application to South Sudan"", Bulletin of Mathematical Biology **80**, 4, 825–839 (2018).

IHME COVID-19 health service utilization forecasting team, "Forecasting COVID-19 impact on hospital bed-days, ICU-days, ventilator-days and deaths by us state in the next 4 months", MedRxiv (2020).

Infection Control, "Face masks 101: Infection control", `https://www.iqair.com/us/newsroom/face-masks-101-infection-control`, (Accessed October 30, 2022) (2020).

Jain, S., A. Venkataraman, M. E. Wechsler and N. A. Peppas, "Messenger RNA-based vaccines: Past, present, and future directions in the context of the COVID-19 pandemic", Advanced Drug Delivery Reviews **179**, 114000 (2021).

Jayk Bernal, A., M. M. Gomes da Silva, D. B. Musungaie, E. Kovalchuk, A. Gonzalez, V. Delos Reyes, A. Martín-Quirós, Y. Caraco, A. Williams-Diaz, M. L. Brown *et al.*, "Molnupiravir for oral treatment of COVID-19 in nonhospitalized patients", New England Journal of Medicine (2021).

Jonathan, K., M. Kosinski-Collins and E. Sundberg, "Coronavirus structure, vaccine and therapy development", Biophysics Society. https://www. biophysics. org/blog/coronavirus-structure-vaccineand-therapy-development (2020).

Karim, S. S. A. and Q. A. Karim, "Omicron SARS-CoV-2 variant: a new chapter in the COVID-19 pandemic", The Lancet **398**, 10317, 2126–2128 (2021).

Katella, K., "Comparing the COVID-19 vaccines: How are they different", Yale Medicine **22** (2021).

Katella, K., ""Omicron and the BA.2 Subvariant: A Guide to What We Know"", `https://www.yalemedicine.org/news/5-things-to-know-omicron`, (Accessed May 09, 2022) (2022).

Katella, K., "Omicron, Delta, Alpha, and More: What To Know About the Coronavirus Variants", `https://www.yalemedicine.org/news/covid-19-variants-of-concern-omicron`, (Accessed March 19, 2023) (2023).

Kim, D., S. T. Ali, S. Kim, J. Jo, J.-S. Lim, S. Lee and S. Ryu, "Estimation of serial interval and reproduction number to quantify the transmissibility of SARS-CoV-2 Omicron variant in South Korea", Viruses **14**, 3, 533 (2022).

King, A. A., M. Domenech de Cellès, F. M. Magpantay and P. Rohani, "Avoidable errors in the modelling of outbreaks of emerging pathogens, with special reference to Ebola", Proceedings of the Royal Society B: Biological Sciences **282**, 1806, 20150347 (2015).

Kissler, S. M., C. Tedijanto, E. Goldstein, Y. H. Grad and M. Lipsitch, "Projecting the transmission dynamics of SARS-CoV-2 through the postpandemic period", Science **368**, 6493, 860–868 (2020).

Koyama, T., D. Weeraratne, J. L. Snowdon and L. Parida, "Emergence of drift variants that may affect COVID-19 vaccine development and antibody treatment", Pathogens **9**, 5, 324 (2020).

La Salle, J. P., *The Stability of Dynamical Systems* (SIAM, 1976).

Lakshmikantham, V. and S. Leela, *Differential and integral inequalities: theory and applications: volume I: ordinary differential equations* (Academic press, 1969).

Lakshmikantham, V., S. Leela and A. A. Martynyuk, *Stability Analysis of Nonlinear Systems* (Springer, 1989).

Lakshmikantham, V. and A. Vatsala, "Theory of differential and integral inequalities with initial time difference and applications", in "Analytic and Geometric Inequalities and Applications", pp. 191–203 (Springer, 1999).

Lau, J. T., H. Tsui, M. Lau and X. Yang, "SARS transmission, risk factors, and prevention in Hong Kong", Emerging Infectious Diseases **10**, 4, 587 (2004).

Li, G., Y. Fan, Y. Lai, T. Han, Z. Li, P. Zhou, P. Pan, W. Wang, D. Hu, X. Liu *et al.*, "Coronavirus infections and immune responses", Journal of Medical Virology **92**, 4, 424–432 (2020).

Liang, S. T., L. T. Liang and J. M. Rosen, "COVID-19: A comparison to the 1918 influenza and how we can defeat it", (2021).

Lin, D.-Y., Y. Gu, B. Wheeler, H. Young, S. Holloway, S.-K. Sunny, Z. Moore and D. Zeng, "Effectiveness of COVID-19 vaccines over a 9-month period in North Carolina", New England Journal of Medicine **386**, 10, 933–941 (2022).

Lindsley, W. G., F. M. Blachere, B. F. Law, D. H. Beezhold and J. D. Noti, "Efficacy of face masks, neck gaiters and face shields for reducing the expulsion of simulated cough-generated aerosols", Aerosol Science and Technology **55**, 4, 449–457 (2021).

Linton, N. M., T. Kobayashi, Y. Yang, K. Hayashi, A. R. Akhmetzhanov, S.-m. Jung, B. Yuan, R. Kinoshita and H. Nishiura, "Incubation period and other epidemiological characteristics of 2019 novel coronavirus infections with right truncation: a statistical analysis of publicly available case data", Journal of Clinical Medicine **9**, 2, 538 (2020).

Luckingham, B., "To mask or not to mask: a note on the 1918 Spanish influenza epidemic in Tucson", The Journal of Arizona History pp. 191–204 (1984).

MacIntyre, C. R., S. Cauchemez, D. E. Dwyer, H. Seale, P. Cheung, G. Browne, M. Fasher, J. Wood, Z. Gao, R. Booy *et al.*, "Face mask use and control of respiratory virus transmission in households", Emerging Infectious Diseases **15**, 2, 233 (2009).

Mahase, E., "COVID-19: Moderna vaccine is nearly 95% effective, trial involving high risk and elderly people shows", BMJ: British Medical Journal (Online) **371** (2020).

Mahase, E., "COVID-19: What new variants are emerging and how are they being investigated?", (2021).

Mancuso, M., S. E. Eikenberry and A. B. Gumel, "Will vaccine-derived protective immunity curtail COVID-19 variants in the US?", Infectious Disease Modelling **6**, 1110–1134 (2021).

Margaret Labban, "The case of remdesivir: How do you calculate the cost of a pandemic drug?", URL `https://www.pharmaceutical-technology.com/pricing-and-market-access/remdesivir-calculate-the-cost-of-a-pandenmic-drug-html`, library Catalog: https://www.cdc.gov/. Publisher: World Health Organization. (Accessed October 27, 2022) (2020).

Marino, S., I. B. Hogue, C. J. Ray and D. E. Kirschner, "A methodology for performing global uncertainty and sensitivity analysis in systems biology", Journal of Theoretical Biology **254**, 1, 178–196 (2008).

Maxmen, A. *et al.*, "Wuhan market was epicentre of pandemic's start, studies suggest", Nature **603**, 7899, 15–16 (2022).

McConeghy, K. W., "Effectiveness of a second COVID-19 vaccine booster dose against infection, hospitalization, or death among nursing home residents—19 states, march 29–july 25, 2022", MMWR. Morbidity and Mortality Weekly Report **71** (2022).

McLeod, R. G., J. F. Brewster, A. B. Gumel and D. A. Slonowsky, "Sensitivity and uncertainty analyses for a SARS model with time-varying inputs and outputs", Mathematical Biosciences & Engineering **3**, 3, 527–544 (2006).

Melesse, D. Y. and A. B. Gumel, "Global asymptotic properties of an SEIRS model with multiple infectious stages", Journal of Mathematical Analysis and Applications **366**, 1, 202–217 (2010).

Michaud, J. and J. Kates, "Is contact tracing getting enough attention in US coronavirus response", Global Health Policy (Assessed on October 25, 2022) (2020).

Moghadas, S. M., M. C. Fitzpatrick, P. Sah, A. Pandey, A. Shoukat, B. H. Singer and A. P. Galvani, "The implications of silent transmission for the control of COVID-19 outbreaks", Proceedings of the National Academy of Sciences URL `https://www.pnas.org/content/early/2020/07/02/2008373117` (2020).

Morens, D. M., J. K. Taubenberger, G. K. Folkers and A. S. Fauci, "An historical antecedent of modern guidelines for community pandemic influenza mitigation", Public Health Reports **124**, 1, 22–25 (2009).

Mrityunjaya, M., V. Pavithra, R. Neelam, P. Janhavi, P. Halami and P. Ravindra, "Immune-boosting, antioxidant and anti-inflammatory food supplements targeting pathogenesis of COVID-19", Frontiers in Immunology p. 2337 (2020).

National Institute of Health, "NIH COVID-19 Treatment Guidelines-Molnupiravir", `https://www.covid19treatmentguidelines.nih.gov/therapies/antiviral-therapy/molnupiravir/`, (Accessed October 30, 2022) (2022).

Ngonghala, C. N., P. Goel, D. Kutor and S. Bhattacharyya, "Human choice to self-isolate in the face of the COVID-19 pandemic: a game dynamic modelling approach", Journal of Theoretical Biology **521**, 110692 (2021a).

Ngonghala, C. N., E. Iboi, S. Eikenberry, M. Scotch, C. R. MacIntyre, M. H. Bonds and A. B. Gumel, "Mathematical assessment of the impact of non-pharmaceutical interventions on curtailing the 2019 novel coronavirus", Mathematical Biosciences **325**, 108364 (2020a).

Ngonghala, C. N., E. A. Iboi and A. B. Gumel, "Could masks curtail the post-lockdown resurgence of COVID-19 in the US?", Mathematical Biosciences **329**, 108452 (2020b).

Ngonghala, C. N., J. R. Knitter, L. Marinacci, M. H. Bonds and A. B. Gumel, "Assessing the impact of widespread respirator use in curtailing COVID-19 transmission in the USA", Royal Society Open Science **8**, 9, 210699 (2021b).

Ngonghala, C. N., H. B. Taboe, S. Safdar and A. B. Gumel, "Unraveling the dynamics of the Omicron and Delta variants of the 2019 coronavirus in the presence of vaccination, mask usage, and antiviral treatment", Applied Mathematical Modelling **114**, 447–465 (2023).

Ohannessian, R., T. A. Duong, A. Odone *et al.*, "Global telemedicine implementation and integration within health systems to fight the COVID-19 pandemic: a call to action", JMIR Public Health and Surveillance **6**, 2, e18810 (2020).

Oliver, S. E., J. W. Gargano, M. Marin, M. Wallace, K. G. Curran, M. Chamberland, N. McClung, D. Campos-Outcalt, R. L. Morgan, S. Mbaeyi *et al.*, "The Advisory Committee on Immunization Practices' interim recommendation for use of Pfizer-BioNTech COVID-19 vaccine - United States, December 2020", Morbidity and Mortality Weekly Report **69**, 50, 1922 (2020).

O'Kelly, E., A. Arora, S. Pirog, J. Ward and P. J. Clarkson, "Comparing the fit of N95, KN95, surgical, and cloth face masks and assessing the accuracy of fit checking", PLOS ONE **16**, 1, e0245688 (2021).

Pacific, W. and S. A. W. Hasan, "Interim statement on booster doses for COVID-19 vaccination", Update **22** (2021).

Pal, M., G. Berhanu, C. Desalegn and V. Kandi, "Severe Acute Respiratory Syndrome Coronavirus-2 (SARS-CoV-2): an update", Cureus **12**, 3 (2020).

Parums, D. V., "Revised World Health Organization (WHO) terminology for variants of concern and variants of interest of SARS-CoV-2", Medical Science Monitor: International Medical Journal of Experimental and Clinical Research **27**, e933622–1 (2021).

Pearson, S., "What is the difference between the Pfizer, Moderna, and Johnson & Johnson COVID-19 vaccines?", GoodRx (Accessed on June 25, 2021) (2021).

Peiris, M. and L. L. Poon, "Severe Acute Respiratory Syndrome (SARS) and Middle East Respiratory Syndrome (MERS)(Coronaviridae)", Encyclopedia of Virology p. 814 (2021).

Pfizer, "Pfizer and BioNTech to submit emergency use authorization request today to the U.S. FDA for COVID-19 vaccine", (2020).

Polack, F. P., S. J. Thomas, N. Kitchin, J. Absalon, A. Gurtman, S. Lockhart, J. L. Perez, G. P. Marc, E. D. Moreira, C. Zerbini *et al.*, "Safety and efficacy of the BNT162b2 mRNA COVID-19 vaccine", New England Journal of Medicine (2020).

Qi, H., B. Liu, X. Wang and L. Zhang, "The humoral response and antibodies against SARS-CoV-2 infection", Nature Immunology **23**, 7, 1008–1020 (2022).

Qian, Y., K. Willeke, S. A. Grinshpun, J. Donnelly and C. C. Coffey, "Performance of N95 respirators: filtration efficiency for airborne microbial and inert particles", American Industrial Hygiene Association Journal **59**, 2, 128–132 (1998).

Rahimi, F. and A. T. B. Abadi, "The Omicron subvariant BA. 2: Birth of a new challenge during the COVID-19 pandemic", International Journal of Surgery (London, England) **99**, 106261 (2022).

Ramos, A., M. Vela-Pérez, M. Ferrández, A. Kubik and B. Ivorra, "Modeling the impact of SARS-CoV-2 variants and vaccines on the spread of COVID-19", Communications in Nonlinear Science and Numerical Simulation **102**, 105937 (2021).

Rella, S. A., Y. A. Kulikova, E. T. Dermitzakis and F. A. Kondrashov, "Rates of SARS-CoV-2 transmission and vaccination impact the fate of vaccine-resistant strains", Scientific Reports **11**, 1, 1–10 (2021).

Ruiz-Medina, B. E., A. Varela-Ramirez, R. A. Kirken and E. Robles-Escajeda, "The SARS-CoV-2 origin dilemma: Zoonotic transfer or laboratory leak?", BioEssays **44**, 1, 2100189 (2022).

Safdar, S. and A. B. Gumel, *Book chapter in "Mathematical Modelling from the Next Generation", Fields Institute for Research in the Mathematical Sciences seminar series. Jummy David and Jianhong Wu, editors. (To appear)* (Springer, 2023).

Safdar, S., C. N. Ngonghala and A. B. Gumel, "Mathematical assessment of the role of waning and boosting immunity against the BA. 1 Omicron variant in the United States", Mathematical Biosciences and Engineering **20**, 1, 179–212 (2023).

Safi, M. A. and A. B. Gumel, "Global asymptotic dynamics of a model for quarantine and isolation", Discrete & Continuous Dynamical Systems-B **14**, 1, 209 (2010).

Sargent, J., S. Kumar, K. Buckley and J. McIntyre, "Johnson & Johnson announces real-world evidence and phase 3 data confirming substantial protection of single-shot COVID-19 vaccine in the US additional data show a booster increases protection1", (2021).

Schlake, T., A. Thess, M. Fotin-Mleczek and K.-J. Kallen, "Developing mRNA-vaccine technologies", RNA Biology **9**, 11, 1319–1330 (2012).

Schneider, K. A., G. A. Ngwa, M. Schwehm, L. Eichner and M. Eichner, "The COVID-19 pandemic preparedness simulation tool: Covidsim", BMC Infectious Diseases **20**, 1, 1–11 (2020).

Scripps Research, "What Are The Parts Of A CORONAVIRUS", `https://www.scripps.edu/covid-19/science-simplified/parts-of-a-coronavirus/`, (Accessed November 04, 2022) (2020).

Self, W. H., M. W. Tenforde, J. P. Rhoads, M. Gaglani, A. A. Ginde, D. J. Douin, S. M. Olson, H. K. Talbot, J. D. Casey, N. M. Mohr *et al.*, "Comparative effectiveness of Moderna, Pfizer-BioNTech, and Janssen (Johnson & Johnson) vaccines in preventing COVID-19 hospitalizations among adults without immunocompromising conditions—United States, March-August 2021", Morbidity and Mortality Weekly Report **70**, 38, 1337 (2021).

Shah, V. K., P. Firmal, A. Alam, D. Ganguly and S. Chattopadhyay, "Overview of immune response during SARS-CoV-2 infection: lessons from the past", Frontiers in Immunology **11**, 1949 (2020).

Sharomi, O. and A. B. Gumel, "Mathematical study of a risk-structured two-group model for Chlamydia transmission dynamics", Applied Mathematical Modelling **35**, 8, 3653–3673 (2011).

Shoukat, A., T. N. Vilches, S. M. Moghadas, P. Sah, E. C. Schneider, J. Shaff, A. Ternier, D. A. Chokshi and A. P. Galvani, "Lives saved and hospitalizations averted by COVID-19 vaccination in New York City: a modeling study", The Lancet Regional Health-Americas **5**, 100085 (2022).

Sidik, S. M., "Vaccines protect against infection from Omicron subvariant-but not for long.", Nature (2022).

Srivastava, A. and G. Chowell, "Understanding spatial heterogeneity of COVID-19 pandemic using shape analysis of growth rate curves", MedRxiv (2020).

Srivastava, N., P. Baxi, R. Ratho and S. K. Saxena, "Global trends in epidemiology of coronavirus disease 2019 (COVID-19)", in "Coronavirus Disease 2019 (COVID-19)", pp. 9–21 (Springer, 2020).

Tan, J. K., D. Leong, H. Munusamy, N. H. Zenol Ariffin, N. Kori, R. Hod and P. Periyasamy, "The prevalence and clinical significance of presymptomatic COVID-19 patients: how we can be one step ahead in mitigating a deadly pandemic", BMC Infectious Diseases **21**, 1, 1–10 (2021).

Tan, S. H., A. R. Cook, D. Heng, B. Ong, D. C. Lye and K. B. Tan, "Effectiveness of BNT162b2 vaccine against Omicron in children 5 to 11 years of age", New England Journal of Medicine **387**, 6, 525–532 (2022).

Tariq, A., Y. Lee, K. Roosa, S. Blumberg, P. Yan, S. Ma and G. Chowell, "Real-time monitoring the transmission potential of COVID-19 in Singapore, March 2020", BMC Medicine **18**, 1–14 (2020).

Thakur, V. and R. Kanta Ratho, "Omicron (B. 1.1. 529): A new SARS-CoV-2 variant of concern mounting worldwide fear", Journal of Medical Virology (2021).

Thieme, H. R., "Local stability in epidemic models for heterogeneous populations", in "Mathematics in Biology and Medicine", pp. 185–189 (Springer, 1985).

Thompson, M. G., "Effectiveness of a third dose of mRNA vaccines against COVID-19–associated emergency department and urgent care encounters and hospitalizations among adults during periods of Delta and Omicron variant predominance—VISION Network, 10 States, August 2021–January 2022", MMWR. Morbidity and Mortality Weekly Report **71** (2022).

Thurner, S., P. Klimek and R. Hanel, "A network-based explanation of why most COVID-19 infection curves are linear", Proceedings of the National Academy of Sciences **117**, 37, 22684–22689 (2020).

Tseng, H. F., B. K. Ackerson, Y. Luo, L. S. Sy, C. Talarico, Y. Tian, K. Bruxvoort, J. E. Tupert, A. Florea, J. H. Ku *et al.*, "Effectiveness of mRNA-1273 against SARS-CoV-2 Omicron and Delta variants", MedRxiv (2022).

U.S. Food and Drug Administration and others, "FDA briefing document", in "Oncology Drug Advisory Committee Meeting, Silver Spring, MD", (2009).

U.S. Food and Drug Administration and others, "Coronavirus (COVID-19) update: FDA issues policies to guide medical product developers addressing virus variants", FDA. February **23**, 2021 (2021a).

U.S. Food and Drug Administration and others, "FDA issues emergency use authorization for third COVID-19 vaccine", Silver Spring, MD: FDA (2021b).

van den Driessche, P. and J. Watmough, "A simple SIS epidemic model with a backward bifurcation", Journal of Mathematical Biology **40**, 6, 525–540 (2000).

van den Driessche, P. and J. Watmough, "Reproduction numbers and sub-threshold endemic equilibria for compartmental models of disease transmission", Mathematical Biosciences **180**, 1-2, 29–48 (2002).

Van der Hoek, L., "Human coronaviruses: what do they cause?", Antiviral Therapy **12**, 4_part_2, 651–658 (2007).

Vermund, S. H. and V. E. Pitzer, "Asymptomatic transmission and the infection fatality risk for COVID-19: implications for school reopening", Clinical Infectious Diseases **72**, 9, 1493–1496 (2021).

Wang, C. J., C. Y. Ng and R. H. Brook, "Response to COVID-19 in Taiwan: big data analytics, new technology, and proactive testing", JAMA **323**, 14, 1341–1342 (2020).

Washam, M., "Bivalent COVID Vaccines: What You Need to Know", `https://www.nationwidechildrens.org/family-resources-education/700childrens/2022/09/bivalent-covid-vaccines`, (Accessed November 08, 2022) (2022).

Weintraub, K., ""Enormous spread of Omicron' may bring 140M new COVID infections to US in the next two months, model predicts."", `https://www.wusa9.com/article/news/verify/how-long-does-it-take-for-the-vaccine-booster-to-get-to-full-protection/65-aa7344c2-fcd5-4c70-bbcd-046e9f697be7`, (Accessed March 22, 2022) (2022).

Wilder, B., M. Charpignon, J. A. Killian, H.-C. Ou, A. Mate, S. Jabbari, A. Perrault, A. Desai, M. Tambe, M. S. Majumder *et al.*, "The role of age distribution and family structure on COVID-19 dynamics: A Preliminary Modeling Assessment for Hubei and Lombardy", Available at SSRN **3564800** (2020).

World Health Organization, "Coronavirus disease 2019 (COVID-19) Situation Report – 46", Tech. Rep. 46, World Health Organization, URL `https://apps.who.int/iris/handle/10665/331443` (2020).

Worldometer., "COVID live update.", Worldometer information URL `https://www.worldometers.info/coronavirus/` (Accessed on March 19, 2023).

Wu, J., F. Xu, W. Zhou, D. R. Feikin, C.-Y. Lin, X. He, Z. Zhu, W. Liang, D. P. Chin and A. Schuchat, "Risk factors for SARS among persons without known contact with SARS patients, Beijing, China", Emerging Infectious Diseases **10**, 2, 210 (2004).

Xue, L., S. Jing, J. C. Miller, W. Sun, H. Li, J. G. Estrada-Franco, J. M. Hyman and H. Zhu, "A data-driven network model for the emerging COVID-19 epidemics in Wuhan, Toronto and Italy", Mathematical Biosciences **326**, 108391 (2020).

Yale Medicine, "Omicron XBB.1.5 'Kraken' Subvariant Is on the Rise: What To Know", `alemedicine.org/news/omicron-xbb-kraken-subvariant`, (Accessed March 19, 2023) (2023).

Yin, Y. and R. G. Wunderink, "MERS, SARS and other coronaviruses as causes of pneumonia", Respirology **23**, 2, 130–137 (2018).

Yuan, S., S.-C. Jiang and Z.-L. Li, "Analysis of possible intermediate hosts of the new coronavirus SARS-CoV-2", Frontiers in Veterinary Science **7**, 379 (2020).

Zheng, J., Y. Deng, Z. Zhao, B. Mao, M. Lu, Y. Lin and A. Huang, "Characterization of SARS-CoV-2-specific humoral immunity and its potential applications and therapeutic prospects", Cellular & Molecular Immunology **19**, 2, 150–157 (2022).

APPENDIX A

PROOF OF THEOREM 2.3.2

Proof. The proof is based on the center manifold theory (Carr, 2012; van den Driessche and Watmough, 2002) and to apply this theory, it is convenient to introduce the following change of variables: let $S = x_1$, $V = x_2$, $E = x_3$, $I_p = x_4$, $I_s = x_5$, $I_a = x_6$, $I_h = x_7$, $R_n = x_8$, $R_{nv} = x_9$. Using this transformation, the vaccination model (2.1) can be re-written in general form $\frac{dX}{dt} = (f_1, f_2, f_3, f_4, f_5, f_6, f_7, f_8, f_9)^T$, with $X = (x_1, x_2, x_3, x_4, x_5, x_6, x_7, x_8, x_9)^T$. Specifically, the model (2.1) can be written in terms of the transformed variables as:

$$\begin{cases} \frac{d\,x_1}{d\,t} = f_1 &= \Pi + \omega_v x_2 - \lambda x_1 - k_1 x_1, \\ \frac{d\,x_2}{d\,t} = f_2 &= \xi_v x_1 - (1-\varepsilon_v)\lambda x_2 - k_2 x_2, \\ \frac{d\,x_3}{d\,t} = f_3 &= \lambda x_1 + (1-\varepsilon_v)\lambda x_2 + (1-\varepsilon_n)\lambda x_8 + (1-\varepsilon_{nv})\lambda x_9 - k_3 x_3, \\ \frac{d\,x_4}{d\,t} = f_4 &= \sigma_E x_3 - k_4 x_4, \\ \frac{d\,x_5}{d\,t} = f_5 &= r\sigma_p x_4 - k_5 x_5, \\ \frac{d\,x_6}{d\,t} = f_6 &= (1-r)\sigma_p x_4 - k_6 x_6, \\ \frac{d\,x_7}{d\,t} = f_7 &= \phi_s x_5 - k_7 x_7, \\ \frac{d\,x_8}{d\,t} = f_8 &= \gamma_s x_5 + \gamma_a\, x_6 + \gamma_h x_7 - (1-\varepsilon_n)\lambda x_8 - k_8 x_8, \\ \frac{d\,x_9}{d\,t} = f_9 &= \xi_v x_8 - (1-\varepsilon_{nv})\lambda x_9 - k_9 x_9, \end{cases} \tag{A.1}$$

with the force of infection under the aforementioned transformation now defined as:

$$\lambda = \frac{(\beta_p\, x_4 + \beta_s\, x_5 + \beta_a\, x_6 + \beta_h\, x_7)}{N},$$

where,

$$\begin{aligned} N &= x_1 + x_2 + x_3 + x_4 + x_5 + x_5 + x_6 + x_7 + x_7 + x_8 + x_9, k_1 = \xi_v + \mu, \\ k_2 &= \omega_v + \mu, k_3 = \sigma_E + \mu, k_4 = \sigma_p + \delta_p + \mu, k_5 = \phi_s + \gamma_s + \delta_s + \mu, \\ k_6 &= \gamma_a + \delta_a + \mu, k_7 = \gamma_h + \delta_h + \mu, k_8 = \xi_v + \mu, \quad \text{and} \quad k_9 = \mu. \end{aligned}$$

The Jacobian of the system (A.1), evaluated at the DFE ($\mathcal{E}_0$), is given by:

$$J(\mathcal{E}_0) = \begin{pmatrix} -k_1 & \omega_v & 0 & -\beta_p J_1 & -\beta_s J_1 & -\beta_a J_1 & -\beta_h J_1 & 0 & 0 \\ \xi_v & -k_2 & 0 & -\beta_p J_2 & -\beta_s J_2 & -\beta_a J_2 & -\beta_h J_2 & 0 & 0 \\ 0 & 0 & -k_3 & -\beta_p J_3 & -\beta_s J_3 & -\beta_a J_3 & -\beta_h J_3 & 0 & 0 \\ 0 & 0 & \sigma_e & -k_4 & 0 & 0 & 0 & 0 & 0 \\ 0 & 0 & 0 & r\,\sigma_p & -k_5 & 0 & 0 & 0 & 0 \\ 0 & 0 & 0 & (1-r)\,\sigma_p & 0 & -k_6 & 0 & 0 & 0 \\ 0 & 0 & 0 & 0 & \phi_s & 0 & -k_7 & 0 & 0 \\ 0 & 0 & 0 & 0 & \gamma_s & \gamma_a & \gamma_h & -k_8 & 0 \\ 0 & 0 & 0 & 0 & 0 & 0 & 0 & \xi_v & -k_9 \end{pmatrix},$$

where, $J_1 = \dfrac{\omega_v + \mu}{\omega_v + \xi_v + \mu}$, $J_2 = \dfrac{(1-\varepsilon_v)\,\xi_v}{\omega_v + \xi_v + \mu}$ and $J_3 = J_2 - J_1$.

Choosing β_p as the bifurcation parameter, and solving for β_p from $\mathbb{R}_{cv} = 1$ (i.e., at the bifurcation point) gives:

$$\beta_p = \frac{1}{(1-\varepsilon_v f_v)\left(\dfrac{\sigma_E}{\sigma_E + \mu}\right)\left(\dfrac{1}{\sigma_p + \delta_p + \mu}\right)(D_p)} = \beta_p^*,$$

where,

$D_p = \left\{1 + d_1 r\sigma_p B_1 + d_2(1-r)\sigma_p B_2 + d_3 r\sigma_p B_1 B_3\right\}$,

with,

$B_1 = \left(\frac{1}{\phi_s + \gamma_s + \delta_s + \mu}\right)$, $B_2 = \left(\frac{1}{\gamma_a + \delta_a + \mu}\right) B_3 = \left(\frac{1}{\gamma_h + \delta_h + \mu}\right)$, $d_1 = \frac{\beta_s}{\beta_p}$, $d_2 = \frac{\beta_a}{\beta_p}$ and $d_3 = \frac{\beta_h}{\beta_p}$.

Let $J_{\beta_p^*}$ denotes the Jacobian of the system (A.1) evaluated at the DFE ($\mathcal{E}_0$). It can be seen that the system (A.1), with $\beta_p = \beta_p^*$, has a simple eigenvalue with zero real part and all other eigenvalues having negative real part (Blayneh *et al.*, 2010). Hence, the center manifold theory (Carr, 2012; Castillo-Chavez and Song, 2004) can be applied to analyze the dynamics of the vaccination model (2.1) near the bifurcation point (where $\beta_p = \beta_p^*$). To apply the theory (in particular, the approach in Castillo-Chavez and Song (2004)), the following computations (associated with the left and right eigenvectors of $J_{\beta_p^*}$, corresponding to the zero eigenvalue) are necessary.

Computation of left and right eigenvectors of $J_{\beta_p^*}$

It can be seen that the left eigenvector of $J_{\beta_p^*}$, corresponding to the zero eigenvalue, is given by:

$\mathbf{v} = [v_1, v_2, v_3, v_4, v_5, v_6, v_7, v_8, v_9]$, where (noting that J_1, J_2 and J_3 are defined above),

$$\begin{aligned} v_1 &> 0 \quad (\text{free}),\ v_3 > 0\,(\text{free}),\ v_8 = v_9 = 0 \\ v_2 &= \frac{\omega_v\, v_1}{k_2},\ v_4 = \frac{k_3\, v_3}{\sigma_E},\ v_5 = \frac{\beta_s\,(-J_1\, v_1 - J_2\, v_2 + J_3\, v_3)}{k_5}, \\ v_6 &= \frac{\beta_a\,(-J_1\, v_1 - J_2\, v_2 + J_3\, v_3)}{k_6},\ v_7 = \frac{\beta_h\,(-J_1\, v_1 - J_2\, v_2 + J_3\, v_3)}{k_7}. \end{aligned} \tag{A.2}$$

Furthermore, the right eigenvector of $J_{\beta_p^*}$, corresponding to the zero eigenvalue, is given by:

$\mathbf{w} = [w_1, w_2, w_3, w_4, w_5, w_6, w_7, w_8, w_9]^T$, where,

$$
\begin{aligned}
w_1 &> 0 \text{ (free)}, \quad w_2 = \frac{k_1\, w_1 + J_1\,(\beta_p\, w_4 + \beta_s\, w_5 + \beta_a\, w_6 + \beta_h\, w_7)}{\omega_v}, \\
w_3 &= \frac{k_4\, w_4}{\sigma_E}, \quad w_4 = \frac{k_5\, w_5}{r\,\sigma_p}, w_5 = \frac{k_7\, w_7}{\phi_s}, \\
w_6 &= \frac{(1-r)\,\sigma_p\, w_4}{k_6}, \quad w_7 > 0\,(\text{free}), \quad w_8 = \frac{k_9\, w_9}{\xi_v}, \quad w_9 > 0\,(\text{free}).
\end{aligned} \tag{A.3}
$$

For computational convenience, we set, without loss of generality, the components of the left eigenvectors v_1 and v_3 in (A.2) to one. Similarly, we set the components w_1,w_7 and w_9, of the right eigenvector, given in (A.3) to unity.

Computation of backward bifurcation coefficients, a and b

The local bifurcation analysis near the bifurcation point ($\beta_p = \beta_p^*$) is determined by the signs of two bifurcation coefficients, denoted by a and b (Carr, 2012; Castillo-Chavez and Song, 2004). Following (Castillo-Chavez and Song, 2004), the expressions for these bifurcation coefficients are, respectively, given by:

$$
a = \sum_{k,i,j=1}^{n} v_k w_i w_j \frac{\partial^2 f_k}{\partial x_i \partial x_j}(\mathcal{E}_0, \beta_p^*), \tag{A.4}
$$

and,

$$
b = \sum_{k,i=1}^{n} v_k w_i \frac{\partial^2 f_k}{\partial x_i \partial \beta_p}(\mathcal{E}_0, \beta_p^*). \tag{A.5}
$$

It can be shown, by substituting the expressions for the eigenvectors (w_k and v_k; $k = 1, \cdots, 9$) given in (A.2) and (A.3) and the partial derivatives of the functions $f_k\,(k = 1, \cdots, 9)$ defined in (A.1) into the expressions (A.4) and (A.5), that the bifurcation coefficients now become:

$$
a = \frac{1}{D_a}\left[(C_a)\left\{(P+Q+R) - (S+T+U)\right\}\right], \tag{A.6}
$$

and,

$$b = \frac{(d_1 w_5 + d_2 w_6 + d_3 w_7 + w_4)(X - Y)}{\omega_v + \xi_v + \mu}, \tag{A.7}$$

where,

$D_a = \Pi\,(\omega_v + \xi_v + \mu), C_a = 2\,\mu\,\beta_p\,(w_4 + d_1\,w_5 + d_2\,w_6 + d_3\,w_7),$

and,

$$\begin{aligned}
P &= \mu(v_3\,w_3 + v_3\,w_5 + v_3\,w_6\ + v_3\,w_7\ + v_8 + v_9 + v_3 w_4 + v_3 w_8 \varepsilon_n + v_3 w_9 \varepsilon_{nv}),\\
Q &= \xi_v(v_3\,w_3 + v_3\,w_5 + v_3\,w_6 + v_3\,w_7 + v_8\,w_8 + v_9\,w_9 + v_1\,w_1\ + v_3\,w_4 + v_3 w_2 \mu\\
&\quad + v_3 w_8 \varepsilon_n + v_3 w_9 \varepsilon_{nv} + v_2 w_1 \varepsilon_v + v_2 w_3 \varepsilon_v + v_2 w_4 \varepsilon_v + v_2 w_5 \varepsilon_v + v_2 w_6 \varepsilon_v + v_2 w_7 \varepsilon_v\\
&\quad + v_2 w_8 \varepsilon_v + v_2 w_9 \varepsilon_v),\\
R &= \omega_v(v_2 w_2 + v_3 w_3 + v_3 w_5 + v_3 w_6 + v_3 w_7 + v_8 w_8 + v_9 w_9 + v_3 w_4 + v_3 w_2 \varepsilon_v\\
&\quad + v_3 w_8 \varepsilon_n + v_3 w_9 \varepsilon_{nv}),\\
S &= \mu(w_3 v_1 + w_5 v_1 + w_6 v_1 + w_7 v_1 + w_8 v_1 + w_9 v_1 + v_1 w_4 + v_8 w_8 \varepsilon_n + v_9 w_9 \varepsilon_{nv}\\
&\quad + v_2 w_2 \varepsilon_v),\\
T &= \xi_v(v_2 w_1 + v_2 w_3 + v_2 w_4 + v_2 w_5 + v_2 w_6 + v_2 w_7 + v_2 w_8 + v_2 w_9 + v_3 w_1 \varepsilon_v + v_3 w_3 \varepsilon_v\\
&\quad + v_3 w_4 \varepsilon_v + v_3 w_5 \varepsilon_v + v_3 w_6 \varepsilon_v + v_3 w_7 \varepsilon_v + v_3 w_8 \varepsilon_v + v_3 w_9 \varepsilon_v + v_8 w_8 \varepsilon_n + v_9 w_9 \varepsilon_{nv}),\\
U &= \omega_v(v_1 w_2 + v_1 w_3 + v_1 w_4 + v_1 w_5 + v_1 w_6 + v_1 w_7 + v_1 w_8 + v_1 w_9 + v_2 w_2 \varepsilon_v\\
&\quad + v_8 w_8 \varepsilon_n + v_9 w_9 \varepsilon_{nv}),\\
X &= \varepsilon_v v_2 \xi_v + \mu v_3 + w_v v_3 + v_3 \xi_v,\\
Y &= \varepsilon_v v_3 \xi_v + \mu v_1 + w_v v_1 + v_2 \xi_v,\\
\beta_s &= d_1 \beta_p, \beta_a = d_2 \beta_p, \beta_h = d_3 \beta_p.
\end{aligned} \tag{A.8}$$

It follows from Item (i) of Theorem 4.1 of Castillo-Chavez and Song (2004) that the vaccination model (2.1) will undergo a backward bifurcation at $\mathbb{R}_{cv} = 1$ whenever the

bifurcation coefficients, a and b (given by (A.6) and (A.7), respectively), are positive. It can be shown that the bifurcation coefficient b is automatically positive as follows. First of all, using the definitions for X and Y in (A.8), the quantity $X - Y$ can be simplified to (by using $v_1 = v_3 = 1$, as mentioned above):

$$X - Y = \xi_v(1 - \varepsilon_v)(1 - v_2), \tag{A.9}$$

which is positive since $\xi_v > 0$, $0 < \varepsilon_v < 1$ and the eigenvector $0 < v_2 < 1$ (from (A.2)). Thus, since $X - Y > 0$, $d_1 > 0, d_2 > 0, d_3 > 0$ and the eigenvectors w_4, w_5, w_6 and w_7 are positive, it follows from Equation (A.7) that the bifurcation coefficient b is automatically positive. Hence, since the bifurcation coefficient b is always positive, we only need to show that the coefficient a is positive for backward bifurcation to occur. In particular, it can be shown from Equation (A.6), and noting the definitions in (A.8) and the expressions for the eigenvectors in (A.2) and (A.3), that the backward bifurcation coefficients a is positive provided the following inequality holds:

$$P + Q + R > S + T + U. \tag{A.10}$$

Thus, it follows from Item (i) of Theorem 4.1 of (Castillo-Chavez and Song, 2004)), that the vaccination model (2.1) will undergo a backward bifurcation at $\mathbb{R}_{cv} = 1$ whenever inequality (A.10) holds. □

APPENDIX B

PROOF OF THEOREM 2.3.3

Proof. Consider the vaccination model (2.1) with $\varepsilon_v = \varepsilon_n = \varepsilon_{nv} = 1$ and $\tilde{\mathbb{R}}_{cv} \leq 1 - f_v < 1$ (with f_v as defined in Equation (2.6)). Furthermore, consider the following linear Lyapunov function:

$$\mathcal{L} = E + a_1\, I_p + a_2\, I_s + a_3\, I_a + a_4\, I_h,$$

where,

$$\begin{aligned} a_1 &= \frac{1}{\sigma_p + \delta_p + \mu}\Big[\beta_p + a_2\, r\, \sigma_p + a_3\,(1-r)\,\sigma_p\Big], a_2 = \frac{1}{\phi_s + \gamma_s + \delta_s + \mu}\left(a_4\,\phi_s + \beta_s\right), \\ a_3 &= \frac{\beta_a}{\gamma_a + \delta_a + \mu}, \text{ and } a_4 = \frac{\beta_h}{\gamma_h + \delta_h + \mu}. \end{aligned}$$

The Lyapunov derivative is given by:

$$\dot{\mathcal{L}} = \dot{E} + a_1\dot{I}_p + a_2\dot{I}_s + a_3\dot{I}_a + a_4\dot{I}_h,$$

so that, upon substituting the equations for the respective derivatives of the model (2.1):

$$\begin{aligned} \dot{\mathcal{L}} = &\left[\beta_p\frac{S}{N} - a_1\left(\sigma_p + \delta_p + \mu\right) + a_2 r\sigma_2 + a_3(1-r)\sigma_2\right] I_p \\ &+ \left[\beta_s\frac{S}{N} - a_2\left(\phi_s + \gamma_s + \delta_s + \mu\right) + a_4\phi_s\right] I_s + \left[\beta_a\frac{S}{N} - a_3(\gamma_a + \delta_a + \mu)\right] I_a \\ &+ \left[\beta_h\frac{S}{N} - a_4(\gamma_h + \delta_h + \mu)\right] I_h + (\sigma_E + \mu)\left(\frac{\tilde{\mathbb{R}}_{cv}}{1 - f_v} - 1\right) E, \end{aligned}$$

from which it follows that (noting that $S(t) \leq N(t)$ for all t in Ω),

$$\dot{\mathcal{L}} \leq (\sigma_E + \mu)\left(\frac{\tilde{\mathbb{R}}_{cv}}{1 - f_v} - 1\right) E.$$

Hence, $\dot{\mathcal{L}} \leq 0$ if $\tilde{\mathbb{R}}_{cv} \leq 1 - f_v < 1$, and $\dot{\mathcal{L}} = 0$ if and only if $E(t) = 0$. Substituting $E(t) = 0$ into the equations of the model (2.1) shows that:
$(S(t), V(t), E(t), I_p(t), I_s(t), I_a(t), I_h(t), R_n(t), R_{nv}(t)) \to (S^*, V^*, 0, 0, 0, 0, 0, 0, 0)$, as

$t \to \infty$ (where S^* and V^* are as defined in Section 2.3.1). Furthermore, it can be shown that the largest compact invariant set in $\{(S(t), V(t), E(t), I_p(t), I_s(t), I_a(t), I_h(t), R_n(t), R_{nv}(t)) \in \Omega : \dot{\mathcal{L}} = 0\}$ is the disease-free equilibrium (ξ_0). Hence, it follows, by LaSalle's Invariance Principle (Hale, 1969), that the disease-free equilibrium (ξ_0) of the model (2.1) is globally-asymptotically stable in Ω whenever $\tilde{\mathbb{R}}_{cv} < 1$. $\square$

APPENDIX C

PROOF OF THEOREM 2.3.4

Before proving the required main result of Theorem 2.3.4, it is necessary to establish the following intermediate results.

Proof of positive invariance and attractivity of Ω_{**}

Since $N(t) \leq \Pi/\mu$ for all t in Ω_{**}, it follows from the first equation of the vaccination model (2.1) that:

$$\begin{aligned}
\frac{dS}{dt} &\leq \Pi + \omega_v V - (\xi_v + \mu)S, \\
&\leq \Pi + \left(\frac{\Pi}{\mu} - S\right)\omega_v - (\xi_v + \mu)S, \\
&\leq \frac{\Pi}{\mu}(\mu + \omega_v) - (\mu + \xi_v + \omega_v)\, S, \\
&\leq (\mu + \xi_v + \omega_v)\,(S^* - S).
\end{aligned}$$

Hence, if $S(t) > S^*$, then $\dfrac{dS}{dt}$ is negative. Thus, $S(t) \leq S^*$ for all t, provided that $S(0) \leq S^*$. Using similar approach for the second equation of the vaccination model (2.1), and using the above bound, leads to the following bound:

$$\begin{aligned}
\frac{dV}{dt} &\leq \xi_v S^* - (\omega_v + \mu)V, \\
&\leq \xi_v \left[\frac{\Pi\,(\mu + \omega_v)}{\mu\,(\mu + \xi_v + \omega_v)}\right] - (\omega_v + \mu)V, \\
&\leq (\omega_v + \mu)(V^* - V).
\end{aligned}$$

Following the same argument as above, we have $V(t) \leq V^*$ for all t, provided that $V(0) \leq V^*$. It follows from these bounds that:

$$\Omega_{**} = \left\{(S, V, E, I_p, I_s, I_a, I_h, R_n, R_{nv}) \in \Omega : S \leq S^*, V \leq V^*\right\}, \tag{C.1}$$

is positively-invariant and attracts all initial solutions in Ω_{**}.

Next generation matrices for the second special case of the model

For the aforementioned (second) special case of the model (2.1), the associated next generation matrix of new infection terms, denoted by F, is as given in Equation (2.5), and the associated next generation matrix of linear transition terms, denoted by $\hat{V}$, is given by:

$$\hat{V} = \begin{bmatrix} \hat{K_1} & 0 & 0 & 0 & 0 \\ -\sigma_E & \hat{K_2} & 0 & 0 & 0 \\ 0 & -r\sigma_p & \hat{K_3} & 0 & 0 \\ 0 & -(1-r)\sigma_p & 0 & \hat{K_4} & 0 \\ 0 & 0 & -\phi_s & 0 & \hat{K_5} \end{bmatrix}, \tag{C.2}$$

with,

$$\hat{K_1} = \sigma_E + \mu, \hat{K_2} = \sigma_p + \mu, \hat{K_3} = \phi_s + \gamma_s + \mu, \hat{K_4} = \gamma_a + \mu \text{ and } \hat{K_5} = \gamma_h + \mu.$$

Proof of Theorem 2.3.4

Proof. Consider the vaccination model (2.1) with $\delta_p = \delta_s = \delta_a = \delta_h = 0$ and $\varepsilon_n = \varepsilon_{nv} = 1$. We further assume that $\hat{\mathbb{R}}_{cv} < 1$. The proof is also based on using a comparison theorem (Lakshmikantham and Leela, 1969; Gumel *et al.*, 2021b; Safdar *et al.*, 2023). Here, too, the equations for the infected compartments of the special case of the model (2.1) can be re-written as:

$$\frac{d}{dt}\begin{bmatrix} E(t) \\ I_p(t) \\ I_s(t) \\ I_a(t) \\ I_h(t) \end{bmatrix} = (F - \hat{V}) \begin{bmatrix} E(t) \\ I_p(t) \\ I_s(t) \\ I_a(t) \\ I_h(t) \end{bmatrix} - \hat{M} \begin{bmatrix} E(t) \\ I_p(t) \\ I_s(t) \\ I_a(t) \\ I_h(t) \end{bmatrix}, \tag{C.3}$$

where the matrices F and $\hat{V}$ are as given in Equations (2.5) and (C.2), respectively, and the matrix $\hat{M}$ (with S^* and V^* are as defined in Section 2.3.1) is given by:

$$\hat{M} = [(S^* - S) + (1 - \varepsilon_v)(V^* - V)] \begin{bmatrix} 0 & \beta_p & \beta_s & \beta_a & \beta_h \\ 0 & 0 & 0 & 0 & 0 \\ 0 & 0 & 0 & 0 & 0 \\ 0 & 0 & 0 & 0 & 0 \\ 0 & 0 & 0 & 0 & 0 \end{bmatrix}. \tag{C.4}$$

Since $S \leq S^*$, $V \leq V^*$ for all $t > 0$ in Ω_{**} (as shown above), it follows that the matrix $\hat{M}$, defined in Equation (C.4), is non-negative. Hence, Equation (C.3) can be re-written in terms of the following inequality:

$$\frac{d}{dt}\begin{bmatrix} E(t) \\ I_p(t) \\ I_s(t) \\ I_a(t) \\ I_h(t) \end{bmatrix} \leq (F - \hat{V}) \begin{bmatrix} E(t) \\ I_p(t) \\ I_s(t) \\ I_a(t) \\ I_h(t) \end{bmatrix}. \tag{C.5}$$

It should be recalled from the local asymptotic stable result for the disease-free equilibrium of the vaccination model (2.1) (given in Theorem 2.3.1) that all eigenvalues of the associated next generation matrix FV^{-1} are negative if $\mathbb{R}_{cv} < 1$ (i.e., $F - V$ is

a stable matrix). It follows that the eigenvalues of the next generation matrix $F\hat{V}^{-1}$, associated with this special case of the model (2.1), are also negative if $\hat{\mathbb{R}}_{cv} < 1$ (i.e., $F - \hat{V}$ is also a stable matrix). Thus, the linearized differential inequality system (C.5) is stable whenever $\rho(F\hat{V}^{-1}) < 1$. Consequently (Sharomi and Gumel, 2011; Gumel *et al.*, 2006; Safdar *et al.*, 2023; Ngonghala *et al.*, 2023),

$$(E(t), I_p(t), I_s(t), I_a(t), I_h(t)) \to (0, 0, 0, 0, 0), \text{ as } t \to \infty.$$

Substituting $E(t) = I_p(t) = I_s(t) = I_a(t) = I_h(t) = 0$ into the differential equations for the rate of change of the $R_n(t)$, $R_{nv}(t)$, $V(t)$ and $S(t)$ compartments of the model (2.1) shows that:

$$R_n(t) \to 0, R_{nv}(t) \to 0, V(t) \to V^* \text{ and } S(t) \to S^*, \text{ as } t \to \infty.$$

Thus, the DFE ($\mathcal{E}_0$) of the second special case of the model (2.1) (with $\delta_p = \delta_s = \delta_a = \delta_h = 0$ and $\varepsilon_n = \varepsilon_{nv} = 1$) is globally-asymptotically stable in Ω_{**} whenever $\hat{\mathbb{R}}_{cv} < 1$. □

APPENDIX D

PROOF OF THEOREM 2.3.6

Proof. Consider the special case of the model (2.1) with $\varepsilon_v = \varepsilon_n = \varepsilon_{nv} = 1$ and $\omega_v = \delta_p = \delta_s = \delta_a = \delta_h = 0$. Setting $\delta_p = \delta_s = \delta_a = \delta_h = 0$ into the model shows that $N(t) \to N^* = \Pi/\mu$ as $t \to \infty$. For the rest of the analysis in this appendix, $N(t)$ will be replaced by the limiting value, N^*. It should be recalled that it has been shown (in Theorem 2.3.5) that this special case of the model has a unique endemic equilibrium (denoted by $\tilde{E}_1$) whenever the associated reproduction number, denoted by $\tilde{\mathbb{R}}_v$, exceeds one. The proof of Theorem 2.3.6 will now be based on using a Krasnoselskii sub-linearity trick introduced by Hethcote and Thieme (1985) (see also Thieme (1985); Esteva and Vargas (2000); Esteva *et al.* (2009); Safi and Gumel (2010); Melesse and Gumel (2010)). First of all, since $N(t) = N^*$, the following relation holds:

$$S(t) = N^* - [V(t) + E(t) + I_p(t) + I_s(t) + I_a(t) + I_h(t) + R_n(t) + R_{nv}(t)] \quad \text{(D.1)}$$

Substituting (D.1) into the model (2.1) gives the following reduced model:

$$\begin{cases} \dot{V} &= \xi_v(N^* - V - E - I_p - I_s - I_a - I_h - R_n - R_{nv}) - (\omega_v + \mu)V, \\ \dot{E} &= \tilde{\lambda}(N^* - V - E - I_p - I_s - I_a - I_h - R_n - R_{nv}) - (\sigma_E + \mu)E, \\ \dot{I}_p &= \sigma_E E - (\sigma_p + \mu)I_p, \\ \dot{I}_s &= r\sigma_p I_p - (\phi_s + \gamma_s + \mu)I_s, \\ \dot{I}_a &= (1-r)\sigma_p I_p - (\gamma_a + \mu)I_a, \\ \dot{I}_h &= \phi_s I_s - (\gamma_h + \mu)I_h, \\ \dot{R}_n &= \gamma_s I_s + \gamma_a I_a + \gamma_h I_h - (\xi_v + \mu)R_n, \\ \dot{R}_{nv} &= \xi_v R_n - \mu R_{nv}. \end{cases} \quad \text{(D.2)}$$

where the associated *force of infection*, $\tilde{\lambda}$, is given by:

$$\tilde{\lambda} = \left(\frac{\beta_p I_p + \beta_s I_s + \beta_a I_a + \beta_h I_h}{N^*} \right). \tag{D.3}$$

The unique endemic equilibrium associated with the reduced system (D.2) now has the form:

$$\tilde{E}_1 = (V^{**}, E^{**}, I_p^{**}, I_s^{**}, I_a^{**}, I_h^{**}, R_n^{**}, R_{nv}^{**}). \tag{D.4}$$

Linearizing the reduced model (D.2), around the endemic equilibrium ($\tilde{E}_1$), gives the following linearized system:

$$\begin{cases} \dot{V} &= -(\xi_v + c_2)V - \xi_v E - \xi_v I_p - \xi_v I_s - \xi_v I_a - \xi_v I_h - \xi_v R_n - \xi_v R_{nv}, \\ \dot{E} &= -b_1 V - (b_1 + c_3)E + \sum_{j=\{p,s,a,h\}} (b_j - b_1) I_j - b_1 R_n - b_1 R_{nv}, \\ \dot{I}_p &= \sigma_E E - c_4 I_p, \\ \dot{I}_s &= r\sigma_p I_p - c_5 I_s, \\ \dot{I}_a &= (1-r)\sigma_p I_p - c_6 I_a, \\ \dot{I}_h &= \phi_s I_s - c_7 I_h, \\ \dot{R}_n &= \gamma_s I_s + \gamma_a I_a + \gamma_h I_h - c_1 R_n, \\ \dot{R}_{nv} &= \xi_v R_n - \mu R_{nv}. \end{cases} \tag{D.5}$$

where, $b_1 = \dfrac{\beta_p I_p^{**} + \beta_s I_s^{**} + \beta_a I_a^{**} + \beta_h I_h^{**}}{N^*}$, $b_j = \dfrac{\beta_j S^{**}}{N^*}$ for $j = \{p, s, a, h\}$ and $c_i (i = 1, \cdots, 7)$ are as defined in Section 2.3.2. The Jacobian associated with the linearized

system (D.5) is given by:

$$J(\tilde{E}_1) = \begin{bmatrix} -(\xi_v + c_2) & -\xi_v & -\xi_v & -\xi_v & -\xi_v & -\xi_v & -\xi_v & -\xi_v \\ -b_1 & -(b_1 + c_3) & \alpha_p & \alpha_s & \alpha_a & \alpha_h & -b_1 & -b_1 \\ 0 & \sigma_E & -c_4 & 0 & 0 & 0 & 0 & 0 \\ 0 & 0 & r\sigma_p & -c_5 & 0 & 0 & 0 & 0 \\ 0 & 0 & (1-r)\sigma_p & 0 & -c_6 & 0 & 0 & 0 \\ 0 & 0 & 0 & \phi_s & 0 & -c_7 & 0 & 0 \\ 0 & 0 & 0 & \gamma_s & \gamma_a & \gamma_h & -c_1 & 0 \\ 0 & 0 & 0 & 0 & 0 & 0 & \xi_v & -\mu \end{bmatrix}$$

with, $\alpha_j = b_j - b_1$ (for $j = \{p, s, a, h\}$). Suppose, now, that the linearized system (D.5) has solution of the form (Esteva and Vargas, 2000; Esteva *et al.*, 2009; Hethcote and Thieme, 1985; Melesse and Gumel, 2010; Safi and Gumel, 2010; Thieme, 1985):

$$\mathbf{Z}(t) = \mathbf{Z}_0 e^{\theta t}, \tag{D.6}$$

with $\mathbf{Z}_0 \in \mathbb{C} - \{0\}$, where $\mathbf{Z}_0 = (Z_1, Z_2, Z_3, Z_4, Z_5, Z_6, Z_7, Z_8), \theta, Z_i \in \mathbb{C}$ (for $i = 1, 2, ..., 8$) and $\mathbb{C}$ denotes the complex numbers (Esteva and Vargas, 2000; Esteva *et al.*, 2009; Hethcote and Thieme, 1985; Melesse and Gumel, 2010; Safi and Gumel, 2010; Thieme, 1985). Substituting a solution of the form (D.6) into the linearized

system (D.5) gives:

$$\begin{aligned}
\theta Z_1 &= -(c_1 + \xi_v)Z_1 - \xi_v(Z_2 + Z_3 + Z_4 + Z_5 + Z_6 + Z_7 + Z_8),\\
\theta Z_2 &= -b_1 Z_1 - (b_1 + c_3)Z_2 + \alpha_p Z_3 + \alpha_s Z_4 + \alpha_a Z_5 + \alpha_h Z_6 - b_1 Z_7 - b_1 Z_8,\\
\theta Z_3 &= \sigma_E Z_2 - c_4 Z_3,\\
\theta Z_4 &= r\sigma_p Z_3 - c_5 Z_4,\\
\theta Z_5 &= (1 - r)\sigma_p Z_3 - c_6 Z_5,\\
\theta Z_6 &= \phi_s Z_4 - c_7 Z_6,\\
\theta Z_7 &= \gamma_s Z_4 + \gamma_a Z_5 + \gamma_h Z_6 - c_1 Z_7,\\
\theta Z_8 &= \xi_v Z_7 - \mu Z_8.
\end{aligned} \tag{D.7}$$

System (D.7) can be simplified by moving all the negative terms in the last six equations of (D.7) to the respective left-hand sides (Esteva and Vargas, 2000; Esteva *et al.*, 2009; Hethcote and Thieme, 1985; Melesse and Gumel, 2010; Safi and Gumel, 2010; Thieme, 1985). Further, the last six equations are then re-written in terms of Z_1 and substituted into the first two equations of (D.7), and all its negative terms are moved to the left-hand side as well. Finally, after adding the first and second equations of (D.7), and moving all the negative terms to the left-hand side. Doing all these lead to the following system (Esteva and Vargas, 2000; Esteva *et al.*, 2009; Hethcote and Thieme, 1985; Melesse and Gumel, 2010; Safi and Gumel, 2010; Thieme, 1985):

$$\begin{aligned}
&[1 + F_1(\theta)]Z_1 + [1 + F_2(\theta)]Z_2 = (MZ)_1 + (MZ)_2,\\
&[1 + F_3(\theta)]Z_3 = (MZ)_3, \;\; [1 + F_4(\theta)]Z_4 = (MZ)_4,\\
&[1 + F_5(\theta)]Z_5 = (MZ)_5, \;\; [1 + F_6(\theta)]Z_6 = (MZ)_6,\\
&[1 + F_7(\theta)]Z_7 = (MZ)_7, \;\; [1 + F_8(\theta)]Z_8 = (MZ)_8.
\end{aligned} \tag{D.8}$$

where,

$$
\begin{aligned}
F_1(\theta) &= \frac{\theta}{\xi_v + c_2} + \frac{a_1}{\xi_v + c_2}, \\
F_2(\theta) &= \frac{\theta}{\xi_v} + \frac{a_1 + c_3}{\xi_v} + \frac{\sigma_E}{(\theta + k_4)}\left(1 + \frac{a_1}{\xi_v}\right) + \frac{r\sigma_p\sigma_E}{(\theta + c_4)(\theta + c_5)}\left(1 + \frac{a_1}{\xi_v}\right) \\
&\quad + \frac{(1-r)\sigma_p\sigma_E}{(\theta + c_4)(\theta + c_6)}\left(1 + \frac{a_1}{\xi_v}\right) + \frac{r\phi_s\sigma_p\sigma_E}{(\theta + c_4)(\theta + c_5)(\theta + c_7)}\left(1 + \frac{a_1}{\xi_v}\right) \\
&\quad + \frac{\sigma_E(\gamma_s + \gamma_a + \gamma_h)}{(\theta + c_1)(\theta + c_4)}\left(1 + \frac{a_1}{\xi_v}\right) + \frac{\sigma_E\xi_v(\gamma_s + \gamma_a + \gamma_h)}{(\theta + \mu)(\theta + c_1)(\theta + c_4)}\left(1 + \frac{a_1}{\xi_v}\right), \\
F_3(\theta) &= \frac{\theta}{c_4}, \;\; F_4(\theta) = \frac{\theta}{c_5}, \;\; F_5(\theta) = \frac{\theta}{c_6}, \;\; F_6(\theta) = \frac{\theta}{c_7}, \;\; F_7(\theta) = \frac{\theta}{c_1}, \;\; F_8(\theta) = \frac{\theta}{\mu},
\end{aligned}
$$

with,

$$
M = \begin{bmatrix}
0 & 0 & 0 & 0 & 0 & 0 & 0 & 0 \\
0 & 0 & \frac{\beta_p S^{**}}{k_3 N^*} & \frac{\beta_s S^{**}}{c_3 N^*} & \frac{\beta_a S^{**}}{c_3 N^*} & \frac{\beta_h S^{**}}{c_3 N^*} & 0 & 0 \\
0 & \frac{\sigma_E}{c_4} & 0 & 0 & 0 & 0 & 0 & 0 \\
0 & 0 & \frac{r\sigma_p}{c_5} & 0 & 0 & 0 & 0 & 0 \\
0 & 0 & \frac{(1-r)\sigma_p}{c_6} & 0 & 0 & 0 & 0 & 0 \\
0 & 0 & 0 & \frac{\phi_s}{c_7} & 0 & 0 & 0 & 0 \\
0 & 0 & 0 & \frac{\gamma_s}{c_1} & \frac{\gamma_a}{c_1} & \frac{\gamma_h}{c_1} & 0 & 0 \\
0 & 0 & 0 & 0 & 0 & 0 & \frac{\xi_v}{\mu} & 0
\end{bmatrix}.
$$

It can be verified that the endemic equilibrium, $\tilde{E}_1 = (V^{**}, E^{**}, I_p^{**}, I_s^{**}, I_a^{**}, I_h^{**}, R_n^{**}, R_{nv}^{**})$, satisfies $\tilde{E}_1 = M\tilde{E}_1$ (Esteva and Vargas, 2000; Esteva *et al.*, 2009; Hethcote and Thieme, 1985; Melesse and Gumel, 2010; Safi and Gumel, 2010; Thieme, 1985). The notation $(M\mathbf{Z})_i$ $(i = 1, 2, ..., 8)$ denotes the ith coordinate of the vector $M\mathbf{Z}$, and the matrix M has non-negative entries. If $\mathbf{Z}$ is a solution of (D.8), then it is possible to find a minimal positive real number r such that (Esteva and Vargas, 2000; Esteva *et al.*, 2009; Hethcote and Thieme, 1985; Melesse and Gumel, 2010; Safi and Gumel,

2010; Thieme, 1985)

$$\|\mathbf{Z}\| = r\tilde{E}_1 \tag{D.9}$$

where, $\|\mathbf{Z}\| = (\|Z_1\|, \|Z_2\|, \|Z_3\|, \|Z_4\|, \|Z_5\|, \|Z_6\|, \|Z_7\|, \|Z_8\|)$ with lexicographic order, and $\|.\|$ is a norm in $\mathbb{C}$. The main goal is to show that $Re(\theta) < 0$. This is illustrated *via* the method of contradiction, as follows. Suppose, now, that $Re(\theta) \geq 0$ and consider the following two cases.

Case 1: $\theta = 0$

Setting $\theta = 0$ in (D.7) reduces it to a homogeneous linear system in the variables Z_i $(i = 1, ..., 8)$, with determinant given by:

$$\Delta = \left[\left\{\mu c_1 \left(c_2 + \xi_v\right) c_3 c_4 c_5 c_6 c_7\right\} \left(\frac{S^{**}(\tilde{\mathbb{R}}_v)}{N^*} - 1\right)\right] - A_2 \tag{D.10}$$

where,

$$\begin{aligned} A_2 = b_1 c_2 [&\sigma_E \left(\mu + \xi_v\right) \left\{c_5 c_7 \left((1-r)\gamma_a \sigma_p\right) + r c_6 \sigma_p \left(\gamma_h \phi_s + c_7 \gamma_s\right)\right\} \\ &+ \mu c_1 \left\{c_4 c_5 c_6 c_7 + \sigma_E \left(c_5 c_7 (c_6 + (1-r)\sigma_p) + r c_6 \sigma_p (c_7 + \phi_s)\right)\right\}] > 0. \end{aligned}$$

To finally determine the sign of Δ, we need to determine the sign of $\left(\frac{S^{**}(\tilde{\mathbb{R}}_v)}{N^*} - 1\right)$. This is explored below. Solving Equation (D.2) at the endemic equilibrium $\tilde{E}_1$ gives:

$$\frac{S^{**}}{N^*} = \frac{c_3 E^{**}}{\beta_p I_p^{**} + \beta_s I_s^{**} + \beta_s I_a^{**} + \beta_h I_s^{**}}. \tag{D.11}$$

Substituting the expressions for $E^{**}, I_p^{**}, I_s^{**}, I_a^{**}$ and I_h^{**} from Equation (2.15) into Equation (D.11), and simplifying, gives (where $\tilde{\mathbb{R}}_v$ is as defined in (2.14)):

$$\frac{S^{**}}{N^*} = \frac{1}{\tilde{\mathbb{R}}_v}, \tag{D.12}$$

so that $\frac{S^{**}}{N^*} - \frac{1}{\tilde{\mathbb{R}}_v} = 0$. Thus, Equation (D.10) now becomes (noting that $A_2 > 0$):

$$\Delta = -A_2 < 0.$$

Since the determinant (Δ) is negative, it follows that the system (D.7) has a unique solution, given by $\mathbf{Z} = \mathbf{0}$ (which corresponds to the disease-free equilibrium, $\mathcal{E}_0$).

Case 2: $\theta \neq 0$.

Since we already assumed that $Re(\theta) > 0$, the remaining task is to show that the system has no non-trivial solution when $Re(\theta) > 0$. Clearly, we have that $F_j(\theta) > 0$, for all $j = \{p, s, a, h\}$, which implies that $|F_j(\theta) + 1| > 1$. We then define $F(\theta) = min(|F_j(\theta) + 1|)$, for $j = \{p, s, a, h\}$. Then, $1 < F(\theta)$ and hence $\frac{r}{F(\theta)} < r$. Since r is a minimal positive real number such that $\|\mathbf{Z}\| \leq r\tilde{E}_1$ (Safi and Gumel, 2010; Melesse and Gumel, 2010; Esteva *et al.*, 2009), which then implies that:

$$\|\mathbf{Z}\| > \frac{r}{F(\theta)}\tilde{E}_1. \tag{D.13}$$

On the other hand, by taking the norm of both sides of the third equation in (D.7) (Safi and Gumel, 2010; Melesse and Gumel, 2010; Esteva *et al.*, 2009), and noting that M is a non-negative matrix, gives:

$$F(\theta)\|Z_3\| \leq |1 + F_3(\theta)|\|Z_3\| = \|(MZ)_3\| \leq M\|Z_3\| \leq rM(\tilde{E}_1)_3 = r(\tilde{E}_1)_3 = rI_p^{**} \tag{D.14}$$

It follows from (D.14) that $\|Z_3\| \leq \frac{r}{F(\theta)}I_p^{**}$, which contradicts (D.13), due to the fact that r is minimal. Hence, $Re(\theta) < 0$. Thus, all eigenvalues of the characteristic equation associated with the linearized system (D.5) will have negative real part, so that the unique endemic equilibrium, $\tilde{E}_1$, of the system (D.2) is locally-asymptotically stable whenever $\tilde{\mathbb{R}}_v > 1$, as required. □

APPENDIX E

FULL FLOW DIAGRAM OF THE MODEL (3.1)

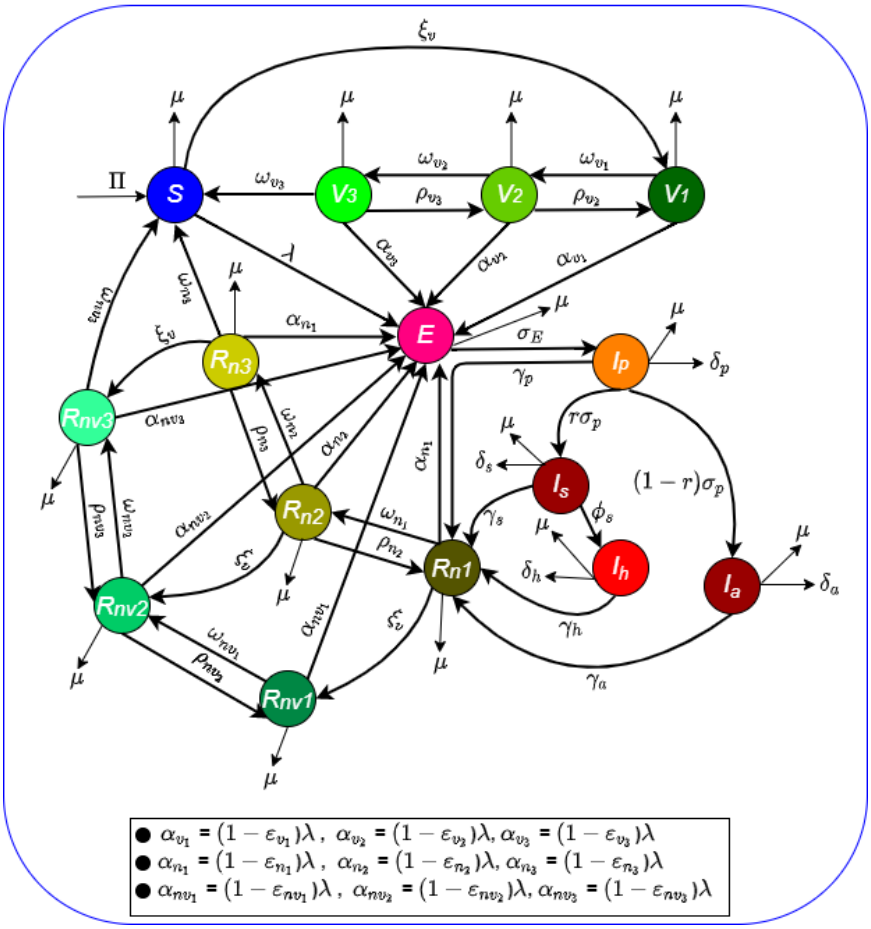

Figure E.1: Complete and Connected Flow Diagram of the Model (3.1).

APPENDIX F

PROOF OF THEOREM 3.3.2

Proof. Consider the model (3.1) with $\varepsilon_{v_i} = \varepsilon_{n_i} = \varepsilon_{nv_i} = 1$ and $\tilde{\mathbb{R}}_v \leq 1 - \sum_{i=1}^{3} f_{v_i} < 1$ (with f_{v_i} as defined in Equation (3.11)), for $i = 1, 2, 3$. Furthermore, consider the following linear Lyapunov function:

$$\mathcal{L} = E + a_1\, I_p + a_2\, I_s + a_3\, I_a + a_4\, I_h,$$

where,

$$\begin{aligned} a_1 &= \frac{1}{\sigma_p + \gamma_p + \delta_p + \mu}\Big[\beta\,\eta_p + a_2\, r\,\sigma_p + a_3\,(1-r)\,\sigma_p\Big], a_2 = \frac{a_4\,\phi_s + \beta\,\eta_s}{\phi_s + \gamma_s + \delta_s + \mu}, \\ a_3 &= \frac{\beta\,\eta_a}{\gamma_a + \delta_a + \mu}, \text{ and } a_4 = \frac{\beta\,\eta_h}{\gamma_h + \delta_h + \mu}. \end{aligned}$$

It follows that the Lyapunov derivative is given by:

$$\dot{\mathcal{L}} = \dot{E} + a_1\dot{I}_p + a_2\dot{I}_s + a_3\dot{I}_a + a_4\dot{I}_h,$$

so that, upon substituting the equations for the respective derivatives of the model (3.1):

$$\begin{aligned} \dot{\mathcal{L}} = &\left[\beta\,\eta_p\frac{S}{N} - a_1\,(\sigma_p + \gamma_p + \delta_p + \mu) + a_2 r\sigma_p + a_3(1-r)\sigma_p\right] I_p \\ &+ \left[\beta\,\eta_s\frac{S}{N} - a_2\,(\phi_s + \gamma_s + \delta_s + \mu) + a_4\phi_s\right] I_s + \left[\beta\,\eta_a\frac{S}{N} - a_3(\gamma_a + \delta_a + \mu)\right] I_a \\ &+ \left[\beta\,\eta_h\frac{S}{N} - a_4(\gamma_h + \delta_h + \mu)\right] I_h + (\sigma_E + \mu)\left(\frac{\tilde{\mathbb{R}}_v}{1 - \sum_{i=1}^{3} f_{v_i}} - 1\right) E, \end{aligned}$$

from which it follows that (noting that $S(t) \leq N(t)$ for all t in Ω),

$$\dot{\mathcal{L}} \leq (\sigma_E + \mu)\left(\frac{\tilde{\mathbb{R}}_v}{1 - \sum_{i=1}^{3} f_{v_i}} - 1\right) E.$$

Hence, $\dot{\mathcal{L}} \leq 0$ if $\tilde{\mathbb{R}}_v \leq 1 - \sum_{i=1}^{3} f_{v_i} < 1$, and $\dot{\mathcal{L}} = 0$ if and only if $E(t) = 0$. Substituting $E(t) = 0$ into the equations of the model (3.1) show that $(S(t), V_1(t), V_2(t), V_3(t), E(t), I_p(t), I_s(t), I_a(t), I_h(t), R_{n_1}(t), R_{n_2}(t), R_{n_3}(t), R_{nv_1}(t), R_{nv_2}(t), R_{nv_3}(t)) \rightarrow (S^*, V_1^*, V_2^*, V_3^*, 0, 0, 0, 0, 0, 0, 0, 0, 0, 0, 0)$ as $t \rightarrow \infty$ (where S^*, V_1^*, V_2^* and V_3^* are as defined in Section 3.3.1). Furthermore, it can be shown that the largest compact invariant set in $\{(S(t), V_i(t), E(t), I_p(t), I_s(t), I_a(t), I_h(t), R_{n_i}(t), R_{nv_i}(t)) \in \Omega : \dot{\mathcal{L}} = 0\}$ (for $i = 1, 2, 3$) is the disease-free equilibrium (ξ_0). Hence, it follows, by LaSalle's Invariance Principle (Hale, 1969), that the disease-free equilibrium (ξ_0) of the model (3.1) is globally-asymptotically stable in Ω whenever $\tilde{\mathbb{R}}_v < 1$. □

APPENDIX G

PROOF OF THEOREM 3.3.3

Proof. Consider the special case of the model (3.1) with $\delta_p = \delta_s = \delta_a = \delta_h = 0$ and $\varepsilon_{n_i} = \varepsilon_{nv_i} = 1$ (for $i = 1, 2, 3$). Further, let $\hat{\mathbb{R}}_v < 1$. For the aforementioned (second) special case of the model (3.1), the associated next generation matrix of new infection terms, denoted by F, is as given in Equation (3.3.1), and the associated next generation matrix of linear transition terms, denoted by $\hat{V}$, is given by:

$$\hat{V} = \begin{bmatrix} \sigma_E + \mu & 0 & 0 & 0 & 0 \\ -\sigma_E & \sigma_p + \gamma_p + \mu & 0 & 0 & 0 \\ 0 & -r\,\sigma_p & \phi_s + \gamma_s + \mu & 0 & 0 \\ 0 & -(1-r)\,\sigma_p & 0 & \gamma_a + \mu & 0 \\ 0 & 0 & -\phi_s & 0 & \gamma_h + \mu \end{bmatrix}. \tag{G.1}$$

The equations for the infected compartments of this special case of the model can be re-written in terms of the next generation matrices:

$$\frac{d}{dt}\begin{bmatrix} E(t) \\ I_p(t) \\ I_s(t) \\ I_a(t) \\ I_h(t) \end{bmatrix} = (F - \hat{V})\begin{bmatrix} E(t) \\ I_p(t) \\ I_s(t) \\ I_a(t) \\ I_h(t) \end{bmatrix} - \hat{M}\begin{bmatrix} E(t) \\ I_p(t) \\ I_s(t) \\ I_a(t) \\ I_h(t) \end{bmatrix}, \tag{G.2}$$

where the matrices F and $\hat{V}$ are as defined in Equations (3.3.1) and (G.1), respectively, and the matrix $\hat{M}$ (with S^*, V_1^*, V_2^* and V_3^* are as defined in Section 3.3.1) is given by:

$$\hat{M} = \beta[(S^* - S) + (1-\varepsilon_{v_1})(V_1^* - V_1) + (1-\varepsilon_{v_2})(V_2^* - V_2) + (1-\varepsilon_{v_3})(V_3^* - V_3)] \begin{bmatrix} 0 & \eta_p & \eta_s & \eta_a & \eta_h \\ 0 & 0 & 0 & 0 & 0 \\ 0 & 0 & 0 & 0 & 0 \\ 0 & 0 & 0 & 0 & 0 \\ 0 & 0 & 0 & 0 & 0 \end{bmatrix}. \tag{G.3}$$

Since $S \leq S^*$, $V_1 \leq V_1^*$, $V_2 \leq V_2^*$ and $V_3 \leq V_3^*$ for all $t > 0$ in Ω_{**}, it follows that the matrix $\hat{M}$, defined in Equation (G.3), is non-negative. Hence, the Equation (G.2) can be re-written in terms of the following inequality:

$$\frac{d}{dt}\begin{bmatrix} E(t) \\ I_p(t) \\ I_s(t) \\ I_a(t) \\ I_h(t) \end{bmatrix} \leq (F - \hat{V}) \begin{bmatrix} E(t) \\ I_p(t) \\ I_s(t) \\ I_a(t) \\ I_h(t) \end{bmatrix}. \tag{G.4}$$

It should be recalled from the local asymptotic stable result for the disease-free equilibrium of the vaccination model (3.1) (given in Theorem 3.3.1) that all eigenvalues of the associated next generation matrix FV^{-1} are negative if $\mathbb{R}_v < 1$ (i.e., $F - V$ is a stable matrix). It follows that the eigenvalues of the next generation matrix $F\hat{V}^{-1}$, associated with this special case of the model (3.1), are also negative if $\hat{\mathbb{R}}_v < 1$ (i.e., $F - \hat{V}$ is also a stable matrix). Thus, the linearized differential inequality system (G.4) is stable whenever $\rho(F\hat{V}^{-1}) < 1$. Consequently (Sharomi and Gumel, 2011; Gumel *et al.*, 2006; Safdar *et al.*, 2023; Ngonghala *et al.*, 2023),

$$(E(t), I_p(t), I_s(t), I_a(t), I_h(t)) \to (0, 0, 0, 0, 0), \text{ as } t \to \infty.$$

Substituting $E(t) = I_p(t) = I_s(t) = I_a(t) = I_h(t) = 0$ into the differential equations for the rate of change of the $R_{n_i}(t)$, $R_{nv_i}(t)$, $V_i(t)$ and $S(t)$ (with $i = 1, 2, 3$) compartments of the model (3.1) shows that:

$$R_{n_i}(t) \to 0, R_{nv_i}(t) \to 0, V_i(t) \to V_i^* \text{ and } S(t) \to S^* \text{ (with } i = 1, 2, 3), \text{ as } t \to \infty.$$

Thus, the DFE ($\mathcal{E}_0$) of the second special case of the model (3.1) (with $\delta_p = \delta_s =$

$\delta_a = \delta_h = 0$ and $\varepsilon_{n_i} = \varepsilon_{nv_i} = 1$ $(i = 1, 2, 3)$) is globally-asymptotically stable in Ω_{**} whenever $\hat{\mathbb{R}}_v < 1$. $\square$